Institut für Elektronik

Heinz-Nixdorf Lehrstuhl für Medizinische Elektronik
Univ. - Prof. Dr. rer. nat. habil. Bernhard Wolf

Multiparameter Methods for Non-invasive Measurement of Blood Glucose

Carlos Eduardo Ferrante do Amaral

Vollständiger Abdruck der von der Fakultät für Elektrotechnik und Informationstechnik der Technische Universität München zur Erlangung des akademischen Grades eines

Doktors-Ingenieurs

genehmigten Dissertation.

Vorsitzender: Univ. - Prof. Dr.-Ing. habil. Gerhard Rigoll

Prüfer der Dissertation:

1. Univ. - Prof. Dr. rer. nat. habil. B. Wolf
2. Univ. - Prof. Dr.-Ing. habil. Alexander W. Koch

Die Dissertation wurde am 28.01.2008 bei der Technischen Universität München eingereicht und durch die Fakultät für Elektrotechnik und Informationstechnik am 10.11.2008 angenommen.

"O Lord, You search out my path and my lying down and are acquainted with all my ways. If I take the wings of the morning and dwell in the uttermost parts of the sea, even there your hand shall lead me, and your right hand shall hold me."

Psalm 139:3, 9 – 10.

"Never forget to open new doors, through them unforgateble adventures, unexpected friends and through love can come... And especially never forget to keep windows opened. They will bring in the end of each day, a wonderful sunset."

ACKNOWLEDGEMENTS

This work is based on research conducted between April 2004 and March 2007 at the Heinz Nixdorf-Chair for Medical Electronics, Technical University of Munich. The study was supported by the German Academic Exchange Service (DAAD) and Heinz Nixdorf Stiftung. Many people have contributed to the writing of this thesis, and therefore deserve to be mentioned.

I am thankful to my supervisor, Professor Dr. Bernhard Wolf, for encouraging me to study this subject, collaborating with ideas and allowing the acquisition of many instruments essential for this work. I thank my second supervisor Martin Brischwein for being a good friend, giving me the opportunity to work in the Department and helping me with technical advices during many experiments. Also important was Dr. Otto and Corinne Brockman for revising the English in the thesis. I also want to thank the colleagues in the Heinz Nixdorf-Chair who provided much needed help and created an encouraging working atmosphere. Especially I thank Ingrid Franz, for being a good counseler and friend in all moments. I am grateful to Professor Décio do Nascimento for having inspired me in the biomedical field and for supporting me in many important decisions.

The company Rohde and Schwarz also had significant participation in this investigation through the donation of equipment and support in impedance analyzer application. I greatly appreciated Dr. Hristo Iglev and Marcus Schmeisser from the department of experimental Physics at the Technische Universität München for providing invaluable support concerning the optical orientation and experimental apparatus. The Central Institute of Medical Engineering (IMETUM) gave us immense help allowing our group to work with the optic spectrometers available in their laboratories. Also sincere thanks to Professor Lars Nørgaard, from the Department of Food Science at the Royal Veterinary and Agricultural University in Denmark, for the extended explanation on PLS algorithms. Professor Dr. Löscher, Dr. Gosen and Dr. Perona from department of Infections and Tropic Medicine at the Ludwig-Maximilians-Universität München and the Bayrische Blutspende also helped our work by donating probes. Doctor Calatzis from the company Dynebyte collaborated with constructive explanations concerning blood preparations.

My gratitude to precious friends Elena Buoso, Marcos, Juliana, Marco Tosi, Elisabeth, Jair, Christina, Ralf, Patrica, Robert, Simone, Lina, Christian, Emma, Nedialko, Lusi, Torsten, Carla, Karl, Lote, Christoph, Liz, Sebastian, Thomas, Wagner, Luciana and Cesar.

To my parents Luiz and Luiza, who are great example in my life, my syster Leticia and nephew Israel. The love and support from my family made this possible.

Finally, I wish to express my gratitude to God, whose presence has given me strength to finish one more phase and whose love has been present in my life, not only through His sacrifice on the cross, but also in every small daily detail.

Munich, January 2008

Carlos Eduardo Ferrante do Amaral

CONTENTS

LIST OF ILLUSTRATIONS

LIST OF TABLES

LIST OF ABREVIATIONS

AC - Alternating Current
A/D - Analógico/Digital
ANN - Artificial Neural Network
ANSI - American National Standards Institute
ATR - Attenuated Total Reflection
BIA - Bio-electrical Impedance Analysis
CCD - Charge Coupled Device
CE - Conformité Européenne
CPU - Central Processing Unit
DC - Direct Current
DDS - Direct-Digital Synthesizer
ECG - Electro Cardio-Gram
EGA - Error Grid Analysis
EIT - Electrical Impedance Tomography
ECF - Extra-Cellular Fluid
FDA - Food and Drug Administration
FFM - Fat Free Mass
FT - Fourier transform
FT-IR - Fourier transform infrared
GOD - Glucose Oxidase
ICF - Intra-Cellular Fluid
IDES - Interdigitated electrodes
IR - Infrared
ISF - Interstitial Fluid
ISFET - Ion selective field effect transistor
LM - Lean Mass
MHC - Metabolic Heat Conformation
MLP - Multilayer Perceptron
MIR - Mid-infrared
NIR - Near infrared

OCT - Optical coherence tomography

PAS - Photoacoustic Spectroscopy

PLS - Partial Least Squares Regression

PRESS - Prediction Error Sum of Squares

RMM - Radiomolecular Magnetism

SD - Standard Deviation

SDRAM - Synchronous Dynamic Random Access Memory

SEC - Standard Error of Calibration

SEP - Standard Error of Prediction

SNR - Signal-to-noise ratio

TBW - Total Body Water

TBF - Total Body Fat

US - Ultrasound

UV - Ultraviolet

VIS - Visible

ABSTRACT

The determination of the blood glucose level is a necessary procedure in diabetes therapy, where the most common technique involves finger-prick capillary measurements, which is invasive, uncomfortable and causes skin injury. Painless glycemic control would improve the quality of life of patients by increasing compliance to monitoring blood glucose levels and thus hyper- and hypoglycaemic episodes. Although research groups have been trying for decades to separate non-invasive glucose information from interference compounds, none of the available commercial devices offers enough precision to replace lancetderived readings. This thesis describes the technologies of bioimpedance and absorption spectroscopy applied simultaneously to transcutaneous glycemic measurement.

Initially, basic electrical and optic theories were studied systematically and, as a result, glucose characteristics were obtained in deionized water and blood. Light spectroscopy studies were done in UV, visible, NIR (1μm to 5 μm) and MIR ranges (5 μm to 40 μm). Complex bioimpedance measurements were scaned from 100 Hz until 30 MHz in Solartron spectrometer, and from 20 kHz until 8 GHz in the network analyzer.

In sequence Femlab simulations helped the design of the concentric electrodes for skin tests. The optimal transcutaneous spectra was found between 3200 nm and 3400 nm. It was measured with a dark chamber adapted to the ATR module, thus avoiding background noises and keeping pressure constant in the target site. In conjuction with the above parameters, information of epidermis temperature (conductance and IR radiation) was also collected with the aim to improve prediction quality. Nevertheless, transcutaneous assays showed correlation of 0.43 for impedance and 0.46 for optic spectroscopy alone. After data was processed through PLS and neural networks method in Matlab, the multiparameter analysis allowed the improvement of correlation to 0.57. Although the sensibility of the transcutaneous method is lower than standard invasive devices, there is still a chance of improvement through laser technology, development of customized circuits and the addition of extra monitoring parameters.

Keywords: Blood glucose monitoring, diabetes mellitus, non-invasive measurement, transcutaneous sensor, bioimpedance, light spectroscopy, multivariable analysis.

CHAPTER 1

INTRODUCTION

1.1 OBJECTIVE AND MOTIVATION

World wide 150 million people suffer from diabetes which is a disease characterized by disturbances in the endocrine metabolic regulation. Approximately 10 % of the cases result from insulin deficiency (diabetes type 1), which often starts during childhood and requires the administration of this hormone usually many times a day. Insulin resistance (diabetes type 2) happens in 90 % of patients, occurring mostly in people over 40 years old. Additional cases occur during pregnancy, where 2 % of women have gestational diabetes. Any kind of diabetes can be dangerous since long-term excess of glucose (hyperglycemia) can cause blindness, damage to the nerves and kidneys (renal failure) or even increase the risk for heart disease, stroke, and birth defects. As well, low levels (hypoglycemia) can result in confusion, coma and even death (HEISE, 2000).

Type 1 diabetes can be controlled by pancreas transplantation, which has been known since 1960 and allows insulin independence in 80% of cases 1 year after surgery. The transplantation of only of islet cells is another alternative that offers less complex surgical interventions. In both therapies the limited number of donors, risks of immunosuppression and complications in medical procedures are major disadvantages. Hybrid systems like bio-artificial pancreas could provide a solution by supplying an unlimited source of islets for transplantation. This technique allows the application of islets from animals or insulin-producing cells engineered from stem cells. Unfortunately these systems still have problems related to biocompatibility, stability of insulin secretion, and a relatively short duration of operation (WOJCICKI and LADYZYNSKI, 2003).

To avoid hyperglycemia or hypoglycaemia, adhering to a diet composed mostly of carbohydrate and monounsaturated fats with limited amounts of sucrose, associated with medicament administration, which is mostly insulin. In order to know the correct medicine volume, a constant monitoring of blood glycemic levels is required, where standard procedure analyzes blood samples from the finger tip. This procedure is uncomfortable and causes low compliance by patients, reason why during the last decades a great number of non-invasive

research has been investigated, unfortunately, without any satisfactory precision (TURA, MARAN and PACINI, 2006).

Although impedance spectroscopy is a simple principle, this technique offers many possibilities of utilisation. One can associate this approach to civil engineering, analyzing the state of construction materials and detecting the existence of failures in the structure. In food industry it is possible to control the validation of products (REN, WANG, AN et al, 1998). The impedance analysis also has special importance in the medical field, as it is used for determination of total body water (TBW), fat free mass (FFM), tissue characterisation, apnea monitoring, venous thrombus detection, tomography, cardiography, pneumography and the analysis of compounds in the blood (JOSSINET and TRILLAUD, 1992). Bio-electrical impedance analysis (BIA) uses electrodes to apply low intensity currents to physiological fluids or tissues. The resulting voltage reflects changes in dielectric or dimensions of the target, thus being able to monitor chemical compositions or even physiological events in the organism. The most important features of BIA are low cost, fast response, simple implementation and safety. Due to the development of fast electronic technology, such parameter is a promising tool for tissue characterization and compound quantification, especially by dielectric spectroscopy in high frequencies.

Photonics involves a wide range of applications in fields such as brain research, intensive care, biopsy, dermatology, surgery, etc... Optical coherence tomography (OCT) and pulse oximetry are examples of the potential of such measurements. This approach uses light sources which work as modulating agents that irradiate parts of the body, and a photodetector for processing the resulting signal. Like in bioimpedance, optical measurements are attractive because of simple principle, low cost, safety and real-time assessment. The field of biomedical photonics is continuously expanding and new applications are envisioned, especially because of the availability of laser technologies (GEDDES e BAKER, 1989; BRONZINO, 2000).

Few published works describe the non-invasive multivariate monitoring of blood glucose, and between all promising methods, complex impedance and optic spectroscopy show appealing technological advantages. Therefore the aim of this thesis is to apply both approaches simultaneously in prediction of glycemic level. Besides the analysis of sensors, classifying algorithms are also described which may improve transcutaneous results.

1.2 OVERVIEW

Chapter 2 reviews the properties of glucose in blood and describes measurement methods with emphasis in non-invasive technologies. First of all, chemical properties of glucose and its concentration in the human body are explained. Next, the chapter shows a theory of traditional glucose oxidation methods and minimally-invasive aproches. Non-invasive methods will be described with emphasis in optical and electrical spectroscopy, including a list of commercial transcutaneous meters. More datailed characteristics of bioimpedance and light methods will be described in independent sections.

In chapter 3 impedance spectroscopy theory is provided. After historical background, basic dielectric definition with enphasis on capacitive-resistive circuits is discussed due to similar characteristics with biological tissues. The next part describes advantages and drawbacks of BIA measurement principles, which can be bipolar or tetrapolar. Other important topics are multifrequential comportament of RC circuits and safety.

A similar analysis of optical methods is discussed in chapter 4. Therefore, historical background, basic optical definition, photo transducers, type of spectrometers and safety are described.

Because one desires to predict the blood glucose concentration in skin, composition and structure of both tissues are described in chapter 5, as well as their physical and optical parameters.

The emphasis in Chapter 6 is the presentation of prediction algorithms, with an explanation of partial least squares (PLS) and artificial neural network (ANN). In both cases, principles of calculation, as well as advantages and limitations are listed.

Impedance transducers, optical sensors and instruments used in the research are analyzed in the chapter 7. The aim of this section is to justify the methodology chosen and to show measurement procedures. Impedance electrodes differ between liquid and tissue assays, been measured through complex impedance spectrometer Solartron 1260 and network analyzer ZVCE. The light tests also used two devices depending on the wavelength range of interest. Ultra-violet, visible and near-infrared investigations were done with Specord 210 spectrometer. Near-infrared and mid-infrared spectra were also measured with FTIR equipment. The PLS and ANN scripts chosen for Matlab are also described.

Experimental results are finally found in chapter 8, which analyzes aqueous assays for impedance and optic approaches, and then it is followed by the blood samples. Moreover, one

measures the characteristics of the skin using both non-invasive methods in association with pressure and temperature control in the finger.

The last chapter discusses the results of the experiment and compares data treatment algorithms, finally, suggesting future corrections and application of this work.

CHAPTER 2

TECHNIQUES FOR BLOOD GLUCOSE MONITORING

2.1 INTRODUCTION

Due to the gravity of diabetes, many efforts have been made to produce precision blood glucometers. There are 3 methods of glucose monitoring: invasive, minimally-invasive and non-invasive. In the present section a general discussion of blood glycemic levels and measurement technologies is presented. Although invasive and minimally-invasive techniques are described, non-invasive approaches are the focus of this work. Impedance and light absorption spectroscopy are the methods chosen for this research and, therefore, they are more detailed explained in more detail in separate chapters.

2.2 PHYSIOLOGICAL ASPECTS

Glucose is the most abundant hematologic monosaccharide and is also the main energy carrier in the human organism. Recommended goals for this carbohydrate levels preceding a meal (preprandial) are less than 100 mg/dL (5.5 mmol/L) in plasma and 89 mg/dL (4.9 mmol/L) in whole blood or capillary. After eating (postprandial) those values should not exceed 140 mg/dL (7.8 mmol/L) in plasma and 125 mg/dL (6.9 mmol/L) in whole blood or capillary, as shown in Table 1 (RENARD, 2005). D-Glucose can be found in two different stereoisomers, i.e. the α- and the β-anomeric form, whose structure can be seen in Figure 1 (HEISE, 2000).

The sugar concentration in blood is controlled by the pancreas. In this entire organ there are clusters of cells called islets of Langerhans, which are formed by alpha or beta types. Alpha clusters produce the hormone glucagon, which raises the level of blood sugar. Beta cells produce insulin, which is responsible for helping the body to transform glucose in to energy. Islets not only produce these metabolic hormones but also continuously monitor glycemic changes with a delay of seconds. This is possible because glucose is quickly transferred from blood to these cells via interstitial fluid surrounding the clusters. The

response from organism not only depends on the absolute magnitude of glucose level, but also on the rate of change (O'CONNELL, HAWTHORNE, HOLMES-WALKER *et al*, 2006).

Table 1 - Glucose level consequences in whole blood.

mmol/l	mg/dL	Interpretation
2.0	35	extremely low, danger of unconsciousness
3.0	55	low, marginal insulin reaction
4.0 -6.0	70-100	normal preprandial in nondiabetic
8.0	150	normal postprandial in nondiabetic
10.0	180	maximum postprandial in nondiabetic
15.0	270	a little high to very high depending on patient
16.5 -20.0	300 -360	danger
22	400	max mg/dL for some metres and strips
33	600	high danger of severe electrolyte imbalance

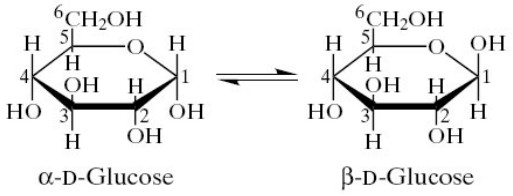

Figure 1 – Glucose molecule structure (HEISE, 2000).

2.3 INVASIVE GLYCEMIC MONITORING

Fully invasive systems can be either bedside clinical devices or self-monitoring meters. Bedside monitors are suitable for intensive care units and use implantable sensors with approximately 1 % precision. These systems allow continuous monitoring, therefore increasing the amount of clinical information such as direction, magnitude, duration, frequency, and causes of fluctuations in blood glucose levels (CLARKE, ANDERSON, FARHY *et al*, 2005). The bio-artificial pancreas uses similar implantable technology to control insulin pumps.

Home monitors, like the equipment in Figure 2, usually have a relative accuracy between 6 – 7 % and read glucose concentrations from blood samples taken from the fingertip. Although disposable test strips for finger-prick capillary measurements normally use reagents associated with electrochemical detectors, optical sensors can also be used for this application.

Figure 2 – "Accu-chek Sensor" from the firm Roche, invasive device (a) to control glucose concentrations in finger blood through disposable strips (b).

Electrochemical (Enzyme) tests are based on amperometric and potentiometric principles. Amperometric electrodes are covered with the enzyme glucose oxidase (GOD) in order to increase the sensor sensitivity (WILKINS and ATANASOV, 1996). Glucose solutions with oxygen produce gluconic acid and oxygenated water as illustrated in Equation 1. In Equation 2 when a 700 mV potential is applied in the solution, glucose concentration can be measured through special semi permeable membranes that control the passage of oxygen to the electrode contact (ABEL and VON WOEDTKE, 2002).

$$\text{GLUCOSE} + O_2 \xrightarrow{\text{GOD}} \text{GLUCONIC ACID} + H_2O_2 \quad (1)$$

$$H_2O_2 \xrightarrow{700\ \text{mV}} O_2 + 2H^+ + 2\acute{e} \quad (2)$$

Enzyme glucose sensors normally use 3 electrodes, as seen in Figure 3. The contact where the measurement occurs is called the work electrode (Platinum - Pt). A reference electrode (Ag/AgCl) is also used to avoid system oscillations, having a constant voltage in its contact (normally - 700 mV). The terminal called counter or auxiliary electrode (Pt) is used to apply a current in the work electrode. Another possibility is to measure the changes in local pH due to the hydrogen produced at the sensor in Equation 2, usually a coated wire pH-selective electrode. Such selective membrane when used with a field effect transistor (ISFET) produces a potentiometric sensor which also reflects glucose changes (ZIMMERMANN, FIENBORK, FLOUNDERS et al, 2004).

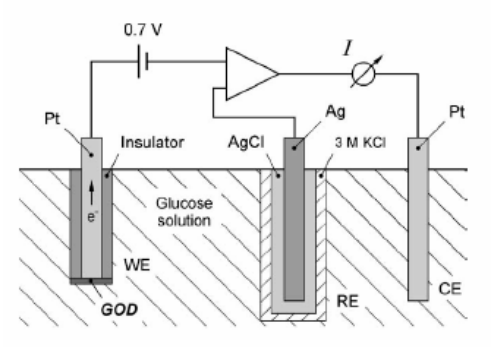

Figure 3 - Schematic diagram of an enzyme-based electrochemical glucose sensor (ZIMMERMANN, FIENBORK, FLOUNDERS *et al*, 2004).

Optical glucose sensors can use a substrate (lectin concanavalin A) with a fluorescent indicator (fluorescein isothiocyanate-dextran) to detect the different analyte concentrations, as illustrated in Figure 4. Excitation light passes through the fiber and into the solution, fluorescing the unbound indicator, and the fluorescent light passes back along the same fiber to a measuring system (MENDELSON, 1995).

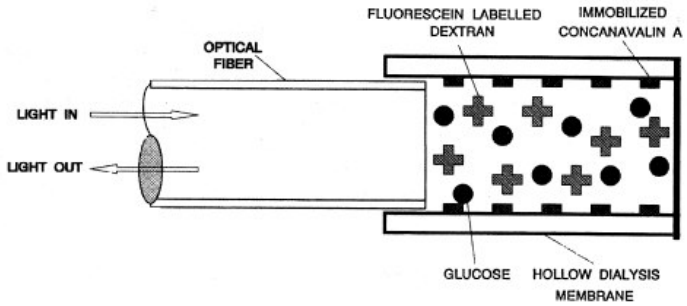

Figure 4 – Schematic diagram of an optic sensor for glucose measurement (MENDELSON, 1995).

Although the invasive result's accuracy can be affected by factors like calibration, ambient temperature, size of blood sample, drugs in blood, hematocrit concentration, humidity and aging of strips, lancet systems are still standard techniques for home monitoring of patients with diabetes. Efforts have been made in order to reduce the level of invasiveness by decreasing blood sample volume to a few microlitters and by measuring areas of the body less sensitive to pain than fingertips, such as the forearm, upper arm, or thigh (KLONOFF, 2005). Most concerning of the drawbacks of such systems are the lack of control during sleeping or manual activities, loss of tracking hyper- or hypoglycaemia episodes, risks of

infection, nerve damage and the discomfort of pricking the finger several times a day, which often leads to non-compliance (PICKUP, HUSSAIN, EVANS *et al*, 2005).

2.4 MINIMALLY-INVASIVE GLYCEMIC MONITORING

Minimally invasive measurements sample the interstitial fluid (ISF) with subcutaneous sensors (GROSS, BODE and EINHORN, 2000). These glucometers also can be bedside units or wearable modules, as illustrated in Figure 5. Even in this method the discomfort causes impediments to patient's therapy, therefore research groups are working to develop a non-invasive glucose control device (KOSCHINSKY and HEINEMANN, 2001). Unfortunately, there are no published reports or patents which show that non-invasive methods have the same accuracy as invasive procedures.

Figure 5 - CGMS System Gold minimally-invasive glucose meter from Medtronic MiniMed. The sensor is inserted under the skin on the abdomen and can monitor interstitial glucose up to 72 hours (GROSS, BODE and EINHORN, 2000).

2.5 NON-INVASIVE GLYCEMIC MONITORING TECHNIQUES

Non-invasive sensors measure either by a direct approach, based on the chemical structure of the glucose molecule, or indirectly by measuring blood sugar effects on a secondary process such as temperature or pH changes (ARNOLD and SMALL, 2005). One option to painless intermittent glucose control is the substitution of blood with others fluids that contain glucose, such as saliva, urine, sweat or tears (SRINIVASAN, PAMULA, POLLACK *et al*, 2003; PARK, LEE, YOON *et al*, 2005). Unfortunately, continuous measurements can only be accomplished through body tissues such as skin, cornea, oral

mucosa, tongue or tympanic membrane (BABA, CAMERON and COTÉ, 2002; ROHRSCHEIB, ROBINSON and EATON, 2003).

Research in this field includes the selection of the measuring principle, choice of measurement site, sensor development, in-vitro evaluation and refinement, in vivo performance tests in laboratory animals and, finally, human trials. The development of such transducers is difficult since it should have a high sensitivity, be capable to detect weak blood signals that lose energy through intervening tissues (bone, fat, skin, etc.), and separate information on glucose from that of other overlapping constituents of higher concentration (proteins, urea, uric acid, hemoglobin, water, etc…) (SIEG, GUY and DELGADO-CHARRO, 2005; KHALIL, 2004).

Recent improvements in technology and treatment algorithms may still enable new works to improve accuracy of the predictions. Figure 6 shows different classifications of blood glucose measurements. Investigations have been published using technologies such as reverse iontophoresis, polarimetry, metabolic heat conformation, ultrasound, thermal emission, electromagnetic, photoacoustic, Raman, light absorption and bioimpedance spectroscopy. Together with the choice of technique and sample region, one should also give attention to factors of the measurement environment. For example, in case of transdermal monitoring, parameters such as sweating, skin color, surface roughness, tissue thickness, breathing artifacts, blood flow, body movements, ambient temperature, pressure, and sample duration also influence the results (BURMEISTER and ARNOLD, 1999; Chen, Liu, Xu, *et al*, 2005). Table 2 shows an update of non-invasive groups with their technique and the target site.

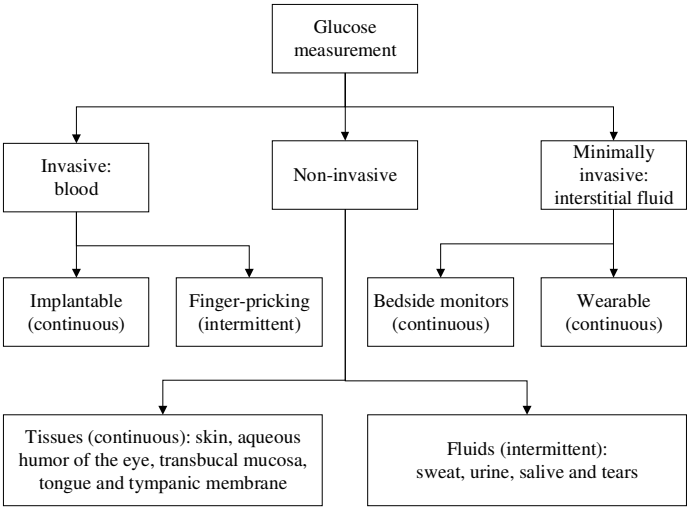

Figure 6 - Overview of technologies for blood glucose control.

Table 2 – Recent non-invasive blood glucose research companies.

Company - Product	Technology - Parameter	Target tissue	URL
- Biocontrol Technology: Diasensor 1000	optic spectroscopy: NIR light 1640 nm, 1670 nm	forearm skin	http://www.mendosa.com/painless.htm
- Biopeak Corporation: Glucotrack	- VIS and NIR light (660 nm, 810 nm, 970 nm, 1054 nm) - ECG - bioimpedance: current (< 1 mA: 1 Hz - 100 kHz) (< 10 mA: 100 kHz - 1 MHz)	wrist skin	http://www.biopeak.com
- Calisto Medical: Glucoband	bio-electromagnetic resonance: current	wrist skin	http://www.calistomedical.com
- Ciba Vision	optic spectroscopy: VIS light (465, 520 nm, 590 nm)	contact lens - tears	http://www.devicelink.com/ivdt/archive/03/05/008.html
- Cygnus (Animas): Glucowatch	interstitial fluid extraction: - current (extraction mA, detection nA) - GOD (hydrogel)	wrist skin	http://www.glucowatch.com
- Fovioptics	optic spectroscopy: VIS light (500 nm - 640 nm)	retinal	http://www.diabetesnet.com/diabetes_technology/fovioptics.php
- GlucoLight Corporation	optical coherence tomography	not available	http://www.glucolight.com
- Glucon: Aprise	photoacoustic: NIR light (800 nm, 960 nm, 1300 nm, 1440 nm,)	forearm skin	http://www.glucon.com
- Infratec	thermal emission spectroscopy: MIR light (4.2 µm – 12.2 µm)	tympanic membrane	http://www.diabetesmonitor.com/metres.htm
- Inlight Solutions	optic spectroscopy: NIR light (1.2 µm - 2.5 µm)	skin	http://www.inlightsolutions.com
- Integrity Applications: GlucoTrack	- ultrasound - complex bioimpedance - temperature	ear lobe skin	http://www.integrity-app.com
- Instrumentation Metrics	optic spectroscopy: VIS and NIR light (700-2500 nm)	skin	www.instrumentationmetrics.com
- LifeTrac: Sugartrac	optic spectroscopy: VIS NIR light (650, 880, 940, 1300 nm)	finger skin	http://www.sugartrac.com
- NIR Diagnostics: GlucoNIR	optic spectroscopy: NIR light (600 nm - 1050 nm)	skin	http://www.nirdiagnostics.com
- Optiscan Biomedical Corporation	thermal emission spectroscopy: MIR light (9.8 µm, 10.9 µm 11.9 µm).	skin	http://www.farir.com
- Orsense	occlusion optic spectroscopy: - VIS light (610 nm, 810 nm) - pressure	finger tip skin	http://www.orsense.com
- Pindi	radiomolecular magnetism (RMM): magnitude of electromagnetic wave (2.48 GHz)	finger tip skin	http://www.pindi.com
- PreciSense	fluorescence resonance energy transfer	skin	http://www.precisense.dk
- Q Step Technologies	polarized light: VIS and NIR light (532 nm, 635 nm, 904 nm)	eye iris	http://www.qstep.com
- Samsung fine Chemicals Company	radiomolecular magnetism: electromagnetic wave (42.58 MHz)	finger skin	www.sfc.samsung.co.kr/en
- Sensys Medical: Sensys GTS	optic spectroscopy NIR light (1300 nm - 1360 nm, 1670 nm 1690 nm, 1930 nm - 1950 nm, 2120 nm - 2280 nm)	skin	http://www.sensysmedical.com/home.html
- Sentek Group: Glucoview	crystalline colloidal array	eye	http://www.diabetesnet.com/diabetes_technology/sentek.php
- Solianis Monitoring (Pendragon): Pendra	bioimpedance: current (1 MHz - 200 MHz)	wrist skin	http://www.solianis.com
- Sontra Medical (Bayer Diagnostics): SonoPrep	- ultrasonic: electromagnetic wave (20 kHz) - electrochemical	skin	http://www.sontra.com
- Heinz Nixdorf-Chair for Medical Electronics (TUM)	- optic spectroscopy: MIR light (8 µm – 10.5 µm) - bioimpedance: current (100 kHz – 3 GHz)	finger tip skin	http://www.lme.ei.tum.de
- VeraLight	fluorescence spectroscopy: VIS light (250 nm - 850 nm)	forearm skin	http://www.veralight.com
- Visual Pathways: GlucoScope	visual pigment bleaching: VIS and NIR light (500 to 950 nm)	anterior chamber of the eye	http://vispath.com
- VivoMedical	electrochemical sweat measurement	finger tip skin	http://www.vivomedical.com
- Hitachi	metabolic heat conformation: - VIS and NIR light (470 nm, 535 nm, 660 nm, 810 nm, 880 nm, and 950 nm) - temperature (skin surface, ambient room, and background radiation)	finger tip skin	http://www.hitachi.com/New/cnews/040223.html

Optimal non-invasive blood sugar meters should be able to detect change in glucose concentrations within l-5 minutes in ranges from 18 to 540 md/dL with approximately 5 % error (WILKINS and ATANASOV, 1996; BOYD and BRUNS, 2001). If the meter does not fit these specifications, the Clarke error grid shown in Figure 7 is another possibility to analyse accuracy of readings. This method classifies the instrument response in five zones from A through E. Zone A represents values that are clinically accurate, zone B values are benign, and values in the C, D, and E zones might lead to an inappropriate treatment (KOVATCHEV, GONDER-FREDERICK, COX CLARKE *et al*, 2004).

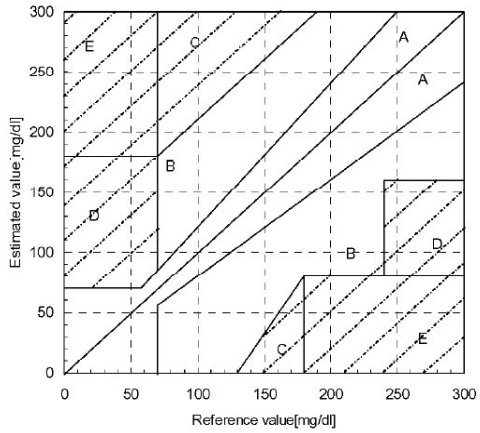

Figure 7 – Clarke error grid for analysis of predicting glucose measurements (FUNAKI, MATSUURA and TANAKA, 2000).

2.5.1 Reverse Iontophoresis

The method of iontophoresis has been used for many decades and utilizes electrical current to deliver charged drug compounds through the skin. Non-invasive monitoring, however, uses transport of glucose in the opposite direction (from the skin outward), therefore, this process has been called ‘reverse iontophoresis’ (LEBOULANGER, GUY and DELGADO-CHARRO, 2004). The GlucoWatch monitor, shown in Figure 8, is a wrist-watch glucose control device manufactured by Animas Technologies that utilizes this technique with two independent potentiostat circuits (POTTS, TAMADA and TIERNEY, 2002). This measurement is possible because neutral molecules, such as glucose, are extracted through the epidermis surface via this electro-osmotic flow to the iontophoretic cathode, along with Na^+ ions.

Figure 8 - GlucoWatch wrist-watch blood glucose monitor from the company Cygnus. Glucose is extracted through reverse iontophoresis, and measured by amperometric biosensor (POTTS, TAMADA and TIERNEY, 2002).

Glucose concentrations extracted through the skin with mA currents are in µmolar ranges, therefore the amperometric circuit needs to detect glucose from 0.9 mg/dL to 3.6 mg/dL. In this electrode, blood sugar is collected in hydrogel discs containing the enzyme glucose oxidase (GOD). These hydrogels, which need to be replaced often, constitute the electrolyte of an amperometric biosensor, working with nA currents to detect H_2O_2 generated by the glucose oxidase-catalyzed reaction (TIERNEY, JAYALAKSHMI, PARRIS *et al*, 1999). After the solute extraction and measurement phases, mathematical algorithms predict the glucose level in the display. This processing not only uses the biosensor response, but also skin temperature and respiration fluctuations, through thermo transducers and conductivity sensors available in the device (TIERNEY, TAMADA, POTTS et al, 2001).

The system is able to read glucose values every 10 minutes for up to 13 hours. Correlation coefficient between the biosensor and finger-stick measurement is about 0.865, and therefore was approved by the U.S. Food and Drug Administration (FDA) for an auxiliary method, without replacing invasive control. Some disadvantages of this technology are the delay of some minutes compared with blood values, skin irritation, inaccuracies of results, long calibration procedures and a two to three hour warm-up period (PANCHAGULA, PILLAI, NAIR *et al* 2000; PARK, LEE, YOON *et al*, 2005]. Another reverse iontophoresis device available is the GluCall from KMH Company, which requires 70 minutes to warm-up and measures glucose values every 20 minutes for up to 6 hours.

2.5.2 Light absorption spectroscopy

Chapter 4 will describe optical absorptions in more details. When light meets biological tissues it can suffer reflection, scattering and transmission proportional to the structure and chemical components of the sample. The possibility of molecular differentiation is, therefore, the reason why the majority of continuous glycemic monitoring efforts are focused in the optical signature spectrum of glucose.

Many spectroscopic investigations have been done in visible and near infrared (NIR) range, namely around 590 nm – 950 nm (YEH, HANNA and KHALIL, 2003), 1212 nm – 1850 nm (MARUO, TSURUGI, CHIN *et al*, 2003; SCHRADER, MEUER, POPP *et al*, 2005; KASEMSUMRAN, DU, MARUO *et al*, 2006) and 2120 nm – 2380 nm (OLESBERG, LIU, VAN ZEE, *et al*, 2004). Such spectra are chosen since the water absorbance is weak, the measuring signal has high energy and there is a wide number of commercial light transducers available. In addition, these wavelengths are found in the therapeutic window (600 nm to 2500 nm) allowing the use of reflectance for superficial layers analysis and transmittance in deep tissues measurements (WEBSTER, 1997). A recent work describes a technology applied to glucose prediction similar to pulse oximetry (detailed in chapter 4). In order to determine the optimal spectra, a fast spectrophotometer was developed, capable of deriving 100 spectra per second (900 nm to 1700 nm), which allowed the analysis of blood volume pulsations in the finger. In Figure 9, initial correlations between predicted (optical) and reference laboratory assays are illustrated and since the results are in regions A and B, it is acceptable for clinical use (YAMAKOSHI and YAMAKOSHI, 2006).

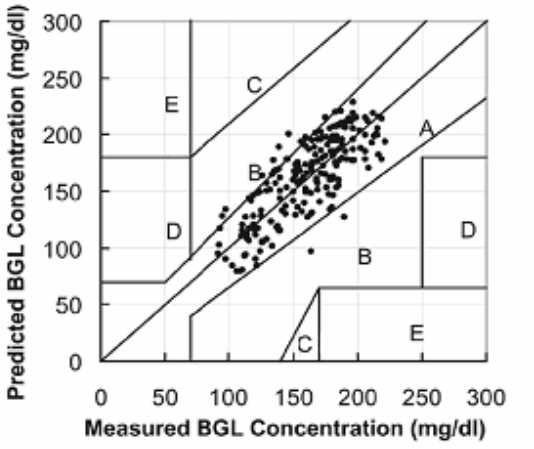

Figure 9 - Comparison of the predicted and measured blood glucose level by error-grid analysis, values in regions A and B are acceptable for clinical use (YAMAKOSHI and YAMAKOSHI, 2006).

On the other hand, the use of middle infrared (MIR) spectra (mostly between 8382 nm and 9708 nm) (MALCHOFF, SHOUKRI, LANDAU *et al*, 2002; MARTIN, MIROV and VENUGOPALAN, 2002; SHEN, DAVIES, LINFIELD *et al*, 2003) gives more distinct glucose peaks. Unfortunaly these spectra have limited light penetration, which exclude their use in transmittance tests. An alternative to increase optic penetration is the measurement with attenuated total reflection (ATR) (HARVEY and MCNEIL, 2006), which uses a light beam guided through a crystal by total reflection and is explained in more detail in chapter 4. If the crystal surface is placed in contact with the skin, the electromagnetic field created by the reflected light reaches the dermis, where the interstitial fluid contains most of the skin's glucose (Thennadil, Rennert, Wenzel *et al*, 2001). Therefore changes in the beam absorption should reflect the optics characteristic of the blood sugar. The use of squalane oil in the crystal interface seems to improve quantitative prediction (TAMURA, FUJITA, KANEKO *et al*, 2004). Table 3 shows a review of optic spectroscopy targets and wavelengths.

Table 3 – Researches in non-invasive glucose documentation by light spectroscopy

Research group - year	Target site	Wavelength (nm)
Cho *et al.* 2004	Finger skin	470 to 950
Baba *et al.* 2003	Eye	532 and 635
Cote *et al.* 1992	Eye	633
Gabriely *et al.*1999	Finger skin	780 to 2500
Saratov *et al.* 2004	Skin	590, 750 and 950
Yeh *et al.* 2003	Forearm skin	590, 660, 890 and 935
Heinemann - *et al.* 1998	Skin	800
Zhao *et al.* 2002	Finger skin	905
Robinson *et al.*1992	Finger skin.	870 to 1300
Fischbacher *et al.*1997	Skin	950 to 1200
tenhunen *et al.*1998	Finger skin	1500 to 1850
Maruo *et al.* 2003	Forearm skin	1600
Kasemsumran *et al.* 2006	Forearm skin	1212 to 1805
Burmeister *et al.*1999	Tongue	1612, 1689 and 1731
Schrader *et al.* 2004	Eye	1859 to 1528 and 1394 to 909
Olesberg *et al.* 2006	Skin	2040 and 2380
Malchoff *et al.* 2002	Tympanic membrane	8500 and 9600
Kajiwara *et al.* 1993	Oral mucosa	3424, 9259 and 9708

In order to compensate the high absorbance by the tissue, some groups have chosen to measure with laser diodes. The SugarTrack (with 650 nm, 880 nm, 940 nm and 1300 nm) or Sensys (750nm-2500nm) are examples of optical equipment for continuous glucose monitoring. Another alternative to improve measurements is occlusion spectroscopy, reported

by the company Orsense. This technique uses a temporary cessation of the tissue blood flow at the finger with the projection of light at 610 nm and 810 nm (COHEN, FINE, MONASHKIN *et al*, 2003).

2.5.3 Photoacoustic spectroscopy

Photoacoustic spectroscopy (PAS) is based on ultrasonic waves created by tissue absorption of pulsating light (WICKRAMASINGHE, YANG and SPENCER, 2004). When laser beams meet cells, heat is generated, causing pressure variations in the sample. These acoustic signals can be detected through a piezoelectric transducer and with the specific incident wavelengths, reflect optical properties of glucose in blood (ALLEN, COX and BEARD, 2005). PAS non-invasive glycemic monitoring devices, like the Aprise from the Glucon company, are already available in the market (GLUCON, 2006). Although this method was shown to correlate with blood sugar levels, it is still necessary to improve the reproducibility and sensitivity in order to decrease interferences from other substances.

2.5.4 Polarimetry

The linear polarization vector of light can be rotated by the path characteristics such as thickness, temperature and concentrations of the crossed sample. Therefore polarimetry has been used for a long time in pharmaceutical and nutritional industries to measure the level of compounds including glucose. Many studies are trying to apply this technique in non-invasive glycemic assays. However, skin is not the optimal target, since high scattering coefficients produce complete depolarization of the beam. Therefore, most investigators focus their attention on the aqueous humor of the eye, which offers a clear optical medium with a reasonable path length and has a lag time of no more than 5 minutes in relation to blood glucose concentrations (CAMERON, BABA and COTÉ, 2004). The average width of the anterior chamber of a human eye is 1 cm, which gives an expected rotation of 4.562 milli degrees for a normal glucose level (5.55 mmol/L) at a wavelength of 633 nm (COTE, 2001).

There are two possible optical paths for polarimetric tests in the eye, as shown in Figure 10. The first uses transmittance configuration where the polarized light passes laterally through the cornea (MCNICHOLS and COTÉ, 2000). In the second approach, the incident beam on the cornea travels into the eyeball, reflecting on the retina, and returning with information on glucose concentration in the aqueous humor (JANG and FOX, 1997).

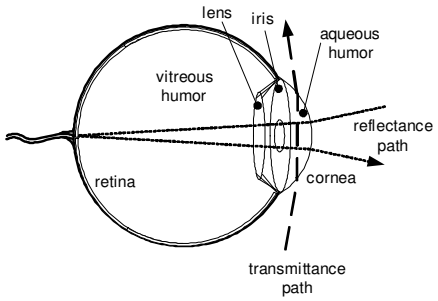

Figure 10 - Transmittance and reflectance optical paths for polarimetric tests in the eye.

Although polarimetry methods suffer negligible influence from temperature and pH drifts, it is still necessary to address these problems in order to successfully quantify concentrations *in vivo* (BABA, CAMERON, THERU et al, 2002). Limitations include safety regulations on light exposure to the eye, motion artifacts, optical noises of other substances and the development of techniques to measure small angles. Recent studies used a Faraday rotator with a single-mode flint glass fibre to improve optic sensitivity of the system, which showed a resolution of 9.9 mg/dL for glucose (YOKOTA, SATO, YYAMAGUCHI *et al*, 2004). Finally, a modified intraocular lens and a liquid-crystal polarization modulator driven by a sinusoidal signal were also proposed to allow *in vivo* measurements of the human eye (RAWER, STORK and KREINER, 2004; LO and YU, 2006).

2.5.5 Fluorescence

It is known that glucose levels in tears reflect concentrations similar to those in blood, therefore, fluorescence is also a sensing technology for painless monitoring (PICKUP, HUSSAIN, EVANS *et al*, 2005). This system can track blood glucose with an approximate 30 minutes lag time and does not suffer interference from fluctuations in the light intensity of the

ambient surrounding. The photonic sensing is done with polymerized crystalline colloidal arrays which respond to different concentrations through diffraction of visible light (KHALIL, 2004).

The sensor is comprised of disposable colorless contact lenses, which require excitation and detection devices. Figure 11 shows recent results of in-vivo assays with these transparent lenses excited in 488 nm. Although the results correlate with control glucose levels, long-term studies addressing confort and toxicity still need to be performed (MARCH, LAZZARO, RASTOGI, 2006). Some of the equipment could be discarded by using colored contact lenses. By changing color in response to the concentration of glucose in the tears, patients could look into a mirror and compare the sensor color to a precalibrated color strip (BADUGU, LAKOWICZ and GEDDES, 2005). Some limitations still need to be solved in colorimetric assays, such as resolution, short lifetimes and biocompatibility (MOSCHOU, SHARMA, DEO *et al*, 2004).

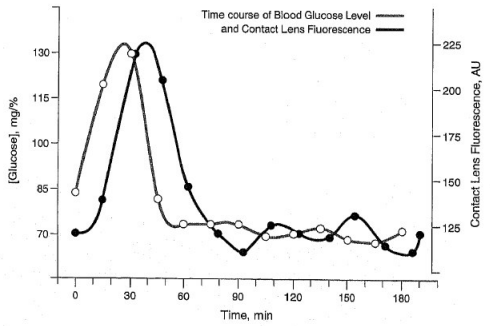

Figure 11 - In-vivo contact lenses data versus standard invasive glucose level control (MARCH, LAZZARO, RASTOGI, 2006).

2.5.6 Raman spectroscopy

The process where a small fraction of scattered light shows wavelengths different from that of the exciting beam is known as the Raman effect. This type of spectroscopy uses laser radiation sources from visible to the MIR range (5 μm to 40 μm) and measures very weak signals in the transparent samples. The measured photons normally have higher wavelengths and lower intensities (10^{-3} times) than the original light, therefore requiring longer collection periods than other optical methods (ELLIS and GOODACRE 2006). Water

has weak scattering indexes, which is the reason why Raman assays are not affected by interference from this substance. Another advantage is that the resulting bands are narrow and have distinct peaks, easing the task of separating signals, in contrast to absorption spectroscopy (BERGER, ITZKAN and FELD, 1997). A recent study reports measurements of glucose in aqueous humor with a 785 nm laser source. An optical fiber was used to focus the beam on the anterior chamber of porcine eyes and also to receive the resulting spectrum. Results suggest that Raman signals from glucose in MIR range can be detectable with this system, nevertheless one should still analyse photothermal damage danger in non-invasive ocular measurements (ERGIN, and THOMAS, 2005).

2.5.7 Metabolic heat conformation

The metabolic heat conformation (MHC) method involves measurements of physiologic indices related to thermal generation, blood flow rate, hemoglobin, and oxyhemoglobin concentrations, all of which should correspond to the glucose levels in the blood (CHO, KIM, MITSUMAKI *et al*, 2004). The first tests used three different temperature measurements (surface finger, ambient room, and background radiation) derived from the fingertip during 10 seconds. In addition, multiwavelength spectroscopy with six wavelengths (470 nm, 535 nm, 660 nm, 810 nm, 880 nm, and 950 nm) was performed, helping to improve glucose signals, as illustrated in Figure 12 (a). The MHC prototype, shown in Figure 12 (b) has a correlation coefficient of 0.91 in laboratory conditions, but the company Hitachi intends to improve its performance in order to obtain sale approval (KO, CHO, KIM et al, 2004).

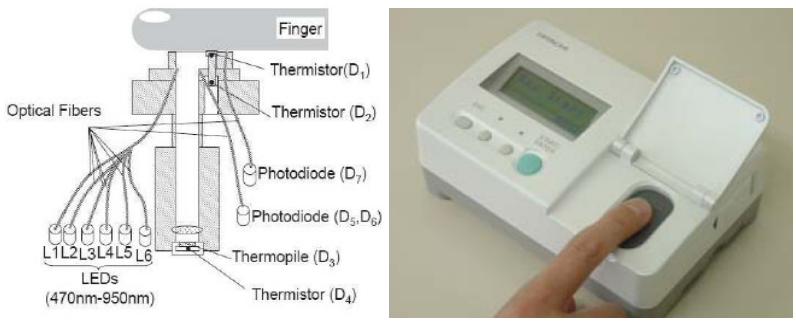

(a) (b)

Figure 12 - Metabolic heat conformation blood sugar monitoring device from Hitachi (KO, CHO, KIM et al, 2004).

2.5.8 Thermal emission spectroscopy

Thermal emission spectroscopy measures IR signals generated in the human body as a result of glucose concentration changes. One promising application of this technology uses a similar concept used in standard clinical tympanic membrane thermometers, with the addition of specific wavelengths for glucose fingerprint (9.8 µm and 10.9 µm). This membrane information is important, because it shares the blood supply with the center of temperature regulation in the hypothalamus. In addition, signals from blood vessels in this organ have to cross a smaller path length than in skin or oral mucosa sites. A prototype was calibrated and tested in patients demonstrating reproducibility and predicting glucose concentrations with a mean error of 12 mg/dL (MALCHOFF, SHOUKRI, LANDAU *et al*, 2002).

2.5.9 Bioimpedance spectroscopy

A detailed description of the impedance mechanisms and techniques will be provided in Chapter 3. Bioimpedance basicly consists of measuring the electrical properties of biological tissues of the whole organism. The first study of a non-invasive continuous glucose monitoring system involving impedance spectroscopy was published by Caduff's group in 2003, as illustrated in Figure 13. As a result of this research, the company Pendragon developed a wrist glucose monitor called Pendra. The equipment gathers information of an LC resonance circuit from 1 MHz until 200 MHz, with the skin working as the dielectric from the capacitor. One limitation of this research is that it requires an equilibration process, where the patient must rest 60 minutes before starting measurements (CADUFF, HIRT, FELDMAN *et al*, 2003).

Pendra was approved in May 2003 in the Conformité Européenne (CE) and for a short time it was available on the market for approximately 3000 €. A post-marketing reliability study showed a difference of 52% (4.3% of the readings in the dangerous zone E from Clarke error grid) when compared with a blood capillary glucometer (WENTHOLT, HOEKSTRA and ZWART, 2005). Therefore, this equipment is suitable only for a small group of patients, whose local dielectric skin characteristics show a minimum resonance frequency (PFÜTZNER, CADUFF, LARBIG *et al* 2004). In 2005 Pendragon was closed, but Caduff's

impedance work has still been investigated through the company Solianis Monitoring (CADUFF, DEWARRAT, TALARY *et al*, 2006).

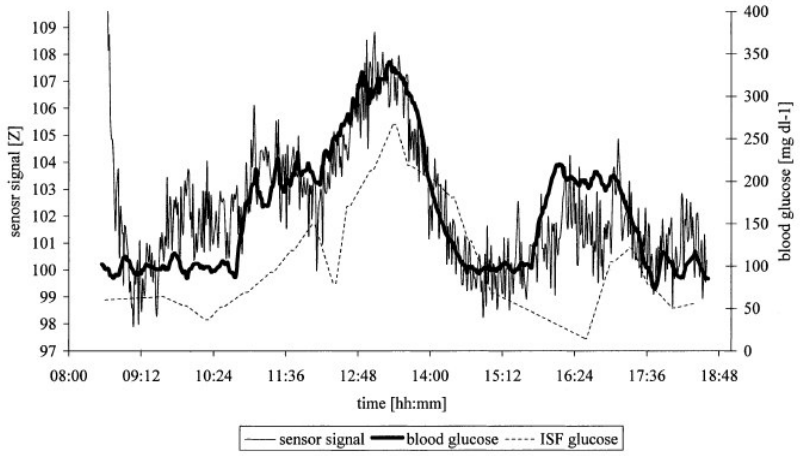

Figure 13 – Impedance sensor signal compared to blood glucose and interstitial fluid glucose levels during glucose clamps with glucose administered intravenously. ISF glucose levels measured by means of the CMA-60 microdialysis, blood glucose continuously measured by the Biostator (CADUFF, HIRT, FELDMAN *et al*, 2003).

2.5.10 Ultrasound based assays

Reverse iontophoresis is not the only method to extract non-invasive glucose molecules from skin. Sonophoresis, which usually enhances transdermal delivery of drugs, can also serve this purpose (KOST, MITRAGOTRI, GABBAY *et al*, 2000). This technique uses a piezoelectric transducer to create 20 kHz ultrasound (US) which increases cutaneous permittivity to interstitial fluid, enabling glucose transport to the epidermis surface. Analyte concentrations can therefore be determined with standard electrochemical glucose sensors. Initial *in vivo* laboratory results have been described predicting glycemic values in rat skins through US (LEE, NAYAK, DODDS *et al*, 2005).

2.5.11 Electromagnetic based assays

Electromagnetic sensors based on eddy currents have been able to detect variation of the dielectric parameters of the blood, which can also be caused by glucose concentration

changes (ALAVI, GOURZI, ROUANE *et al*, 2001). Conductivity detection of blood inside a plastic tube was possible at a resonant frequency of 2.664 MHz in static and moving samples, showing a glycemic sensitivity of 80 mg/dL (GOURZI, ROUANE, GUELAZ *et al*, 2005). Studies from Öz group also described magnetic glucose assays. This work reported that even localized nuclear magnetic resonance (NMR) performed well in detecting glycogen metabolism in the human brain (OZ, HENRY, SEAQUIST *et al*, 2003).

CHAPTER 3

IMPEDANCE SPECTROSCOPY

3.1 INTRODUCTION

Although impedanciometry is relatively simple method, there are many possibilities for application. These include the analysis of materials, detecting of failures in structures, controlling the product to validation, and especially obtaining of physiological parameters in medicine.

In pure metals, the current value comes from the electrons movement and in solutions like acid, bases and salts, the electrical charge's transport is done through free ions. However, in such substances, factors like temperature and concentration can influence the ionic dissociation quantity, changing its conductor properties (HUANG, CHENG, PENG *et al*, 2000). The current in organisms is mostly ionic for both inside and outside the cells (GEDDES and BAKER, 1989). One can call bioimpedance the opposition that biological tissues present for the electricity. Applying a direct current in these solutions, there will be a polarisation effect, where an ionic layer is formed in which electrode, impeding the current flow. Therefore, only alternating current (AC) can be used in bioimpedanciometry (GRIMNES and MARTINSEN, 2000). Although studies with electric impulses have been already realized (NEVES, LEITE and SOUZA, 2000), sinus waves are still mostly used in this type of measurement, since it is easy to create and treat these waves.

Besides the signal characteristics, other factors can also influence this technique. The organism has tissues with different substances, compositions and shapes, resulting in different resistivities for each organ. While muscles and blood are good conductors, skin, fat and bones act mostly as isolators (N. I. H., 1994; LIEDTKE, 1997). Due these properties, one possible application of bioimpedance is tissue characterisation. However, even in isolated tissues, the electric characteristics can change with electrode position because different shapes of cells change the current density (GRIMNES and MARTINSEN, 2000). In Figure 14, in the same organ, there is a lower resistance between electrodes 3 and 4 than between electrodes 1 and 2.

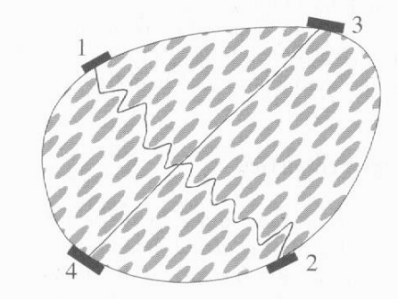

Figure 14 – Asymmetric measurement with bioimpedance, there is a lower resistance between electrodes 3 and 4 than between electrodes 1 and 2 (GRIMNES and MARTINSEN, 2000).

This section shows the basic principles of complex impedance, describing sensors and measurement techniques. Finally, concepts involving patient safety and applications are described.

3.2 HISTORICAL BACKGROUND

Electrical impedance has been studied in medical applications for a long time. Grimnes and Martinsen reviewed some important research: in 1911 Hoeber discovered the current dispersion β, which corresponds to the electric comportment of tissues in medium frequencies. In 1930 this dispersion was explained by Fricke, Cole and Curtis. Nyober introduced in 1940 the blood resistivity definition (Ω.m). The dispersion α (low frequency analyze) was studied by Schwan in 1957. The relation between bioimpedance and Total Body Water was discovered in 1962 by Thomasset (GEDDES and BAKER, 1989). In 1966 Kubicek developed a study with NASA astronauts to create the first cardiac monitor applied in medicine with bioimpedance (N. I. H., 1994). The idea of tissue imaging was introduced by Pullen in 1970. The first image was realized in 1978 by Henderson with 144 electrodes. Barber and Brown realized the first *in vivo* impedance image test in 1983 and simultanesly applied the principle of volumetric electrical resistivity of Kubicek to measure the total body water. In 1985 Sramek, Bernsein and Quail developed a method to measure cardiac debit through impedance. Improvements in the cardiac impedance analysis were made in 1986 by Bernstein, allowing to determine the stroke volume, cardiac output, systemic vascular resistance (SVR) and left cardiac work (LCW).

3.3 PHYSICAL PRINCIPLES

Electrical resistance is the opposition to the current flow, which depends on the dimensions and resistivity (ρ) of the object, as seen in Equation 1.

$$R = \frac{\rho L}{A} \tag{1}$$

where:

- R is the component resistance, Ω (Ohm);
- A is the cross-sectional area, m^2 (square metres);
- ρ is the resistivity, Ω.m (Ohm metres);
- L is the length of the object, m (metres).

Elements that are purely resistive do not accumulate energy and therefore have a constant resistance independent of the applied signal frequency. However, in inductors and capacitors, there is an opposition to the electrical current called reactance, whose intensity varies with the signal frequency, shown in Equation 2 and Equation 3.

$$Xc = \frac{1}{2\pi f C} \tag{2}$$

where:

- Xc is the capacitive reactance, Ω (Ohm);
- f is the frequency, Hz (Hertz);
- C is the capacitance, F (Farad).

$$Xl = 2\pi f L \tag{3}$$

where:

- Xl is the inductive reactance, Ω (Ohm);
- f is the frequency, Hz (Hertz);
- L is the inductance, H (Henry).

The complex result of resistive and reactive vectors is called impedance (*Z*), where the resistive component (*R*) is located in the real axis and its reactive components (*Xc* ou *Xl*) in the imaginary axis. The modulus (|*Z*|) and phase (θ) of the impedance in Figure 15 can be calculated through Equations 4 and 5.

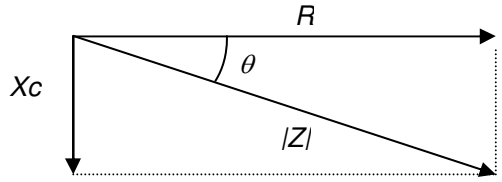

Figure 15 – Example of impedance in its rectangular and polar modes.

$$|Z|^2 = R^2 + Xc^2 \tag{4}$$

$$\tan(\theta) = \frac{Xc}{R} \tag{5}$$

where:

- |*Z*| is the impedance modulus, Ω (Ohm);
- *Xc* is the capacitive reactance, Ω (Ohm);
- *R* is the resistance, Ω (Ohm);
- θ is the phase angle, ^{o} (Degree).

The Ohm law defines impedance as the result of the division between the measured voltage and the applied current, as seen in Equation 6.

$$V = ZI \tag{6}$$

where:

- *V* is the voltage, V (Volt);
- *Z* is the impedance, Ω (Ohm);
- *I* is the electric current, A (Ampère).

3.4 TRANSDUCERS

Bioimpedance sensors are basically electrodes, which, in contrast with most of the transductors, are not affected significantly by pressure and temperature variations.Due to its reduced size, these devices do not interfere in the physiological events, reason why bioimpedance has been widely accepted in the medical community.

It is desirable to use materials with constant characteristics in a large frequency spectrum. The Silver-Silver Chloride electrode (Ag/AgCl) is commonly used in our days. This component with a diameter of 1.5 cm has approximately 200 Ω in 30 Hz, and after 10 kHz this value decreases to 150 Ω (WEBSTER, 1998). Other materials which can also be used to contact with the skin are aluminium and steel. An electrode with this composition and area of 0,94 cm^2 in 1 kHz offers a resistance of 37 Ω in serie with a capacitance of 4 μF (TORRENTS and PALLÀS-ARENY, 2002). Platinum electrodes (Pt) are commonly used as well in chemometric assays, but low frequency utilization should be avoided due to highly polarizable characteristics (BRONZINO, 2000).

The cable that connects the electrode with the measurement circuit is also observed. In high frequencies it is important to use coaxial cables in order to reduce eventual noises. Another component that should be chosen carefully is the gel used to improve the signal propagation in the epithelial surface. This occurs because the electrolytes fill empty spaces between the electrode surface and the tissue, therefore decreasing the electrode-skin impedance. Hydrogels (gels with a higher concentration of water) cause higher variations of impedance as gels with higher density (MC ADAMS, JOSSINET, LACKERMERMAIER *et al*, 1993).

3.5 MEASUREMENT

BIA measurements normally use either two electrodes (bipolar) or four electrodes (tetrapolar). With two electrodes, the current carrying electrodes and signal pick-up electrodes are the same. In this case, the contact interface of the electrode with the skin can have a parasite resistance that causes errors in the read impedance. The lower the measurement frequency, the higher is the value of such error (TORRENTS and PALLÀS-ARENY, 2002). This additional impedance depends upon the contact area in the electrode, the type of material

used as the dielectric, hair concentration and skin moisture (OLDHAM, 1996). In 1884 Bouty introduced the method of measurement with four electrodes shown in Figure 16.

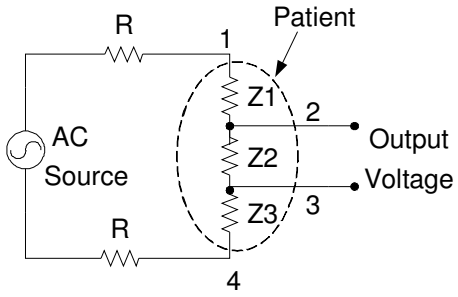

Figure 16– Tetrapolar measurement method, which can eliminate most part of patient-electrode errors (GEDDES and BAKER, 1989).

Thetrapolar measurement is the most commonly technique because most of the errors from patient-electrode impedance is eliminated. The constant current is applied in the person through electrodes 1 and 4. The output voltage, which depends on the corporal impedance, is read in electrodes 2 and 3. The greater the distance between these reading electrodes, the more uniform is the current in the tissue (GEDDES and BAKER, 1989).

The majority of the available impedance devices have some common blocks, seen in Figure 17. The excitation circuit normally uses an oscillator, which can be analog, or a Direct-Digital Synthesizer (DDS), and a current source, to avoid harming the patient. The signal acquisition is made through amplifiers (differential and instrumentation types) with high input impedance and fast response. In case of analog impedance measurement, a voltmeter block is required, which can have different levels of complexity, depending on the signal frequency and amplitude. The resulting signal is then digitalized by A/D converters, which allow the application of algorithms and digital filters. The central processing unit (CPU) interprets the results, controls computer interfaces, reads keyboard commands and shows the results in graphic displays. In order to measure a wide spectrum of frequencies, the circuits should have variable oscillators, amplifiers with fast response and wide bandwidth, A/D converters with high sample rate and short processing time.

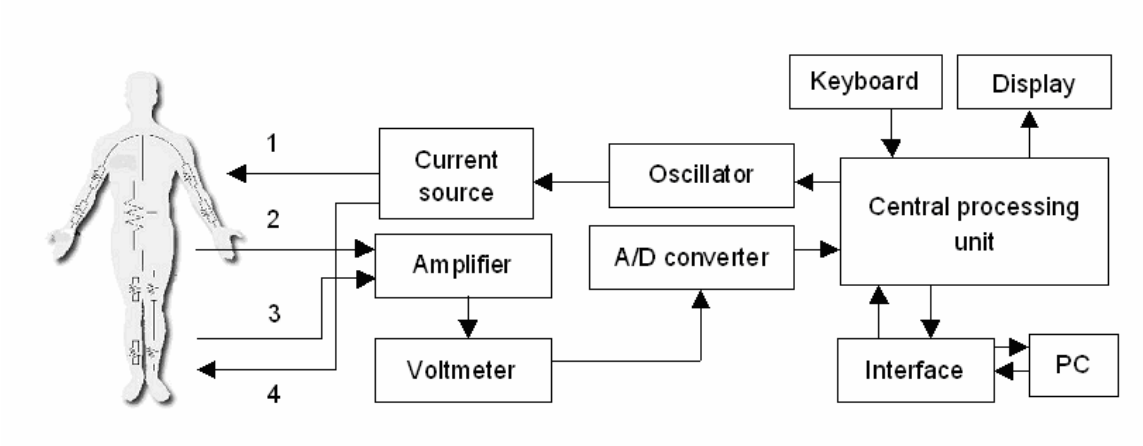

Figure 17 - Basic block diagram of a tetrapolar impedance circuit, if contact 1 is connected to 2, and 3 to 4, it is possible to have a bipolar measurement.

3.6 SPECTRAL ANALYSIS

Tissues are composed of many similar cells covered with an electrolytic fluid. Each cell can be defined as a variety of structures responsible for metabolism, reproduction and maintenance, revested by a membrane. This membrane, whose thickness is about 7 nm, is composed of lipids with isolating characteristics and proteins, responsible for the transport of water, ions and others chemical substances that cross its structure by osmosis (GEDDES and BAKER, 1989). The electric comportment from the cellular membrane is equivalent to a capacitor, which is mostly around 20 $\mu F/cm^2$. In all organs the resistive and capacitive components are higher as the inductive component and therefore it is not considered (GRIMNES and MARTINSEN, 2000).

Cells present high capacitance reactance for low frequency currents (until 5 kHz). In cases where higher frequencies are applied, this parameter decreases, and in 1 MHz the current crosses the whole cytoplasm (GRIMNES and MARTINSEN, 2000). Tissues also have similar comportment to the cells. In high frequencies current can cross the cellular membrane, flowing through both extra cellular and intra cellular fluids. Therefore in lower frequencies, tissues with greater cellular density will show higher impedance than tissues with more of extracellular fluid. Figure 18 shows a graph of the impedance modulus variation with frequency for biological tissues (THOMASSET, 1997).

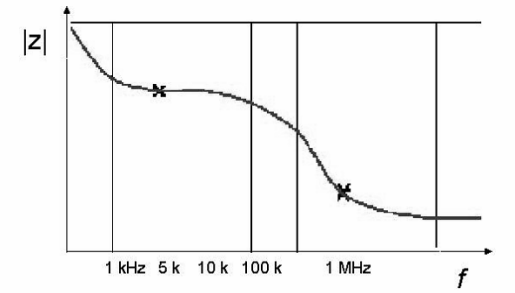

Figure 18 – Impedance modulus of biological tissue with the frequency (THOMASSET, 1997).

The permissibility comportment of a biological tissue depending on the frequency of the crossing signal is called dispersion. There are three fundamental types: α, β and γ (BLAD and BALDETORP, 1996). The dispersion α happens in low frequencies and is due to the diffusion phenomenon of free ions outside the cells. The dispersion β, also called structural relationship, comes from the charge and discharge of the cellular membrane capacitance through intra and extra-cellular liquids. This type of dispersion is found in the frequencies from 100 kHz until 30 MHz. The dispersion γ is caused by the bipolar relationship of the free water molecules in the medium. It occurs in the range from 10 GHz until 100 GHz (LÓPEZ, MADRID and FELICE, 2001).

Figure 19 illustrates the electric current in tissues: for low frequencies (LF) the ions flow outside the cells, in high frequencies (HF), the signal crosses both intra-cellular fluid (ICF) and extra-cellular fluid (ECF). Figure 20 represents one equivalent circuit for the tissue comportment with frequencies. The value of the resistance *Ro* corresponds to the extra-cellular fluid and the value *Rp* to the intra-cellular fluid. For low frequencies the total impedance is only given by *Ro*. In high frequencies, over 1 MHz, the capacitor *Cp* decreases its reactance and the total impedance can be calculated by the parallel between *Rp* and *Ro* (THOMASSET, 1997).

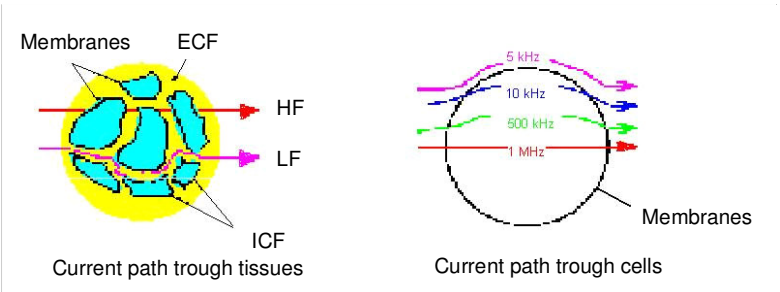

Figure 19 – Tissue currents for low and high frequencies (THOMASSET, 1997).

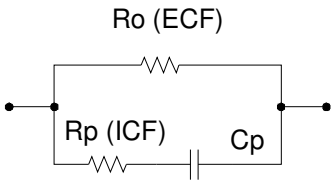

Figure 20 – Tissue equivalent circuit.

The relationship between the total impedance in high frequencies (Z_{1MHz}) and the resistances *Ro* and *Rp* is shown in the Equation 7.

$$\frac{1}{Z_{1MHz}} = \frac{1}{R_o} + \frac{1}{R_p} \tag{7}$$

where:

- Z_{1MHz} is the impedance in high frequencies, Ω (Ohm);
- R_o is the extra-cellular resistance, Ω (Ohm);
- *Rp* is the intra-cellular resistance, Ω (Ohm).

The characteristic frequency is the value where the impedance presents the maximum capacitive reactance value, shown for the circuit above in Equation 8.

$$fc = \frac{1}{2\pi Cp(Ro + Rp)} \tag{8}$$

where:

- *fc* is the characteristic frequency, Hz (Hertz);
- R_o is the extra-cellular resistance, Ω (Ohm);
- *Rp* is the intra-cellular resistance, Ω (Ohm);
- *Cp* is the typical capacitance for each tissue, F (Farad).

In the majority of tissues the characteristic frequency is found between 10 kHz and 200 kHz, while for blood this value is around 2 and 3 MHz (BLAD and BALDETORP, 1996). Table 4 shows characteristic frequencies measured in swines. Tissues with high water concentration, like tumors, also show high characteristic frequencies (ORSYPKA and GERSING, 1995).

Table 4 – Characteristic frequency in swines (CINCA, WARREN, RODRÍGUEZ-SINOVAS *et al*, 1998).

Organ	Chracteristic frequency (kHz)
Liver	0.39
Pancreas	123
Lung	0.46
Musses	0.2
Blood	2020

Cole represented the resistive *R* and capacitive *Xc* comportment of tissue impedance with the frequency. In the ideal circuit of Figure 21 (a), the impedance changes with frequency as shown in curve |*Z*| with extremities always in the axis origin. The curve drawn by the modulus is centered in ((*Ro – Ro//Rp*)/2 + *Ro//Rp)*. For a DC signal the impedance would have value *Ro*. With the frequency, increasing this parameter decreases anti-clockwise until it reaches *Ro//Rp*. When measuring biological tissues, the circumference centre is found under the resistance axis, as illustrated in Figure 21 (b). The value of α is empiric, and should therefore be chosen in order to match both graphs (GEDDES and BAKER, 1929).

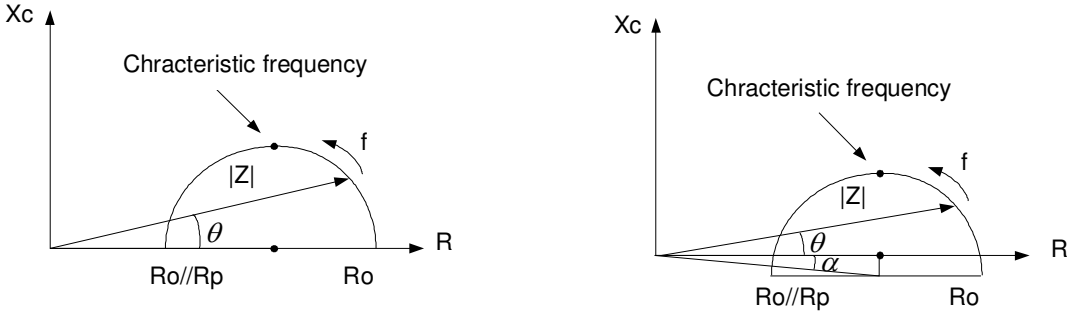

(a) (b)

Figure 21 – Teoretical (a) and real (b) Cole–Cole graph.

One important data in the Cole graph is the phase angle (θ), which in theory can change between 0^o and 90^o and in most people is found between 3^o to 10^o. For medium frequencies, a small θ means a decrease in the capacitive reactance, corresponding to cellular death. A high phase angle means an increase in the capacitance, which means that there is a great number of cellular membranes (RIGAUD, HAMZAOUI, CHAVEUAU *et al*, 1994). Each tissue has one specific curve in the Cole diagram, and the sum of different organs results in a typical graph for total body impedance as shown in Figure 22 from 10 kHz until 800 kHz. The muscles impedance is responsible for most of the measured values (THOMAS, WAR and CORNISH, 1998).

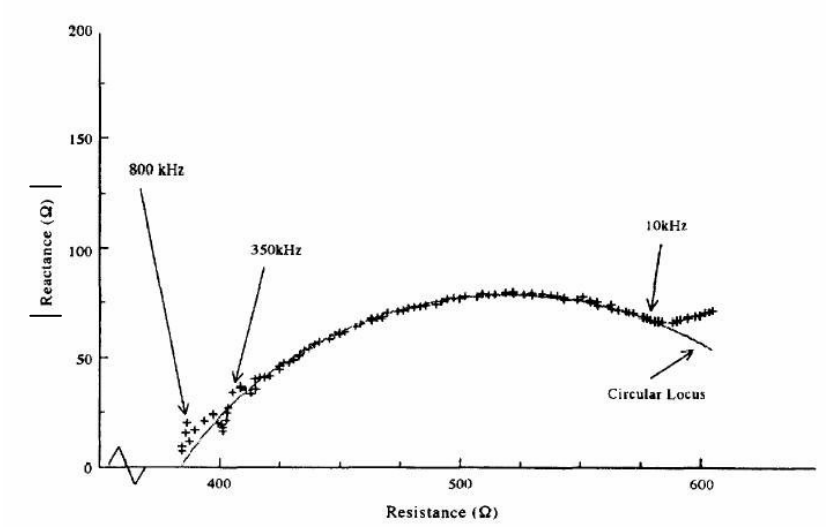

Figure 22 – Total body impedance measured by tetrapolar configuration measured between the right hand and left foot (THOMAS, WARD and CORNISH, 1998).

3.7 SAFETY

Because the impedanciometry measures the voltage created by applying an external current in the body, special care should be taken in order to avoid physical harm to the measured person. The current value should be small enough to be undetectable by the patient, not stimulate nerves and muscles and induce warming in tissues. If someone with wet skin holds conductors in each hand, an alternated current of only 0.5 mA already can be noted. For constant currents, those values are from 2 to 10 mA. In some cases a current of only 6 mA is able to excite muscle tissues. However, the magnitude of current used in impedanciometry should be higher than biological noises as mioelectric signals or interference of equipments in

hospital, such as heaters, infrared lamps or motors. In order to decrease disturbances caused by bioelectric signals, between 10 and 100 Hz, frequencies over 1 kHz are adopted. The smaller the wave length, the higher the current intensity that can be used. Figure 23 represents the limit current (let-go) that one person can support without exciting muscles. This value tends to be stable in the region with higher sensibility and outside of these limits increases quickly (WEBSTER, 1998). The diameter of the electrode is another important factor, the smaller the area of the electrode, the fewer parasite capacitances will result, but the pain limit is also reduced.

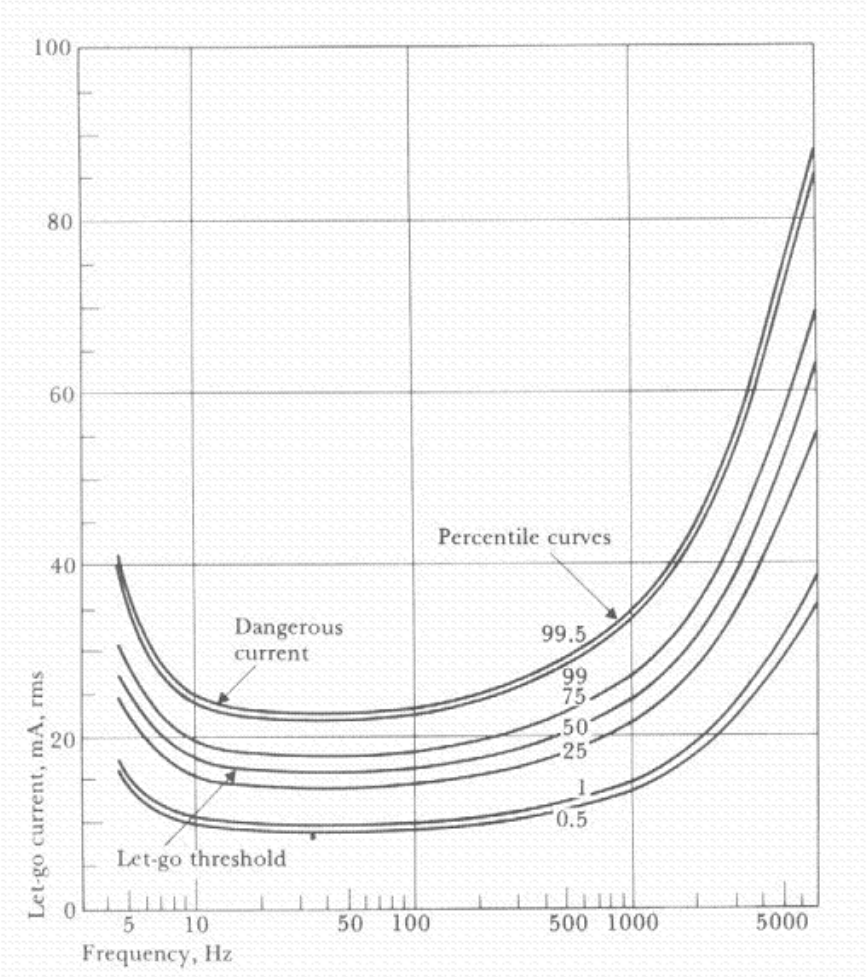

Figure 23 – Let-go current versus frequency, with higher values for up 1 kHz (WEBSTER, 1998).

The American Health Institute suggests a current maximum value of 800 μA to be used in impedanciometry, with a frequency of 50 kHz (N. I. H., 1994). In practice, one uses currents around 50 μA, for frequencies under 1 kHz. Over 100 kHz it is possible to use

currents in miliamperes. Special attention is also required for the measurement voltage, Boone and Holder suggest values between 25 μV and 160 mV (GRIMNES and MARTINSEN, 2000). The placement of the electrodes influences the decision of electric values as well. When the current crosses the body, it can flow through muscles, bones, nerves, glands, organs and corporal fluids. Some of these elements, such as vocal chords, can be easily damaged by only a few miliamperes of current. Therefore in more sensitive regions one should reduce the maximum intensity of applied signals.

One option to decrease the chance of stimulating a patient is the use of short duration waves. The higher the time of applied signal, the lower the current that can be applied (WEBSTER, 1998). In organisms, the most excitable nervous fibers require a minimum duration of 0.2 ms. Therefore, the use of current pulses in impedanciometry should have frequencies higher than 5 kHz.

Another necessary procedure to prevent the compromise of the health of patients is to replace the electric network alimentation by low tension batteries, thus avoiding electric shocks in case of system failure. For people with implanted pacemakers bioimpedance measurements are not recommended because the BIA current can affect the functionality of the equipment.

3.8 APPLICATIONS

When changes in dimensions or conductivity of the organism happens, it is possible to monitor the many physiological events through BIA. Because this technique does not require any special transductor, but only electrodes, it is possible to non-invasively detect blood flow, cardiac activity, respiratory frequency, renal volume, bladder state, uterus contractions, nervous activity, arterial pressure and salivation. Therefore this method can be found in areas like cardiology, anaesthesia, surgery, emergency rooms, obstetrics, genecology and internal medicine. Although the modulus $|Z|$ is mostly analyzed alone in physiological events, sometimes others components (Xc, R and θ) can present important alterations (GEDDES and BAKER, 1989).

It is known that in some disorders, changes in electric parameters from organisms happens before appearing as clinical and organic symptoms. Therefore, a possible application of this method is the detection of pathological agents even in the incubation period, which could help the prevention and treatment of diseases (REN, WANG, AN *et al*, 1998).

The impedanciometry is a fast technique to measure the erythrocytes in blood, this is possible because the red cell impedance is almost 9 times greater than plasma. The coagulation time is also a parameter that can be monitored by BIA, because clotting changes the plasma quantity and therefore its electrical conductivity. Finally, it is also possible to determine the volume of solid cells in blood by such technology, with only the patient immersing his finger in a prepared solution (ÜLGEN and SEZDI, 1998).

When electrodes are positioned in the thoracic area, values reflecting cardiac activities are easily obtained, since blood impedance decreases with the increase of the circulation speed. Respiratory frequency can also be modulated by cardiac impedance signals, this approach is widely used especially in neonatal ICU, where premature children are monitored to avoid apnea or heart infarct (HUANG, HONG, CHENG *et al,* 1998).

The utilisation of BIA for image measurement and has the advantage of not harming the organism, in opposition to X rays whose excess use can cause cellular modification. The visualisation of impedance distribution inside the human body is done through a conductivity matrix. In order to map one region, one should connect the sensors around the local of interest (BAYOD, HERMANT and FARGES, 1999).

One common application of bioelectric impedance is the determination of total body water (TBW) in its distribution both intra and extracellular, which helps the determination of the fat-free mass (FFM) or lean mass (LM) and the total boy fat (TBF), requiring only the age, size and sex of the patient (GRIMNES and MARTINSEN, 2000).

CHAPTER 4

LIGHT ABSORPTION SPECTROSCOPY

4.1 INTRODUCTION

Spectroscopy measurement can be done basically through absorption, scattering and emission approaches. Scattering spectroscopy, such as Raman spectroscopy, measures physical electromagnetic properties by analyzing the amount of light that a substance scatters at certain wavelengths, incident angles, and polarization angles. Emission spectroscopy reads light spectra radiated by the substance, whose energy can result from sources, such as temperatures or chemical reactions. Absorption spectroscopy quantifies the concentrations of substances through the detection of transmitted or reflected photons, which have the same wavelength as the incident beam. In this chapter only absorption effect is described since all assays were done based on this phenomenon.

4.2 HISTORICAL BACKGROUND

Optical methods are among the oldest and best-established techniques for measuring biochemical analytes and are at the core of medical and biological research. The microscope, created in the 16^{th} century, represents the first technology in medical light spectroscopy. Isaac Newton's publication in 1704 unleashed the scientific pursuit of today's science of spectroscopy. Carl Scheele formulated the concept of radiant heat in 1777 (GÜNZLER and GREMLICH, 2002).

In the year 1800, Sir William Herschel discovered the existence of infrared radiation. The first IR spectrometer was constructed by Melloni in 1850. The second major event of importance to medical image was the discovery of X-rays by Wilhelm Röntgen in 1895. Another important step t is the discovery of Raman scattering in 1928 by Chandrasekhara Venkata Raman. In addition, research like the mathematic study of Fourier to process spectra, the development of interferometry by Michelson and the invention of the laser by Schawlow and Townes in 1960 had great relevance to biomedical optics (JACKSON, 2004).

4.3 PHYSICAL PRINCIPLES

The Beer-Lambert Law describes the attenuation of incident light (I_0) crossing a material with absorbing properties, as seen in Figure 24. When an incident beam (I_0) enters the sample, the intensity of transmitted light (I) decreases exponentially as shown in Equation 3.

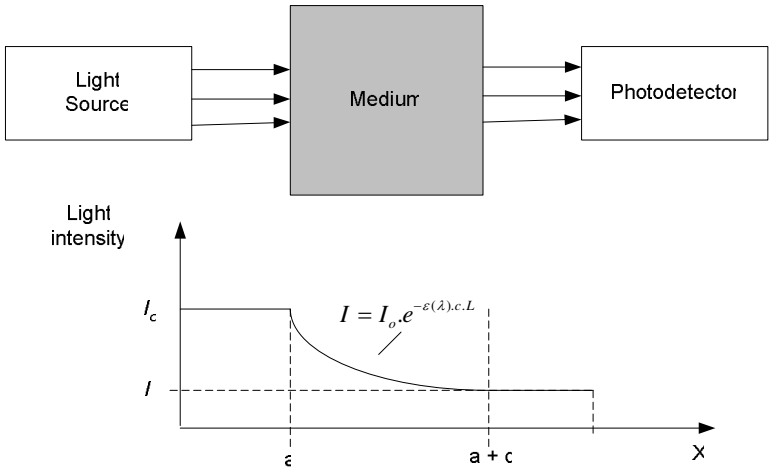

Figure 24 - Beer-Lambert Law, relationship that relates the absorption of light to the properties of the material penetrated (WEBSTER, 1997).

$$I = I_o.e^{-\varepsilon(\lambda).c.L} \tag{9}$$

where:

- I is the intensity of transmission light;
- I_0 is the intensity of incident light;
- ε is the absorptivity (extinction coefficient) of the substance at a specific wavelength, mol^{-1} cm^{-1} (1/mol centimetres);
- c is the concentration of absorbent, mol (mol);
- L is the optical path length in the medium, cm (centimetres).

The transmittance (T) of light crossing a medium with an absorbance substance is the ratio of transmitted light (I) to the incident light (I_0), and absorbance is the negative natural logarithm of the transmittance, as shown in Equation 10 (HOF, 2003).

$$A = -\ln T = -\ln \frac{I}{I_o} = -\varepsilon(\lambda)cL \tag{10}$$

where:

- A is the absorbance, AU (absorbance unit);
- T is the transmittance, no units;
- I is the intensity of transmission light;
- I_0 is the intensity of incident light;
- ε is the absorptivity (extinction coefficient) of the substance at a specific wavelength, mol^{-1} cm^{-1} (1/mol centimetres);
- c is the concentration of absorbent, mol (mol);
- L is the optical path length in the medium, cm (centimetres).

Even if more than one substance absorbs light in a medium, the Beer-Lambert Law is still valid (Equation 11).

$$At = \varepsilon_1(\lambda)c_1L_1 + \varepsilon_2(\lambda)c_2L_2 + ... + \varepsilon_n(\lambda)c_nL_n \tag{11}$$

where:

- A is the absorbance, AU (absorbance unit);
- ε is the absorptivity (extinction coefficient) of the substance at a specific wavelength, mol^{-1} cm^{-1} (1/mol centimetres);
- c is the concentration of absorbent, mol (mol);
- L is the optical path length in the medium, cm (centimetres).

4.4 TRANSDUCERS

Instrumentation for optical measurements generally consists of light sources, optical components to generate a light beam with specific characteristics and to direct this light to some modulating agent, and photodetectors for processing the optical signal (MENDELSON, 1995).

There are many possible light sources available, such as highly coherent gas semiconductor diode lasers, broad spectral band incandescent lamps, and light-emitting diodes (LEDs). The advantages of LEDs are the small size, selective wavelengths, low cost and energy consumption. On the other hand, tungsten lamps provide a broader range of wavelengths, higher intensity, and better stability, but require a strong power supply and produce heat (ALLEN, COX and BEARD, 2005).

Optical elements also offer a variety of alternatives and are used to manipulate radiation in optical instrumentation. Some examples are lenses, mirrors, light choppers, beam splitters, and couplers for directing the light from the source into the small aperture of a fiber optic or a specific area on a waveguide surface and collect the light from the sensor. Optical filters, prisms, and diffraction gratings are the most common components used to provide a narrow bandwidth of excitation when a broadwidth light source is utilized (MENDELSON, 1995).

Factors such as sensitivity, noise, spectral, and response time must be considered in the choice of photodetectors. Normally either photomultipliers or semiconductor quantum photodetectors, such as photoconductors and photodiodes are used. The compactness and simplicity of the circuitry involved with photodiodes make these components more attractive (YOTTER and WILSON, 2003).

4.5 MEASUREMENT

Body optical properties can be measured either with transmittance or reflectance approaches. Reflection configuration measures lower light intensities than transmission, as the amount of radiation crossing the tissue is greater than the amount reflected. On the other hand, refelectance probes, shown in Figure 25 (a), allow the sensors to be placed on locations such as the chest, cheek, or forehead (ZHAO, 2002).

In transmission mode in Figure 25 (b), the detector is placed in line with the light source reading the maximum amount of the transmitted light. The photodiode should be placed as close as possible to the target. A disadvantage of transmission mode is the limited measurement sites, such as fingertip, nasal septum, cheek, tongue, and ear (WEBSTER, 1997).

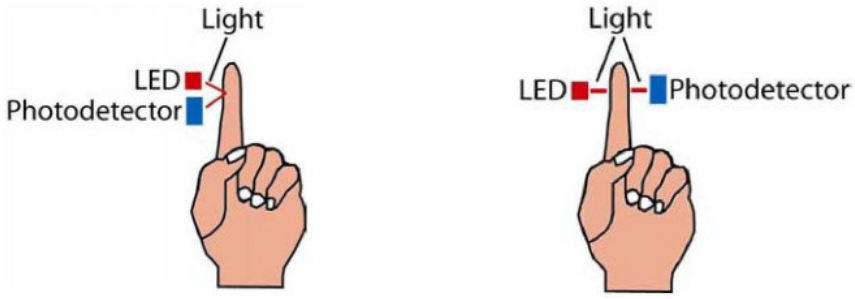

(a) (b)

Figure 25 - Reflectance (a) and transmittance (b) models (ZHAO, 2002).

The signal obtained from a photodetector provides a voltage or a current proportional to the measured light intensity. The output from a photodetector can be applied to a preamplifier before the measurement stage, which can be analog or digital (MENDELSON, 1995).

The optic analysis with a wide spectral range requires special devices called spectrophotometers, which can be built by a variety of techniques. Common radiation sources for the IR spectrometer are Nernst glower (constructed of rare-earth oxides), Globar (constructed of silicon carbide), and tungsten lamps tungsten lamps. Such components produce continuous radiation, but with different radiation energy profiles (SHERMAN, 1997).

Dispersive light spectrometers consist of three basic components: radiation source, monochromator, and detector, as illustrated in the schematic diagram of Figure 26 (THERMO NICOLET, 2002). After photom production, the light is split in two beams, and through a set of mirrors, is directed to a sample and to a reference chamber (double-beam principle). After passing the sample chamber, both signals are combined into one common path by means of a rotating chopper mirror. The control of the measurement wavelength is done through a mechanical filter called monochromator, this diffraction prisms or grating focuses a narrow band of frequencies on a mechanical slit (ANALYTIK JENA 2004). Each wavelength is measured one at a time, with the slit monitoring the spectral bandwidth and the grating moving to select the wavelength being measured. After crossing the slit, the detector measures the magnitude of the resulting radiation (SABLINSKAS, 2003).

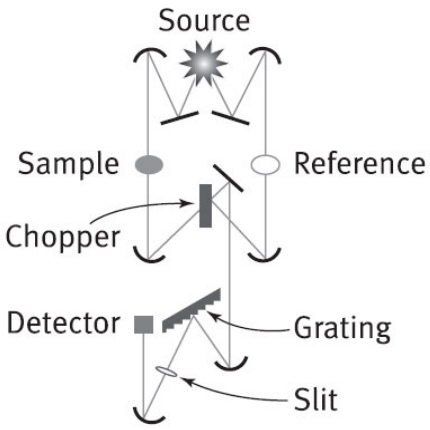

Figure 26 - Dispersive spectrometers measurement principle (THERMO NICOLET, 2002).

Fourier transform (FT) spectrometers have replaced dispersive instruments for most applications due to their superior speed and sensitivity. Unlike dispersive instruments, FT spectrometers acquire single channel spectra of sample and reference, as seen in Figure 27. This equipment has source, interferometer, sample, and detector blocks. The same types of radiation sources are used for both types of spectrometers, however, the source is often water-cooled in FTIR instruments to provide better power and stability (SABLINSKAS, 2003).

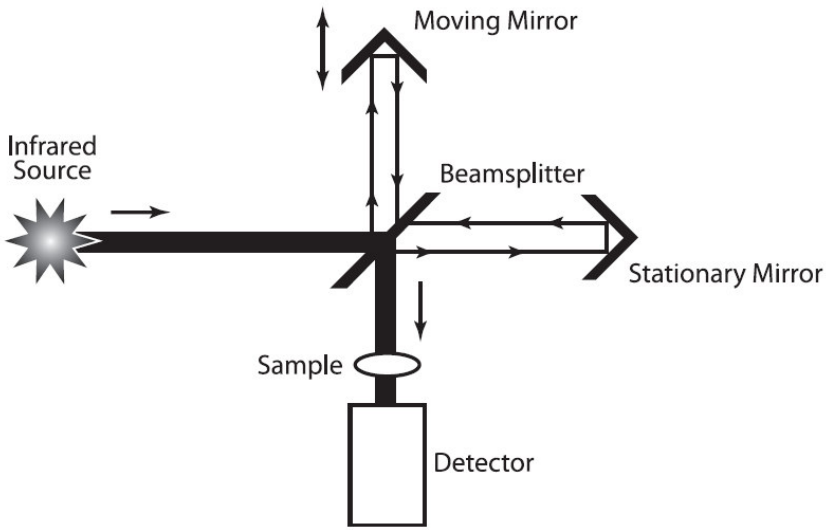

Figure 27 - Interferometer Diagram (THERMO NICOLET, 2002).

The interferometer consists of a beamsplitter, a moving mirror, and a fixed mirror. The beamsplitter transmits about 50% and reflects about 50% of the incident radiation. After the divided beams are reflected from the two mirrors, they are rejoined at the beamsplitter, which results in obtained an interference pattern as the optical path difference is varied by the moving mirror (SHERMAN, 1997). The resulting beam then passes through the sample

chamber and is measured on the detector. The spectrum of a given sample is generated by calculating the ratio of the background signal, obtained by the first scanning and stored in memory, to the signal obtained by scanning the sample (THERMO NICOLET, 2002).

Many FTIR spectrometers offer the possibility to measure with ATR technique, which involves placing a little sample preparation on top of a crystal with a high refractive index. This is a great advantage, since only a small amount of sample without special preparation is required. Attenuated total reflectance occurs when a beam of radiation enters from a more-dense into a less-dense medium. Such phenomenon is shown in Figure 28, where an infrared beam from the instrument is passed into the accessory and up into the crystal. It is then reflected at its surface, penetrating 0.5 μm to 2 μm into the sample, and back towards the detector. Therefore, the reflectance behaviour depends on the refractive indexes of the crystal and of the sample lying on its top (SHAW and MANTSCH, 2000).

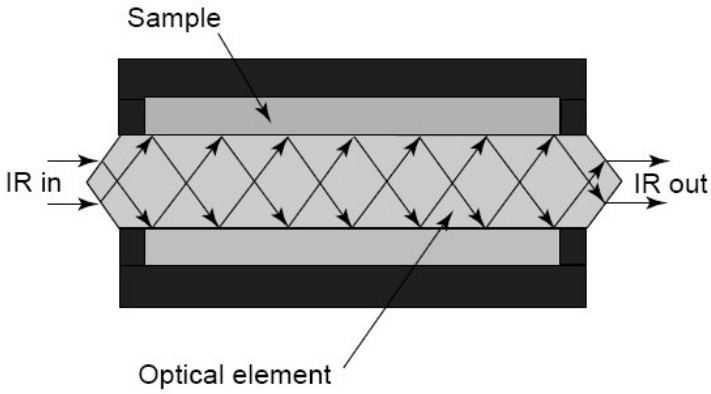

Figure 28 - Schematic representation of multiple internal reflection effect in Attenuated Total Reflectance module (SHAW and MANTSCH, 2000).

4.6 SPECTRAL ANALYSIS

Spectroscopy is used in physical and analytical chemistry for the identification of a substance's concentration through its optic spectrum. Figure 29 shows the electromagnetic spectra and its effects in biological tissues.

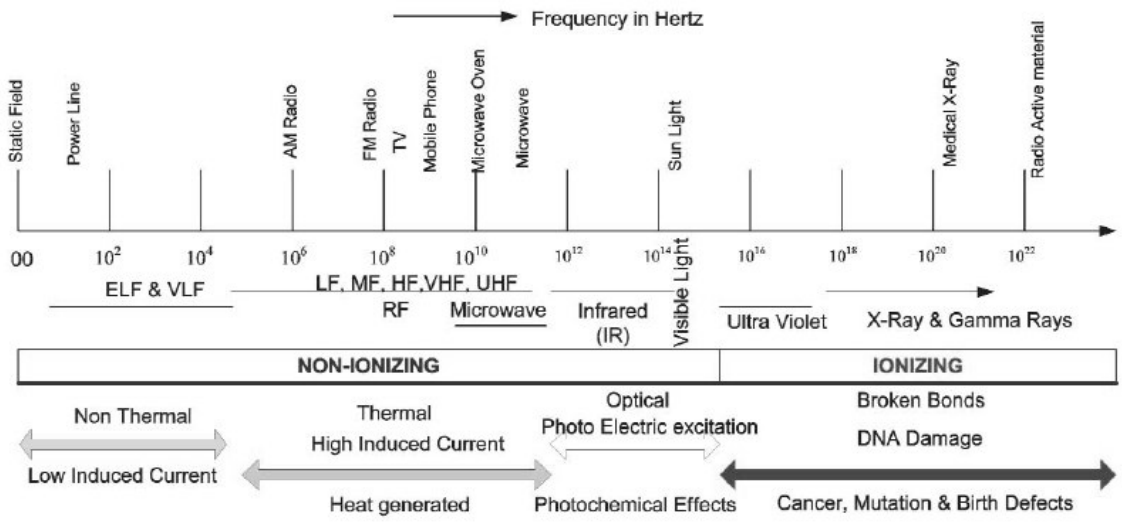

Figure 29 – Electromagnetic spectra (ZAMANIAN and HARDIMAN, 2005)

The range of frequencies covered by radiation in the infrared region of the electromagnetic spectrum is comparable to the natural frequencies at which atoms or molecules will vibrate in the absence of an applied field, as seen in Figure 30. Thus when IR is incident on a system of matter, resonance will occur around the natural frequencies, whereby energy is transferred from the incident field to the system and its amplitude of vibration is increased (HOLLIS, 2002).

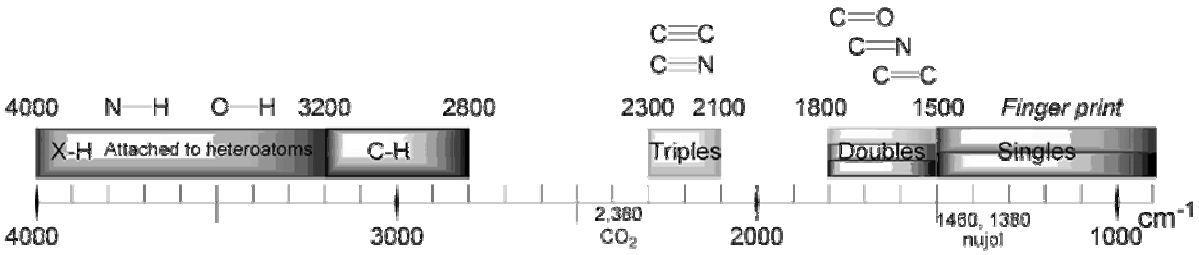

Figure 30 - Molecular vibrations in MIR range (HOLLIS, 2002).

Water constitutes 70% of hydrated tissues, followed by the connective tissue proteins and lipids. Photons are absorbed by water at wavelengths longer than the middle infrared (MIR) range, while proteins are strongly absorbing in the ultraviolet (UV) region. Fortunately, the optical absorption capacity of water, proteins and lipids is small in the red and near-infrared region, as seen in Figure 31. Therefore, ranges from 600 nm to 2300 nm, which allow light to penetrate from a few hundred micrometers to a few millimeters into tissues, can be exploited for purposes of diagnosis, imaging or therapy (KHALIL, 2004).

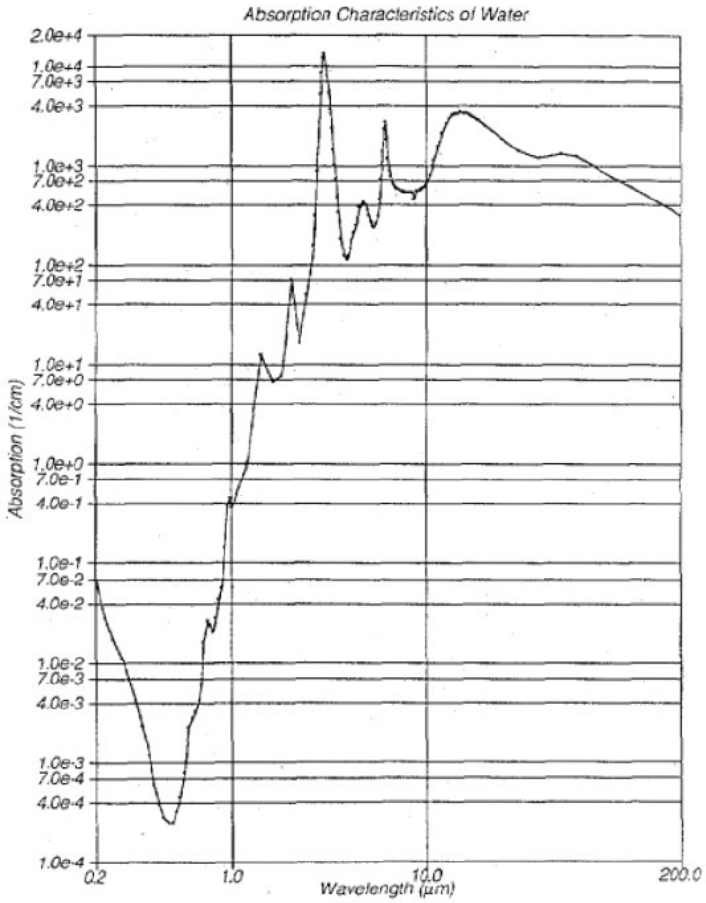

Figure 31 – Typical water absorption spectra (KINNUNEN, 2006).

Glucose NIR spectral range has overtone bands that are broad and weak, on the other hand, bands in the MIR are sharp and have a higher absorption coefficient, as illustrated in Figure 32 (cm^{-1} = 10000000/nm) and Figure 33. These spectral bands are dominated by C-C, C-H, and OH stretching and bending vibrations. The 8.3 μm – 12.5 μm fingerprint region of the IR spectrum of glucose has bands at 11.961 μm, 10.976 μm, 9.891 μm, 9.551 μm, 9.293 μm, and 8 μm that have been assigned to C-H bending vibrations. A 9.746 μm band corresponds to C-O-H bend vibration. Spectral measurements in this frequency interval were used to determine glucose in serum and blood (KHALIL, 2004).

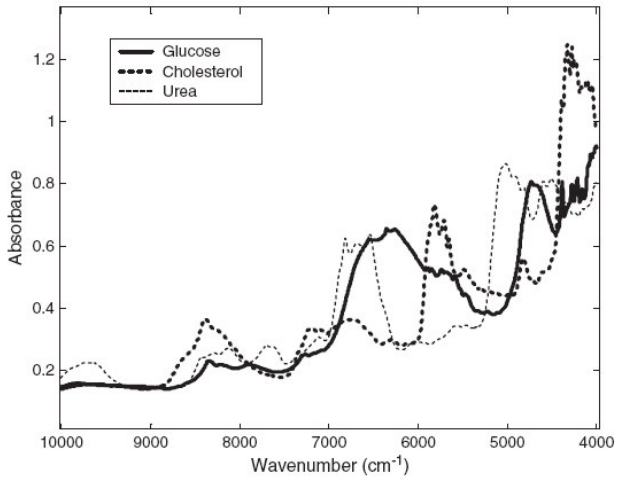

Figure 32 – Typical NIR glucose absorption spectra (KANG, KASEMSUMRAN, WOO *et al*, 2006).

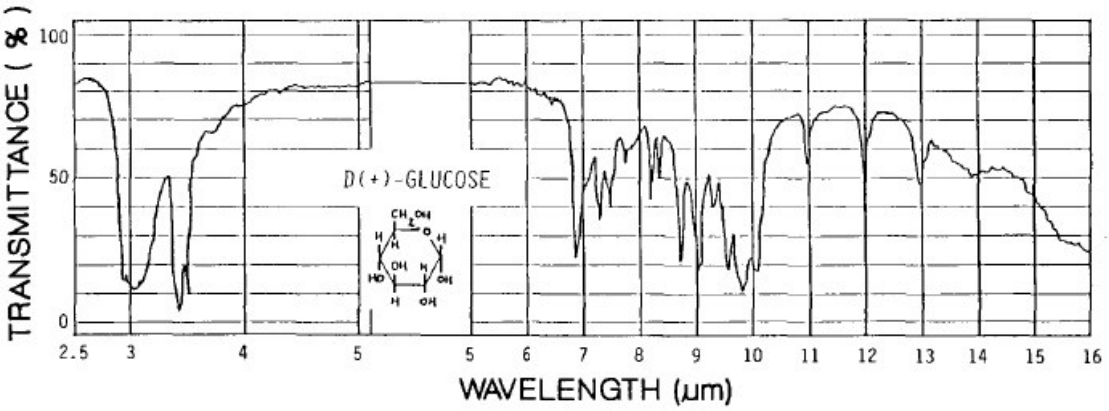

Figure 33 - Typical MIR glucose transmittance spectra (MENDELSON, CLERMONT, PEURA *et al*, 1990.)

4.7 SAFETY

The human organism is constantly exposed to sources of optical radiation such as sunlight, electrical lamps, lasers and oher incandescent sources. Light absorption in the tissue varies depending on the wavelength of the light radiated. The energy of intense optical radiations can be absorbed by water electrons in tissue near the body's surface causing heating, redness and even burning. Optical radiations are not very penetrating, therefore, eye and skin are the organs of greatest concern. Normally, the eye is well adapted to protect itself against light radiation from the natural environment, as seen in Figure 34. In addition, biological protective measures are also known, such as clothing to shield against the harmful

effects of skin exposure. However, high levels of electromagnetic radiation or overexposure may be harmful, therefore, many standards and regulations for optical equipments are implemented to protect the tissues (SLINEY, 1997).

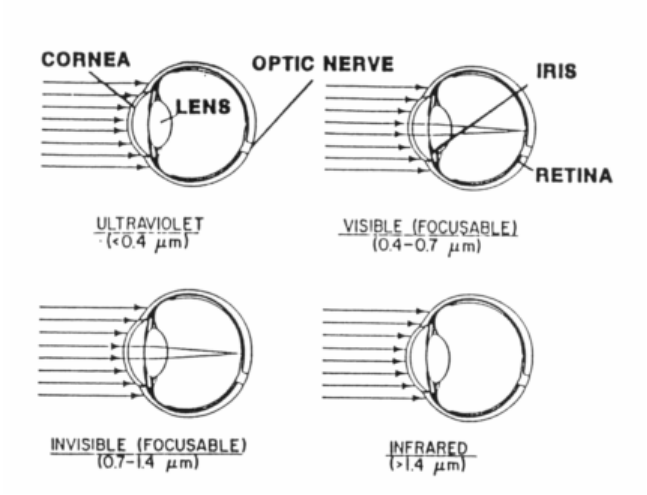

Figure 34 - Absorption of light in the Ocular System (INDIANA UNIVERSITY, 2006).

The visible frequencies of the electromagnetic spectrum (Figure 35) are interpreted by our eyes as different colors (MENDELSON, 1995). Radiation with wavelengths in the ocular focus region (0.4 μm – 1.4 μm) is transmitted through the cornea and focused by the lens on the retina with a magnification of up to 100,000 times. Strong light intensity with wavelengths in this range, such as lasers, have the greatest potential for seriously damaging the eye, and are able to form permanent lesions on the retina (INDIANA UNIVERSITY, 2006).

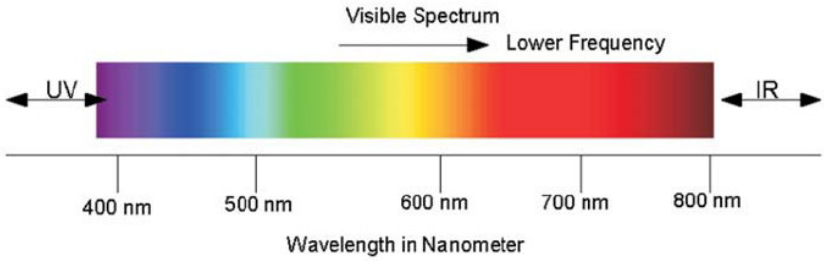

Figure 35 - Visible light spectrum (ZAMANIAN and HARDIMAN, 2005).

IR radiation is usually emitted by flash lamps, furnaces, molten metal or glass, fireplace embers and hot objects, invisible to the human eye. Visible light energy is emitted by objects only at a high temperature, where as infrared energy is emitted by all objects at normal temperatures. Some studies have shown that infrared energy can have therapeutic

effects on the organism, helping to rebuild connective tissue. Visible and infrared high-powered laser radiation can cause depigmentation, ulceration, and scarring of the skin as well as damage to underlying organs. Laser radiation, with frequencies outside the ocular focus region, are absorbed by the cornea and do not harm the retina. In the infrared frequencies, excessive exposure causes a loss of transparency or surface irregularities in the cornea. As an example, 10 mW/cm^2 is the occupational ocular exposure limit from 780 nm to 1400 nm (BOZKURT and ONARAL, 2004).

The ultraviolet (UV) radiation has a high photon energy range and can also be found in normal conditions, especially in sunlight, black lights and welding arcs. These wavelengths produce photochemical changes and may have both positive and negative consequences, depending on the level of exposure, duration and differences in the susceptibility to the light. The benefits of UV are warmth, photosynthesis in plants, and vitamin D synthesis in the human body. This radiation usually does not have immediate negative symptoms, however, when an organism is overexposed, it produces ionizing effects which may damage genetic information, causing skin cancer, immune system suppression, and premature aging. UV negative effects to eyes produce intolerance to light, tearing, removal of the surface in scales and cloudiness in the connective tissue or main body of the cornea. For this reason, certain medical germicidal lamps (λ = 254 nm) have limits as low as 0.1 $\mu W/cm^2$ for a 24-hour period and 0.5 $\mu W/cm^2$ for a seven-hour period (ZAMANIAN and HARDIMAN, 2005).

Strong lights such as lasers also require attention to the radiation period, and are divided in to continuous and pulsed mechanisms. Continuous wave lasers produce thermal processes whereby a steady stream of photons is absorbed by the target until the natural cooling ability of the tissue is overwhelmed and its temperature rises to damaging levels. Pulsed laser mechanism is one of acoustical blast or shock damage. Table 5 corresponds to the laser intensity limits from the American National Standards Institute - ANSI Z136.1. Class 1 low-power lasers have no risk to the skin or eyes, class 2 pose no risk to the skin and minimal risk to the eyes. Class 3b are medium-power lasers whose direct beam and reflections pose potential risks to the skin and immediate risks to the eyes. Class 4 high-power lasers have a primary beam and reflection that have immediate risks to the skin and eyes (INDIANA UNIVERSITY, 2006).

Table 5 – Laser safety standard (American National Standards Institute - ANSI Z136.1)

Wavelength (μm)	Laser Type	Wavelength (μm)	Pulse Duration (s)	Class 1 (J)	Class 3b (J)	Class 4 (J)
Ultraviolet						
0.180 to 0.400	Excimer (ArF)	0.193	20×10^{-9}	$\leq 1.9 \times 10^{-6}$ *	> Class 1 but ≤ 0.125	> 0.125
	Excimer (KrF)	0.248	20×10^{-9}	$\leq 1.9 \times 10^{-6}$ *	> Class 1 but ≤ 0.125	> 0.125
	Neodymium:YAG Quadrupled (Q-sw)	0.266	20×10^{-9}	$\leq 1.9 \times 10^{-6}$ *	> Class 1 but ≤ 0.125	> 0.125
	Excimer (XeCl)	0.308	20×10^{-9}	$\leq 4.3 \times 10^{-6}$ *	> Class 1 but ≤ 0.125	> 0.125
	Nitrogen	0.337	20×10^{-9}	$\leq 3.6 \times 10^{-6}$ *	> Class 1 but ≤ 0.125	> 0.125
	Excimer (XeF)	0.351	20×10^{-9}	$\leq 4.3 \times 10^{-6}$ *	> Clas 1 but ≤ 0.125	> 0.125
Visible						
0.400 to 0.700	Rhodamine 6G (Dye Laser)	0.450-0.650	1×10^{-6}	$\leq 0.2 \times 10^{-6}$	> Class 1 but ≤ 0.03	> 0.03
	Copper Vapor	0.510, 0.578	25×10^{-9}	$\leq 2 \times 10^{-7}$	> Class 1 but ≤ 0.03	> 0.03
	Neodymium:YAG Doubled (Q-sw)	0.532	20×10^{-9}	$\leq 2 \times 10^{-7}$	> Class 1 but ≤ 0.03	> 0.03
	Ruby (Q-sw)	0.6943	20×10^{-9}	$\leq 2 \times 10^{-7}$	> Class 1 but ≤ 0.03	> 0.03
	Ruby (Long Pulse)	0.6943	1×10^{-3}	$\leq 4 \times 10^{-6}$	> Class 1 but ≤0.03	> 0.03
Near Infrared						
0.700 to 1.4	Ti:Sapphire	0.700-1.000	6×10^{-6}	$\leq 1.9 \times 10^{-7}$	> Class 1 but ≤ 0.03 C_A	> 0.03 C_A
	Alexandrite	0.720-0.800	1×10^{-4}	$\leq 0.76 \times 10^{-6}$	> Class 1 but ≤ 0.03 C_A	> 0.03 C_A
	Neodymium:YAG (Q-sw)	1.064	20×10^{-9}	$\leq 2 \times 10^{-6}$	> Class 1 but ≤ 0.15	> 0.15
Far Infrared						
1.4 to 10^3	Erbium:Glass (Q-sw)	1.540	10×10^{-9}	$\leq 7.9 \times 10^{-3}$	> Class 1 but ≤ 0.125	> 0.125
	Co:Magnesium-Fluoride	1.8-2.5	80×10^{-6}	$\leq 7.9 \times 10^{-4}$	> Class 1 but ≤ 0.125	> 0.125
	Holmium	2.100	250×10^{-6}	$\leq 7.9 \times 10^{-4}$	> Class 1 but ≤ 0.125	> 0.125
	Hydrogen Fluoride	2.600-3.000	0.4×10^{-6}	$\leq 1.1 \times 10^{-4}$	> Class 1 but ≤ 0.125	> 0.125
	Erbium	2.940	250×10^{-6}	$\leq 5.6 \times 10^{-4}$	> Class 1 but ≤ 0.125	> 0.125
	Carbon Dioxide (Q-sw)	10.6	100×10^{-9}	$\leq 7.9 \times 10^{-5}$	> Class 1 but ≤ 0.125	> 0.125
	Carbon Dioxide	10.6	1×10^{-3}	$\leq 7.9 \times 10^{-4}$	> Class 1 but ≤ 0.125	> 0.125

* Assuming that both eye and skin maybe exposed, i.e., 1.0 mm beam (area of limiting aperture = 7.9×10^{-3} cm^2).

4.8 APPLICATIONS

New laser sources, detectors and measurement techniques are powerful methods for the study of diseases on all scales, from single molecules, to specific tissues and whole organs. Optic technology is widely utilized in the biological and medical specialtys fields such as ophthalmology, dermatology, oncology, radiology, anaesthesiology, gynaecology, neurosurgery, gastroenterology, cardiology, cardiothoracic surgery, neonatology, immunology and clinical chemistry.

The cancer therapy photosensitizing drugs activated by specific wavelengths are absorbed by tumors. The light-excited drug interacts with molecular oxygen to produce a toxic oxygen species, known as singlet oxygen, which mediates cellular death (WANG, HEBDEN and TUCHIN, 2004).

Hyperbilirubinemia is one of the most common problems encountered in term newborns and if not treated may cause seizures and brain damage. When infants are exposed to blue light (410 nm to 460 nm), a photochemical reaction occurs in the skin, changing unconjugated bilirubin into more soluble metabolites which are then excreted into the bile and the urine. The effectiveness of phototherapy depends upon the irradiance delivered by the light source, and the amount of skin exposed to the light (ROSEN, ROSEN, HIS *et al*, 2004).

Optical coherence tomography allows non-invasive visualization of specific tissues and organs. The algorithms applied to optical imaging are similar to x-ray tomography methods. A source and detector are scanned around the surface of the tissue volume of interest, and the measurements are inverted to reconstruct the optical properties within the tissue volume as a function of position (HEBDEN, BOAS, GEORGE *et al,* 2003). Laser spectroscopic microscopes are able to obtain high resolution images and 3-D reconstructions, and may have enough resolution to measure single protein molecules. In addition this technology is able to manipulate samples, moving or rotating probes and even cutting specific parts of cells, such as membranes (SATO, ISHIGURE and INABA, 1991).

Intravascular catheters also use light in fiber optics to determine concentration of gases such as oxygen, carbon dioxide and pH, which is essential for clinical diagnosis and management of respiratory and metabolic problems (MENDELSON, 1995). Oxygen saturation of arterial blood can also be measured through non-invasive assays. The basis of this technology is to measure red (660 nm) and infrared (950 nm) light effects in the tissue. Pulse oximeter beams radiate though fingers or ears, where most of the energy is absorbed by tissue, bone and venous blood, however, these values of absorption are relatively constant. Arterial blood however is pulsatile, and therefore can be distinguished from other artifacts. The basic pulse oximetry system is shown in Figure 36 (WEBSTER, 1997).

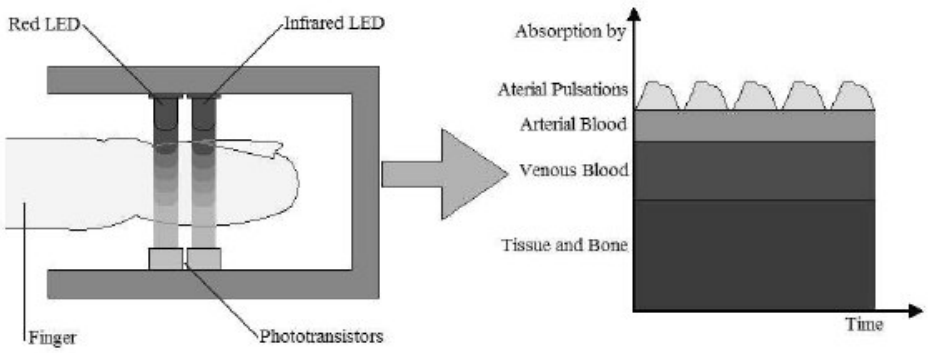

Figure 36 – Measurement of oxygen saturation of arterial blood through pulse oximetry (WEBSTER, 1997).

CHAPTER 5

PROPERTIES FROM BIOLOGICAL TISSUES

5.1 INTRODUCTION

Optical and electrical non-invasive diagnostics of the human body depend strongly on the composition and morphology of tissues in the measurement site. Blood glucose changes these complex properties in almost all of the organism's parts. The first obstacle to light and current penetration is the skin, which can also contain glycemic information from blood due the dermal microcirculation, therefore optic and electrical properties of both tissues are analyzed in this section.

5.2 SKIN

5.2.1 Composition

The skin is a barrier that protects from excessive water loss, entry of potentially hazardous substances and cell damage due to ultraviolet radiation. The epithelial tissue consists of epidermis, dermis, and subcutaneous layers, which is composed mainly of fatty tissue and provides no blood information. The epidermis illustrated in Figure 37 changes its thickness depending on the body part, for example, 50 μm in eyelids, 176 μm in fingertips and even 1 mm in palms and soles (ZHAO, 2002; WHITTON and EVERALL, 1973). It can be subdivided into stratum corneum (most external), stratum granulosum, stratum spinosum, and stratum basale. The cells from the stratum corneum are constantly being shed from the body, forming a lipid matrix surface of approximately 10–20 μm thick. The density of the stratum corneum is the principal obstacle to non-invasively measuring the underlying tissue (MAGNENAT-THALMANN, KALRA, LÉVÊQUE *et al*, 2002). The other sublayers of epidermis are made of keratinocytes and melanocytes, which are pigment cells responsible for skin color. Correlation from epidermis readings with blood levels may be wrong, since this layer is avascular and receives all nutrients via diffusion from the dermis (ZHAO, 2002).

The dermis thickness varies from 0.3 mm in the eyelids to about 3 mm in the palm and soles. One-half of its volume is made of collagen and elastic fibers, ISF accounts for about 45%, and the rest corresponds to blood vessels, nerves, hair follicles and sweat glands. Its upper layer is the papillary dermis and contains the vascular network and sensory nerve endings. The reticular dermis, which is the deeper layer, consists of loose connective and epithelial-derived structures such as glands and follicles (ZHAO, 2002). Standard home monitoring techniques take samples from dermal capillary blood, whose vessels change its diameter with stress, temperature, aging and disease state (SIEG, GUY and DELGADO-CHARRO, 2005).

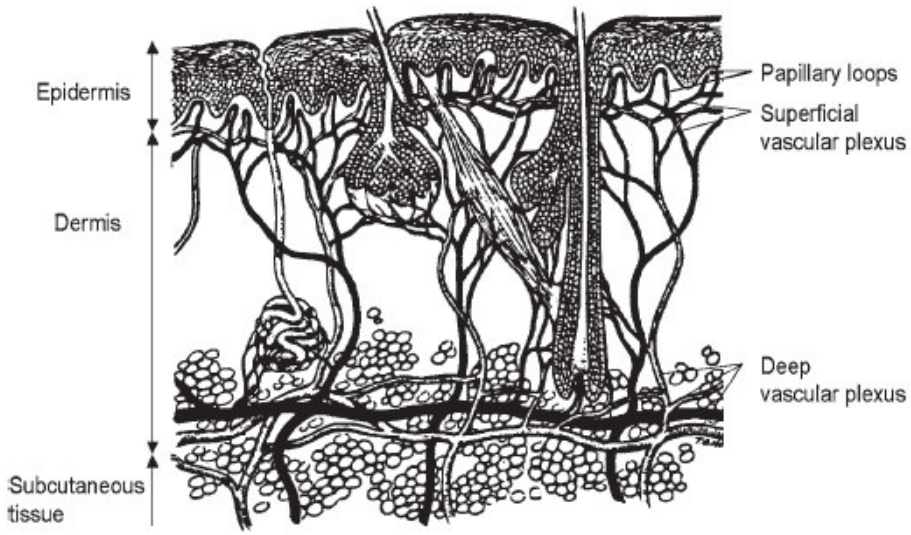

Figure 37 – Human skin model with epidermis, dermis, and subcutaneous layers (SIEG, GUY and DELGADO-CHARRO, 2005).

5.2.2 Electrical properties

The skin electric comportment is similar to a capacitor, for DC currents it has high impedance, but for alternated signals this value decreases proportionally to the applied frequency. This effect is mainly caused by the stratum corneum, which in 10 kHz accounts for about 50 % of the total epithelial impedance with a concentric electrode (GRIMNES and MARTINSEN, 2000). On the other hand, at 100 kHz, such values decrease 10 %. The epithelial impedance has modulus between 300 Ω and 1 MΩ per square centimetre and a

phase angle approximately 71.5° in the kHz range, therefore the smaller the electrode surface, the lower the impedance value (GEDDES and BAKER, 1989).

Many factors such as sweat, measurement site, gland activity and ambient humidity can reflect large influences in the electrical parameters of cutaneous tissue. The surface temperature, which has glucose influence, also changes bioimpedance measurement, Cornish, Thomas and Ward analyzed between 10 kHz and 100 kHz got a resistance of 110 Ω and a reactance of 130 Ω in 20° C. With the skin in 40° C, the values decreased to 70 Ω of resistance and 110 Ω of reactance (GEDDES and BAKER, 1989). Another factor that should be taken in consideration during BIA experiments is that the epithelial impedance variation is not linear with the applied signal. For values higher than 10 μA/cm^2, increasing the signal amplitude causes the impedance magnitude to decrease (LACKERMEIER, PIRKE, MC ADAMS *et al*, 1996). Beside the signal frequency and surface characteristics, the distance between the electrodes also changes the depth penetration of electrical current, as seen in Figure 38, where high frequency signals reach approximately half of the distance *L*.

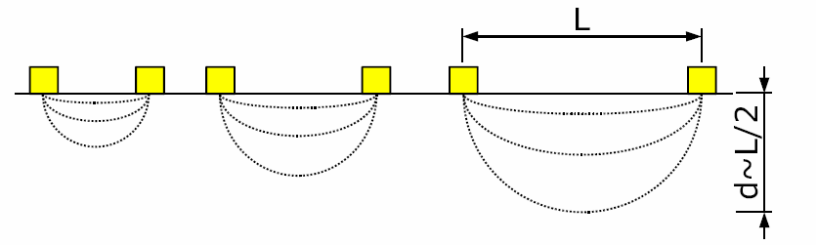

Figure 38 – The depth penetration of high current lines in the skin is approximately half of the distance between electrodes (ABERG, GELADI, NICANDER *et al*, 2002).

5.2.3 Optic properties

The epidermis is a light-absorbing layer, where melanin and other specific pigments are present for ultraviolet photo protection. However, at near-infrared wavelengths, the transmittance of light through the stratum corneum and epidermis is 90–95%, independent of skin pigmentation. In the dermis, light scattering is more important, being principally responsible for light absorption at wavelengths less than 600 nm (SIEG, GUY and DELGADO-CHARRO, 2005). Beyond this threshold, a sharp decrease in absorption by hemoglobin and skin pigment allows significant penetration of red light and NIR radiation.

The most penetrating optical wavelength is 1150 nm, at which about one-quarter of the incident radiation traverses the entire dermis. Thereafter, absorption by water becomes considerable and is the reason for the 600 nm to1300 nm region being called the “optical window” of the skin (KHALIL, 1999). Between 1520 nm and 1850 nm, scattering predominates, and absorptions by water and fat is already significant (Figure 39). Between 2000 nm and 2500 nm, absorption dominates, with water, fat, and protein as the primary absorbers (SIEG, GUY and DELGADO-CHARRO, 2005). Chemical, structural, and physiological variations, such as skin temperature, hydration state, or local skin blood flow, affect the tissue’s optical properties and the depth of light penetration. For example, light penetration depth in skin is increased by lowering its temperature (KHALIL, 2004).

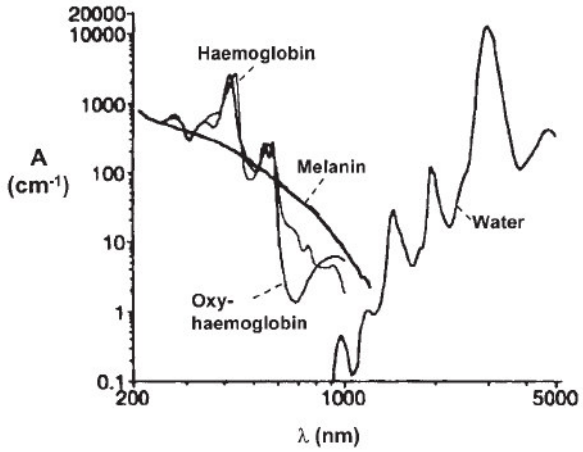

Figure 39 - Principal light-absorbing molecules in the skin (SIEG, GUY and DELGADO-CHARRO, 2005).

The MIR spectrum of the skin, as determined by ATR accessories, showed overlap between bands of glucose and those in skin components. Table 6 summarizes the low frequency vibrations in such frequencies for water, glucose, and human skin. Although bands in the 10 μm range are specific to glucose in aqueous solutions, there is a high probability of having C-C, C-H, and C-O bending vibrations from other skin components coinciding with them. The C-C bands in the spectrum of skin do not relate only to glucose, as it is a minor component compared with proteins and fats (KHALIL, 2004).

Table 6 - Vibrations in the MIR band frequencies of water, glucose, and human skin (KHALIL, 2004).

Water (nm)	Glucose (nm)	Skin (nm)
	11961	
		11737
	10976	10905
	9891	
	9746	9661
	9551	
	9293	9285
		8944
8695		8591
	8000	8032

5.3 BLOOD

5.3.1 Composition

Blood is a specialized circulating tissue responsible for immunological functions, waste removal, transport of hormones, regulation of pH in the organism, control of body temperature, clotting, supplying of oxygen and nutrients. Failures in any of these processes can result in serious damage to the organism, therefore, whole blood monitoring is an important tool in clinical diagnostics. This tissue can be divided into a liquid part, called plasma, and a solid component (hematocytes) formed by erythrocytes for respiration, white corps (leukocytes), which defend the body against infections and diseases and platelets (thrombocytes) that act in clotting, as shown in Figure 40. The plasma is comprised of 90% water and forms more then 55% of blood volume (Table 7). The rest of the volume is almost all occupied by red blood cells (Table 8), since its size (10 μm of diameter) and number are much higher than the other substances (GEDDES and BAKER, 1989).

Generally, about 70% of the total blood volume is related to the venous vasculature, 20% is arterial and about 5% is capillary blood. The arterio-venous glucose difference also plays a role in integral tissue probing within spectroscopic assays. Under physiological conditions, the difference can vary considerably as a result of nutritional and metabolic activities (HEISE, 2000).

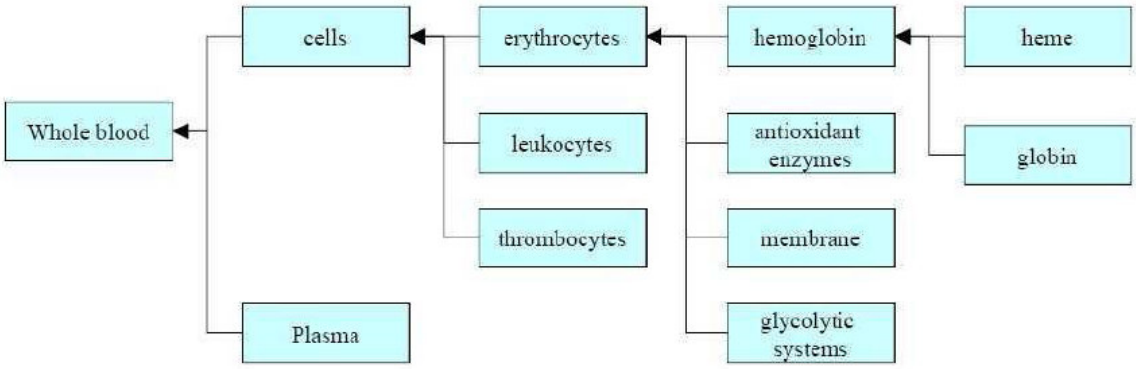

Figure 40 – Liquid and cellular components of human blood (ZHAO, 2002).

Table 7 – Concentration of plasma components (SCHNECK, 1995)

Constituent	Concentration Range (mg/dl plasma)	Typical Plasma Value (mg/dl)	Molecular Weight Range	Typical Value	Typical size (nm)
Total protein, 7% by weight	6400–8300	7245	21,000–1,200,000	—	—
Albumin (56% TP)	2800–5600	4057	66,500–69,000	69,000	15 × 4
α_1-*Globulin* (5.5% TP)	300–600	400	21,000–435,000	60,000	5–12
α_2-*Globulin* (7.5% TP)	400–900	542	100,000–725,000	200,000	50–500
β-*Globulin* (13% TP)	500–1230	942	90,000–1,200,000	100,000	18–50
γ-*Globulin* (12% TP)	500–1800	869	150,000–196,000	150,000	23 × 4
Fibrinogen (4% TP)	150–470	290	330,000–450,000	390,000	(50–60) × (3–8)
Other (2% TP)	70–210	145	70,000–1,000,000	200,000	(15–25) × (2–6)
Inorganic ash, 0.95% by weight	930–1140	983	20–100	—	— (Radius)
Sodium	300–340	325	—	22.98977	0.102 (Na^+)
Potassium	13–21	17	—	39.09800	0.138 (K^+)
Calcium	8.4–11.0	10	—	40.08000	0.099 (Ca^{2+})
Magnesium	1.5–3.0	2	—	24,30500	0.072 (Mg^{2+})
Chloride	336–390	369	—	35.45300	0.181 (Cl^-)
Bicarbonate	110–240	175	—	61.01710	0.163 (HCO_3^-)
Phosphate	2.7–4.5	3.6	—	95.97926	0.210 (HPO_4^{2-})
Sulfate	0.5–1.5	1.0	—	96.05760	0.230 (SO_4^{2-})
Other	0–100	80.4	20–100	—	0.1–0.3
Lipids (fats), 0.80% by weight	541–1000	828	44,000–3,200,000	= Lipoproteins	Up to 200 or more
Cholesterol (34% TL)	12–105 "free" 72–259 esterified, 84–364 "total"	59 224 283	386.67	Contained mostly in intermediate to LDL β-lipoproteins; higher in women	
Phospholipid (35% TL)	150–331	292	690–1010	Contained mainly in HDL to VHDL α_1-lipoproteins	
Triglyceride (26% TL)	65–240	215	400–1370	Contained mainly in VLDL α_2-lipoproteins and chylomicrons	
Other (5% TL)	0–80	38	280–1500	Fat-soluble vitamins, prostaglandins, fatty acids	
Extractives, 0.25% by weight	200–500	259	—	—	—
Glucose	60–120, fasting	90	—	180.1572	0.86 D
Urea	20–30	25	—	60.0554	0.36 D
Carbohydrate	60–105	83	180.16–342.3	—	0.74–0.108 D
Other	11–111	61	—	—	—

Table 8 - Concentration of hematocytes (SCHNECK, 1995)

Cell Type	Number Cells per mm³ Blood*	Corpuscular Diameter (μm)*	Corpuscular Surface Area (μm²)*	Corpuscular Volume (μm³)*	Mass Density (g/cm³)*	Percent Water*	Percent Protein *	Percent Extractives*†
Erythrocytes	4.2–5.4	6–9 (7.5)	120–163	80–100	1.089–1.100	64–68	29–35	1.6–2.8
(red blood cells)	× 10⁶ ♀	Thickness	(140)	(90)	(1.098)	(66)	(32)	(2)
	4.6–6.2	1.84–2.84						
	× 10⁶ ♂	"Neck"						
	(5 × 10⁶)	0.81–1.44						
Leukocytes	4000–11000	6–10	300–625	160–450	1.055–1.085	52–60	30–36	4–18
(white blood cells)	(7500)					(56)	(33)	(11)
Granulocytes								
Neutrophils:	2–6 × 10³	8–8.6	422–511	268–333	1.075–1.085	—	—	—
55–70% WBC (65%)	(4875)	(8.3)	(467)	(300)	(1.080)			
Eosinophils:	45–480	8–9	422–560	268–382	1.075–1.085	—	—	—
1–4% WBC (3%)	(225)	(8.5)	(491)	(321)	(1.080)			
Basophils:	0–113	7.7–8.5	391–500	239–321	1.075–1.085	—	—	—
0–1.5% WBC (1%)	(75)	(8.1)	(445)	(278)	(1.080)			
Agranulocytes								
Lymphocytes:	1000–4800	6.75–7.34	300–372	161–207	1.055–1.070	—	—	—
20–35% WBC (25%)	(1875)	(7.06)	(336)	(184)	(1.063)			
Monocytes:	100–800	9–9.5	534–624	382–449	1.055–1.070	—	—	—
3–8% WBC (6%)	(450)	(9.25)	(579)	(414)	(1.063)			
Thrombocytes	(1.4 ♂),	2–4 (3)	16–35	5–10	1.04–1.06	60–68	32–40	Neg.
(platelets)	2.14 (♀)–5	Thickness	(25)	(7.5)	(1.05)	(64)	(36)	
(2.675 × 10⁵)	×10⁵	0.9–1.3						

5.3.2 Electrical properties

Characterization of blood bioimpedance properties is important for the development of methods estimating clinical indices such as haematocrit, glucose level and hydration. The electrical impedance of blood is dependent on the plasma, the cell interior (mostly red cells), the cell membrane, volume fraction and the temperature (ZHAO, 1993). Therefore erythrocyte volume and shape also changes dielectric parameters from this tissue, especially at 3 MHz. The plasma and cell interior consist of conducting fluids with electrical resistivities, while cell membranes consist of phospholipids and proteins with dielectric properties that can be simulated by capacitors around 0.8 μF cm^{-2}. The blood plasma, which transports glucose, has conductivity about three times higher than for the cell cytoplasm (BEVING, ERIKSSON, DAVEY *et al*, 1994). Figure 41 shows the characteristic spectra of blood samples using a parallel bipolar electrode structure with 10 mV signal.

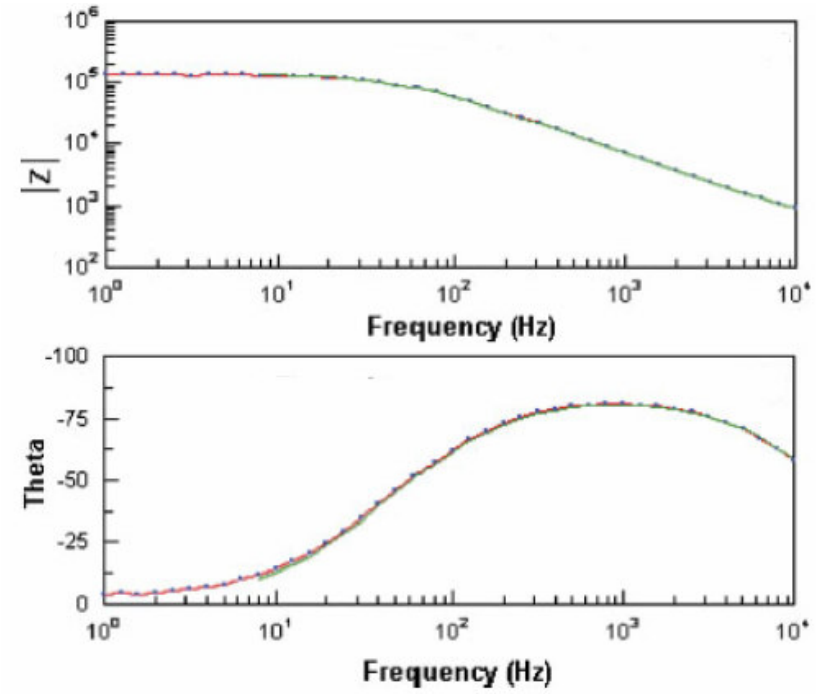

Figure 41 – Characteristic spectra of blood samples measured with a parallel bipolar electrode structure with 10 mV signal (SOSA, BERNAL-ALVARADO and JIMENEZ-MORENO, 2005).

5.3.3 Optic properties

The optical properties of blood especially depend especially on erythrocyte concentration, shape, velocity, aggregation, osmolarity and sedimentation. Hemoglobin is the protein that forms these cells, and it is responsible for delivering oxygen from the lungs to the body tissues and returning waste gases to the lungs to be exhaled. The oxygenated state haemoglobin is known as oxyhemoglobin (HbO_2), while the de-oxygenated form is known as deoxyhemoglobin (Hb). Arterial blood, which in adults is usually about 98% oxygen saturated, is bright red, whereas venous blood, which is approximately 75% saturated, appears dark red to purple in colour (BOZKURT and ONARAL, 2004).

Wavelengths longer than 950 nm are strongly absorbed by water and in its window of transparency (700nm – 900 nm) the most dominant absorption of NIR light is haemoglobin (Figure 39). From 4.6 µm to 5.4-µm, the attenuation is mainly due to of the water contents of the blood. In the 7-10 µm regions, hemoglobin again has a stronger absorption than water, contributing to a larger total attenuation coefficient (GUO, WANG, PENG *et al*, 2004).

In principle, serum or blood glucose may be quantified either by using MIR spectroscopy or by exploiring sets of NIR absorptions, corresponding to vibrational combination bands (2000 nm – 2500 nm), the first overtone absorptions (1400 nm – 1800 nm), or the second overtone bands (950 nm – 1250 nm) (SHAW and MANTSCH, 2000).

MIR glucose characteristic frequencies in the MIR are 8.68 μm, 9.017 μm, 9.259 μm, and 9.66 μm (Figure 42). Only the 9.66 μm peak is limited to glucose in the context of other blood constituents. For example, the 7.326 μm peak is identified in albumin, hemoglobin, and other constituents. The 9.259 μm peak is identified in albumin and hemoglobin; and the 9.017 μm peak is identified in hemoglobin. However, if interstitial fluid is used for glucose detection, thus eliminating the effects of hemoglobin, then the 9.017 μm peak may be used. In addition, the presence of large peaks near a characteristic peak may mask its appearance. For example, a strong urea peak at 8.620 μm masked the characteristic glucose peak at 8.680 μm. While albumin will still cause added absorption at the 9.259 μm peak, the frequency is potentially usable because changes in albumin concentration have little effect on the absorption spectra (MARTIN, MIROV and VENUGOPALAN, 2002). Table 9 shows examples of research with glucose characteristic frequencies and target site.

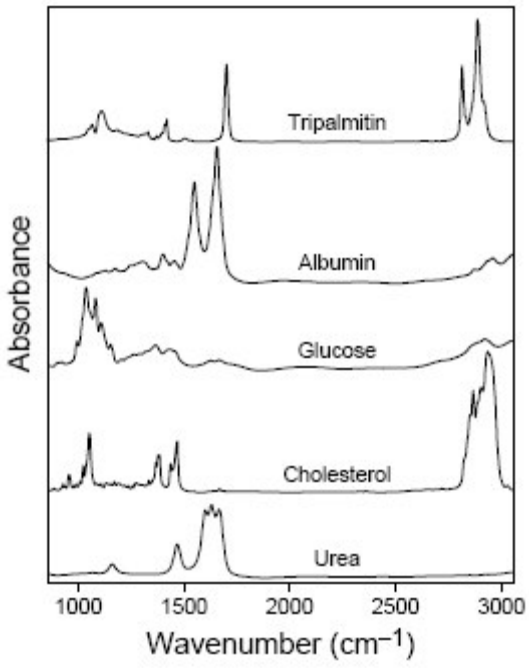

Figure 42 - MIR absorption spectra for serum constituents (SHAW and MANTSCH, 2000).

Table 9 – Research with glucose characteristic frequencies and target site.

Research group - year	Target site	Wavelength (nm)
Cho - Noninvasive measurement of glucose by metabolic heat conformation - 2004	Finger skin	470, 535, 660, 810, 880, 950
Baba – The use of polarized light for biomedical applications - 2003	Eye	532, 635
Cote - Noninvasive Optical Polarimetric Glucose Sensing using a True Phase Measurement Technique - 1992	Eye	633
Gabriely - Transcutaneous Glucose Measurement using near-infrared spectroscopy - 1999	Finger skin	780 – 2500
Yeh - Temperature-modulated Localized Reflectance Measurements - 2003	Forearm skin	590, 660, 890, 935
Heinemann - Non-invasive continuous glucose monitoring in Type I diabetic patients - 1998	Skin	800
Zhao - Pulsed photoacoustic techniques and glucose determination in human - theses - 2002	Finger	905
Robinson - Noninvasive glucose monitoring in diabetic patients - a preliminary evaluation - 1992	Finger skin	870 - 1300
Fischbacher - Enhancing calibration models for non-invasive near-infrared - 1997	Skin	950 - 1200
Tenhunen - Non-invasive glucose measurement based on selective near infrared- 1998	Finger skin	1500 - 1850
Maruo - Noninvasive Blood Glucose Assay Using a newly developed Near-Infrared System - 2003	Forearm skin	1600
Kasemsumran - Improvement of partial least squares models for in vitro and in vivo glucose - 2006	Forearm skin	1373–1429, 1495–1545, 1565–1696, 1790–1805
Niessner - New concept for the non-invasive determination - 1996	-	1554, 1304 (reference)
Burmeister - Evaluation of Measurement Sites for Noninvasive - 1999	Tongue	1612, 1689, 1731
Schrader - Non-invasive glucose determination in the human eye - 2004	Eye	1859 – 1528 1394 – 909
Olesberg - Tunable Laser Diode System for Noninvasive Blood Glucose Measurements - 2005	Blood	2325 –2212
Olesberg - Noninvasive Blood Glucose Monitoring in the 2.0-2.5 micrometer Wavelengh Range - 2001	Skin	2120, 2270, 2320
Toumi - Noninvasive Blood Glucose Analysis using Near Infrared Absorption spectroscopy - 2000	Blood	2257
Olesberg - In Vivo Near-Infrared Spectroscopy of Rat Skin - 2006	Skin	2040 2380
Toumi - Noninvasive Blood Glucose Analysis using Near Infrared Absorption – 1999	Liquids measurement	1686 2257
Kanukurthy – Wireless NIR glucose sensor controller	Arm skin	2120, 2270, 2320
Malchoff - A Novel Noninvasive Blood Glucose Monitor – 2002	Tympanic membrane	8500 (reference), 9600
Kajiwara - Noninvasive measurement of blood glucose concentrations by analysing fourier transform infra-red absorbance spectra through oral mucosa - 1993	Oral mucosa	3424 (reference), 9259, 9708
Martin - Using two discrete frequencies within the middle infrared - 2002	Serum	8382 (reference) 9661, 9259, 9017
Shen - The use of Fourier-transform infrared spectroscopy - 2003	Blood	9242, 9149
Lilienfeld-Toal - A novel approach to non-invasive glucose measurement by mid-infrared spectroscopy - 2005	Forearm skin	

CHAPTER 6

SPECTRA PREPROCESSING AND CALIBRATION MODELS

6.1 INTRODUCTION

As already seen, blood is a complex fluid consisting of many compounds with spectra overlapping in a wide range of measurements. In this case there are a great number of variables, which makes it difficult to find a model that relates them all. Baseline preprocessing can eliminate undesired substances overlapping as well as decrease errors caused by instrumentation and temperature instabilities (RANDALL, 1995). After the choice of one or more correction techniques, attention must be given to the data treatment, which is explained in this chapter. The derivation of a model to recover quantitative information of complex mixtures spectra requires calibration procedures, which are able to predict analyte specific information without knowing the relationship between the variables (HAM, COHEN, KOSTANIC *et al*, 1996).

Dimension reduction can be achieved by treating spectral data in a partial least squares (PLS) system. The resulting factors can be used as input in artificial neural networks (ANN), which are ideal to treat multisensor information and to monitor of data with noises and perturbations that introduce non-linearity into the model. (NYSTROM, LINDHOLM-SETHSON, STENBERG *et al*, 2003; LISZKA-HACKZELL, 1999).

6.2 PREPROCESSING

In chemometrics it is recommended to preprocess any data in order to remove slopes from the original spectrum, caused by instrumentation instability, overlapping bands, and environment influence. This procedure is useful especially when comparing curves or measuring peak intensities, and can be implemented by either physical or mathematical means. Physical methods such as chemical treatments of the sample may be helpful, but they contaminate the probe and can slow down the analysis. Manual estimation, polynomial fitting, frequency filtering, and derivative processing can be classified as processing methods for sloping removal (LEGER and RYDER, 2006).

6.2.1 Visual inspection

The baseline can be manually estimated by visual inspection, which has been done extensively in many fields and requires the choice of explicit points in the graphic. A basic whole spectrum processing corresponds to a linear baseline, which draws a line through 2 points and turns it into the horizontal axis. Drawbacks from this treatment are that the process is very slow, as each spectrum must be carefully inspected, and the quality of the correction will be greatly dependent on the experience of the user (GÜNZLER and GREMLICH, 2002).

6.2.2 Polynomial fitting

Polynomial fitting is the estimation of the baseline as a mathematical equation in order to subtract it from the original spectrum, such as in Figure 43. The baseline can be assumed to be a sloping line, or a function resulting from the selection of many points. It is also possible to assume that the baseline would have an exponential, logarithmic, or power dependence (VICKERS, WAMBLES, MANN, 2001).

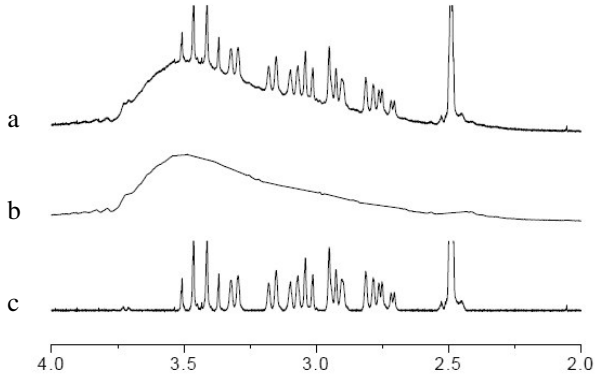

Figure 43 – Example of baseline processing, which removes slopes (b) from the original curve (a) to improve peaks analysis in (c) (WILLIAMS, MAIER and POTOCKY-PACAY, 2001).

The simplest polynomial is an offset, where a constant is subtracted from each channel. This is interesting when only two different signal frequencies are significant to a specific measurement. In this case, one wavelength is sensitive to changes in the species being measured, and the other wavelength is unaffected by changes in the analyte concentration,

being a reference to compensate fluctuations. Therefore, when many spectrums are collected, the elimination of offsets in the reference improves the quantification of solutes through a more accurate and stable measurement (MENDELSON, 1995). Figure 44 compares spectra of blood samples with different glucose concentrations before (a) and after (b) baseline correction in 8.47 µm. As a result the peaks of glucose concentration at 9.66 µm can be better distinguished.

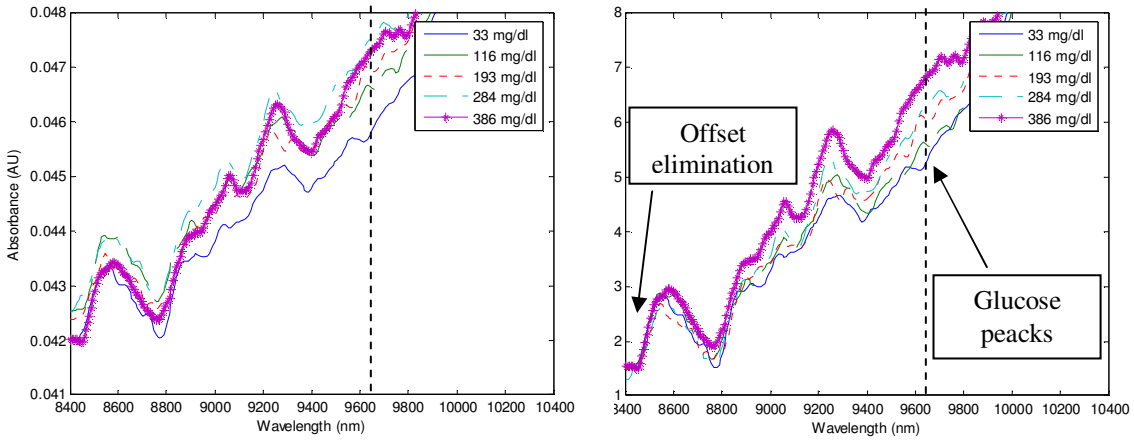

(a) (b)

Figure 44 – Example of blood spectra before (a) and after (b) baseline correction in 8.47 µm in order to increase analyte information in 9.6 µm.

6.2.3 Filtering

Digital fitering is a signal processing method used to remove specific frequency components from measured data. Low frequency errors in signal spectrum are mostly due temperature and instrument drifts, while high frequency noises are produced by substances overlapping and by measurement problems (HAM, COHEN, KOSTANIC *et al*, 1996; SMALL, ARNOLD, and MARQUARDT, 1993). Filters are appealing treatment, since this tool allows the control of the centre frequency and bandwidth, separating analyte information (DING, SMALL and ARNOLD, 1999). In Figure 45 a blood spectra with 181 points is processed by a 1st Order Butterworth bandpass filter with 25f and 0.25f cutoff frequencies. As a result the amplitude differences due to each glucose concentration can be better investigated in 9.79 µm.

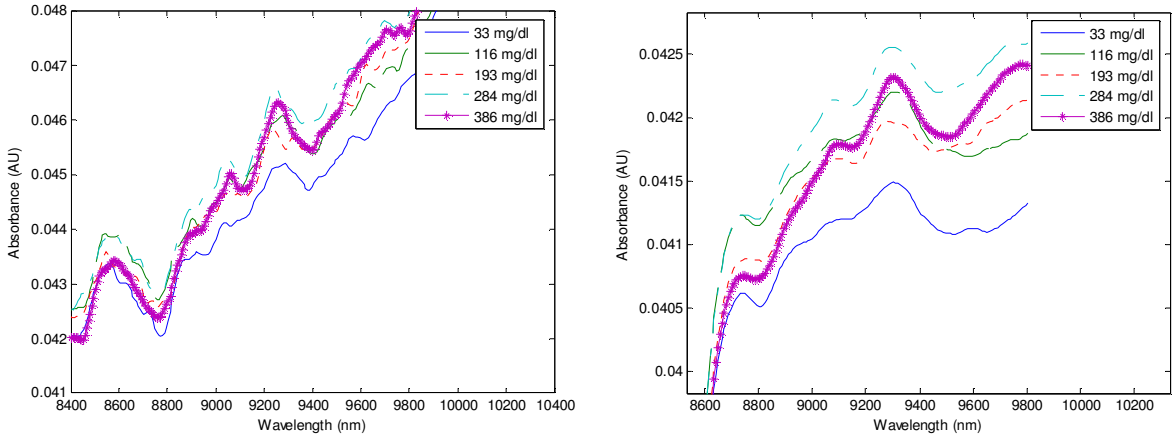

(a) (b)

Figure 45– Bandpass Butterworth digital filtering, the result curves (b) show better signal-to-noise ratio as the original (a).

6.2.4 Second Derivative

A derivative is the instantaneous rate of quantity change of a function, which can be used to characterize increasing or decreasing rate and maximum or minimum values. Figure 46 (b) shows the second derivate of the filtered signal (a), which decreases the amplitude and is very sensitive to signal variations.

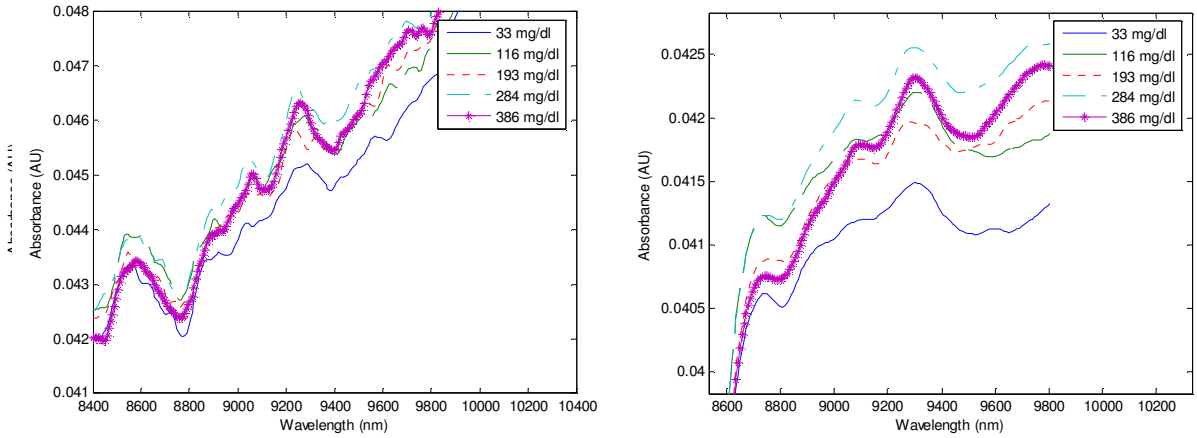

(a) (b)

Figure 46– Second derivative (b) of the filtered data (a), signal amplitude is decreased but signal variations are better observed.

The derivative spectrum retains proportionality to the analyte concentration, and therefore can still be used for quantification. Calculating the first derivative of the spectrum should lead to the removal of constant offsets, while the second derivative should solve both constant offsets and linear drifts in the spectrum. One disadvantage of this process is that the interpretation of the signal is difficult since the resulting spectrum is different from the original and can not return to the first characteristic (LEGER and RYDER, 2006).

6.3 PARTIAL LEAST SQUARES REGRESSION

6.3.1 Definition

Partial Least Squares regression is a bilinear calibration method which uses the concentration active during the decomposition of the spectrum in (Figure 47) in order to maximise the significance of the factors (latent variables) *T* and *Q*, which are included in the model and replace large unrelated input variations. The resulting model has few relevant dimensions (typically 5–15 loading vectors), which are enough to provide quantitation (SHAW and MANTSCH, 2000). Therefore, such regression is useful in cases where there are many variables available with redundancy and unknown relationship to the responses (SMALL, ARNOLD, and MARQUARDT, 1993).

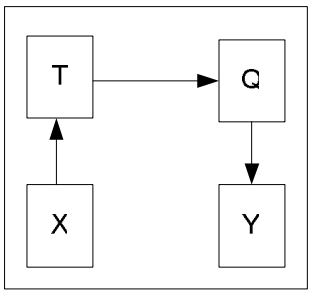

Figure 47 – PLS calibration matrix decomposition *T* and *Q*, which replaces large unrelated input variations (RANDALL, 1995).

Although numerous algorithms have been developed for calculating PLS parameters, all of them define the concentration of any analyte Y as result of the spectra matrix X multiplied by the regression coefficients matrix B, as seen in Equation 12.

$$Y = XB + E \tag{12}$$

where:

- Y is the concentration matrix;
- X is the spectra matrix;
- B is set of regression coefficients;
- E is the error matrix.

Usually, X and Y are centered by subtracting their means and scaled by dividing by their standard deviations. Then the algorithm decomposes each variable into the score of latent variables T and Q (Equations 13 and 14), chosen so that the relationship between successive pairs of scores is strongly correlated (SONG, JANG, CHO *et al*, 2004).

$$X = TW^{-1} \tag{13}$$

where:

- X is the spectra matrix;
- T is the X score matrix;
- W is the X loading (weight) matrix.

$$Y = TQ + E \tag{14}$$

where:

- Y is the concentration matrix;
- T is the X score matrix;
- Q is the Y loading matrix.

In Figure 48 a data set with two strongly correlated variables x1 and x2 can be changed to two orthogonal factors (latent variables) *t1* and *t2* that are linear combinations of

original descriptors. As a result, a single-factor model can be obtained that relates activity y to the first latent variable *t1*. This principle is the reason why the column size of the scores is much smaller than that of the original variables, therefore allowing dimension reduction (HAALAND and THOMAS, 1988).

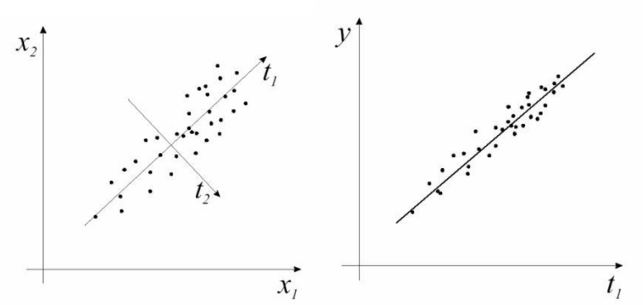

Figure 48 – Example of PLS dimension reduction where t_1 replaces x_1 and x_2 since they are strongly correlated (RANDALL, 1995).

Prediction is possible through a set of regression coefficients *B* that directly relates the centred/scaled *X* with the centred/scaled *Y*, as shown in Equation 15.

$$B = W.Q \tag{15}$$

where:

- *B* is set of regression coefficients;
- *W* is the *X* loading (weight) matrix;
- *Q* is the *Y* loading matrix.

Therefore, for a new sample X_{TEST} will predict Y_{PRED} concentrations as in Equation 16.

$$Y_{PRED} = X_{TEST} B \tag{16}$$

where:

- Y_{PRED} is the prediction concentration matrix;
- X_{TEST} is a spectra matrix;
- *B* is a set of regression coefficients.

6.3.2 Calibration

To obtain a reliable model, the quantification process is usually subdivided into training and prediction phases. In the training step a large dataset of random order, which covers as much of the concentration ranges possible, is loaded in the system input and the algorithm automaticly extracts the necessary characteristics to represent the given information (WANG, YAN, LIU *et al*, 2005). In this process, spectra and concentration measurements that do not fit with the rest of the dataset, called outlines, can be identified. These values may arise from different kinds of errors and may affect the future predictions. Once detected, the wrong data must be corrected or removed from the set. However, whenever possible one should try to understand the reason for every discrepancy. The validation of the prediction capacity of the PLS is important to determine the precision of the model, it is suggested that the size of the independent validation data should be at least a quarter of the training set, whith the difference being that the order of the information does not have influence in the response (FAUSETT, 1994).

6.3.3 Topology

The selection of an optimal number of factors (variables that change the spectrum such as glucose, temperature, etc…) is an important point in PLS. If the number of factors becomes too large the model will fit the samples perfectly, but will fail to predict new data (over-fitting), on the other hand under-fitting may lead to systematic errors. Only a few latent factors account for most of the variation in the response, therefore the root mean square error of cross validation (RMSECV), represented by Equation 17, can be calculated, allowing the analysis of the performance as a function of the number of scores (KANG, KASEMSUMRAN, WOO *et al*, 2006).

$$RMSECV = \sqrt{\frac{1}{N}\sum_{i=1}^{N}(Y_{TEST} - Y_{PRED})^2} \tag{17}$$

where:

- *RMSECV* is the root mean square error of cross validation;
- Y_{TEST} is the original concentration matrix;
- Y_{PRED} is the prediction concentration matrix.

6.4 ARTIFICIAL NEURAL NETWORKS

6.4.1 Definition

ANN is a non-linear statistical data modelling of biological neural systems that simulate mathematical functions such as complex relationships between inputs and outputs or data patterns. This adaptive system is divided in layers and interconnected through a great number of neurons or nodes, as shown in Figure 49 (DESPAGNE, and MASSART, 1998).

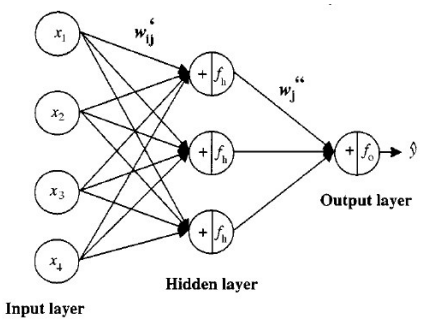

Figure 49 – Example of neural network topology with four inputs, one intern layer and one output node (DESPAGNE, and MASSART, 1998).

Each node is associated with a computational device that receives a number of input signals, associated with weights to represent stimulating or inhibiting influences. The projection of this sum is applied to a transfer function to produce activation of the neurons that is forwarded towards the nodes until it reaches the network output, as shown in Equation 18 (TRAJANOSKI, REGITTNIG and WACH, 1998).

$$\hat{y} = f_o\left[\theta'' + \sum_{j=1}^{nh} w_j'' f_h\left(\sum_{i=1}^{nd} w_{ij}' x_i + \theta'\right)\right] \tag{18}$$

where:

- y is the output signal;
- x is the input signal;
- w is the connection weight;
- f_o is the output transfer function;
- f_h is the hidden layer transfer function;
- θ'' is the output bias;
- θ' is the input bias.

The most important feature of the neural network approach is that any continuous function defined on a compact domain can be fitted with a pre-defined arbitrary degree of accuracy. In addition, the flexibility and ability to maintain a decent performance even in the presence of significant amounts of noise in the input increases the use of this tool in prediction, classification and control problems (WANG, YAN, LIU *et al*, 2005).

6.4.2 Calibration

ANNs require sets of training and validation data similar to PLS. Backpropagation is the most commonly used training algorithm because it improves the response of the network by adjusting the parameters by gradient-descent minimization of an error function, teaching the system to associate specific outputs with each of inputs. Adjustable parameters are the weights and biases that act as offset terms by shifting the transfer functions horizontally (FAUSETT, 1994). These values are first randomized between –1 and +1. The training starts by processing forward a set of samples of known response. At the end, the magnitude of the error between experimental and predicted responses is calculated and used to adjust all variables of the system, in a reverse step that finalizes an iteration or epoch. The repetition of this sequence with a large number of spectra of random order and wide concentration ranges will improve the relationship between x and y, enabling the ANN to produce reasonable output for unknown input. On the other hand, unnecessary interactions can lead to overfitting, therefore a stop criterion should be used. The decision rule can be either a maximal number of

epochs or a standard error of prediction (SEC), with a formula similar to RMSECV (LIN, HSIAO, ZENG *et al*, 1998).

6.4.3 Topology

Like biological neurons, a single neuron is not sufficient enough to perform a specific task. Therefore, the nodes have to be connected to another. The most widely architecture used is a multilayer perceptron (MLP), which requires a thorough understanding in order to achieve a satisfactory ability to generalize. There are numerous rules that give an indication of how large a neural network should be, most of them are based on the size of the train data set or the number of input and output nodes. If the total number of neurons is too small, the resulting neural network will not be able to accurately represent the train data and errors will be significant. On the other hand, a large number of nodes could lead to redundant paths, heavy processing algorithms and overfitting (LOBANOV, BORISOV, GORDON *et al*, 2001).

The number of input nodes are chosen by starting with a small number of variables and than adding new neurons one at a time until the prediction performance of the system does not improve any more. It is recommended that one response be evaluated for each model at a time and therefore a single output cell should be used. The only exception to this rule is for situations where one wants to predict several correlated responses, such as the concentrations of different constituents of a mixture in a closed system (DESPAGNE, and MASSART, 1998).

A neural network with only one hidden layer can approximate any function with any desired accuracy, as long as there are enough neurons in the hidden layer and that the activation functions are non-linear. One important advantage in this case is that the model obtained with one hidden layer is quasi-independent from the set of initial weights. However, for some functions the number of neurons needed between input and output can be very large. For this situation, a neural network with two hidden layers might have better performance. The disadvantage of more hidden nodes is that different sets of initial random weights can lead to different combinations of transfer functions to build empirical models. Therefore it is recommended to systematically reduce the number of hidden neurons as much as possible, in order to achieve simpler and more robust models (FAUSETT, 1994).

6.4.4 Transfer functions

The most commonly used nonlinear transfer functions in the hidden layer are the sigmoid or hyperbolic tangent (Figure 50) that are bounded, easily differentiable and exhibit a linear portion in their centre, so that data sets that are only slightly non-linear can also be modelled (DESPAGNE, and MASSART, 1998).

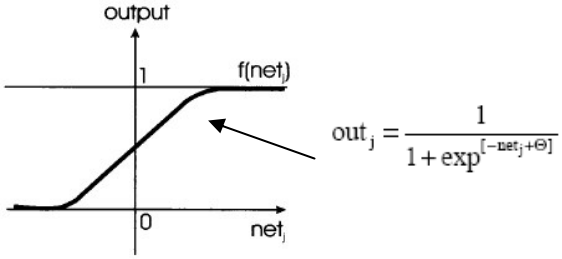

Figure 50 - Standard sigmoid transfer function of neuron.

6.5 EXAMPLES OF GLUCOSE QUANTIFICATION

There is a wide application range of calibration models in glucose assays, some of the important works with serum, whole blood and skin in ascending order of error are summarized in Table 10.

Table 10 - MIR and NIR spectroscopic determination of blood glucose.

Sample	Path length (mm)	Spectral regions (nm)	Pretreatment/Calibration	SEP (mg/dL)
Plasma	-	2000– 2500	Gaussian Bandpass filter (0.052f +-0.013f) PLS - 9 factors	7.27
Serum	0.39	1477 - 2498	Butterworth bandpass Filter (first-order) (0.15f +-0.1271f) PLS - 14 factors	13.2
Whole blood	ATR	8333 - 10526	PLS - 11factors	14.55
Whole blood	ATR	6666 - 13333	PLS 14 factors ANN - 1 hidden layer sigmoidal, output linear	15.6
Whole blood	ATR	6666 - 13333	ANN	16.36
Skin arm	-	1616–1733	PLS - 4 factors	17.19
Serum	ATR	2500 - 22222	PLS - 7 factors ANN – 1 hidden layer sigmoidal, output linear	18.7
Skin back of ear lobe	ATR	6666 - 10526	PLS - 6 factors	19.12
Whole blood	ATR	6666 - 13333	PLS - 16 factors	20
Serum	1	1373–1429, 1495–1545 , 1565–1696, 1790–1805	PLS - 8 factors	25.31
Whole blood	1	1515 -1818, 2062 - 2353	PLS - 8 factors	38..18

The parallel monitoring of more than one parameter can improve the sensibility of measurements in both invasive and non-invasive assays. Initial bloodless glycemic studies have already been reported with simultaneous measurement of bioimpedance and near-infrared spectroscopy in the skin (DING, SMALL and ARNOLD, 1999). Another example is the Glucotrack device from the company Integrity Applications, which is a commercial multiparameter monitoring device, where glucose is predicted with ultrasound, conductivity, and heat capacity. Therefore the following chapters study the parallel measurement of impedance and optic spectroscopy associated with PLS and ANN methods.

CHAPTER 7

MATERIALS AND METHODS

7.1 INTRODUCTION

In order to achieve significant results for impedance and light spectroscopy in non-invasive blood glucose detection, it is important to investigate which signal characteristics are optimal for this application and, at the same time, do not harm the patient. In the case of bioimpedance, the shape and material of the electrode may have significant influence over the results. Therefore, simulations of signal penetration in skin are performed, helping the choice of the transductor characteristics. The biomedical department from the Technical University of Munich has spectrometers available for measuring with electrical and optical technologies. The knowledge of the limitations from each device, also explained in this section, is essential to determine the confidence range of the read data. In addition, fast performance algorithms for treatment of the multivariate information are also found in this text.

Before explaining procedures for transcutaneous assays, the setup of glucose measurements in water and blood are described, which helps the analysis of skin tests, and also gives information for the improvement of invasive diagnostics. It is known that parameters like sweating, skin colour, surface roughness, tissue thickness, breathing artifacts, blood flow, body movements, ambient temperature, pressure and sample time all have influence in the results of transdermal monitoring analysis. Thus, the last part of this chapter corresponds to the description of *in vivo* investigations, taking in consideration the equipment limitations and safety, as well as variable factors of the measurement environment.

7.2 ELECTRODES

7.2.1 Liquid electrodes

Many layouts and sizes of electrodes are available to measure impedance of fluid and tissue. Interdigitated electrodes (IDES) offer high sensibility and wide surface scanning, and

are often applied in cell culture analysis to detect number, morphology and adhesion changes (EHRET, BAUMANN, BRISCHWEIN, *et al*, 1998). Due to the insulating behaviour of the lipid membranes, living cells increase the impedance of the system, especially the capacitive component. Some disadvantages of such structures are that the resulting impedance is sensitive to room temperature variations and therefore no tetrapolar assays can be performed. Figure 51 shows the design of platinum IDES in a glass base developed at the Technical University of Munich.

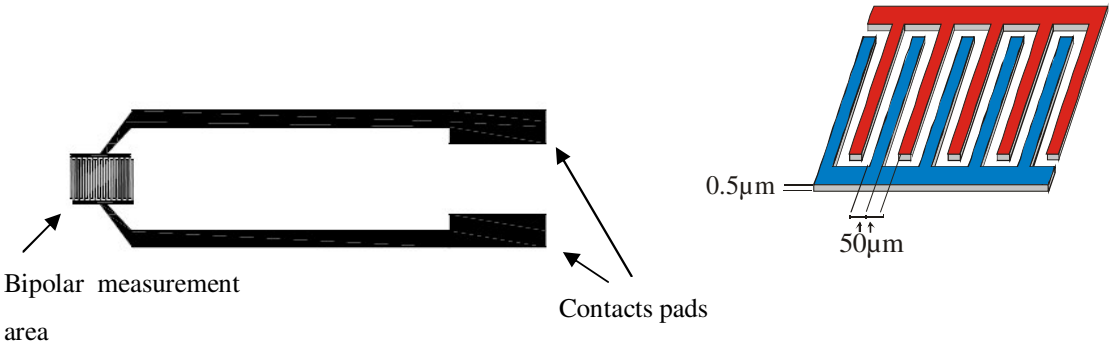

(a) (b)

Figure 51 – IDES (a) manufactured in the Heinz Nixdorf-Chair for Medical Electronics, the small dimensions of the electrodes (b) allows measuring cell proliferation rate.

The electrode configuration of Figure 52 is manufactured from a glass substract in order to investigate four point impedances. Like in IDES, the distance between each finger is 50 μm. The small size of the sensor and tracks produces low parasite capacitance, and allows the measurement of high frequencies.

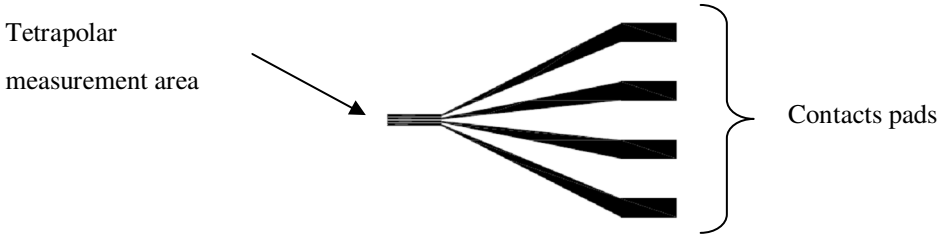

Figure 52 – Tetrapolar layout for liquids tests, the size of the sensor as well as tracks were designed in order to have low reactance in high frequencies.

7.2.2 Skin electrodes

Since the epidermis does not contain strong glucose information, superficial current densities produced by IDES are not distributed enough to allow non-invasive measurements, therefore a greater distance between the electrodes is required. Many applications of skin impedance use concentric electrodes approaches, such as in Figure 53. This configuration is less sensitive to interferences from temperature variations and produces symmetric electric fields between the contacts, avoiding the accumulation of high electric gradients due to corner effects.

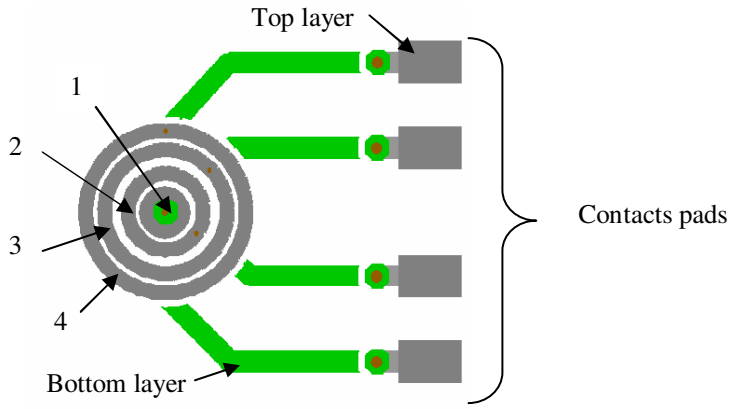

Figure 53 – Concentric tetrapolar configuration used for skin tests. The symmetric electric fields avoid the accumulation of high electric gradients due to corner effects.

A computer simulation of a circular layout in Femlab with 5 millimetres diameter and gold contacts is shown in Figure 54. The potential distribution when applying a 100 mV (250 kHz) signal proves that the electrical current crosses the subcutaneous layer and reaches high vascularized tissues, and thus allows for monitoring of blood analytes.

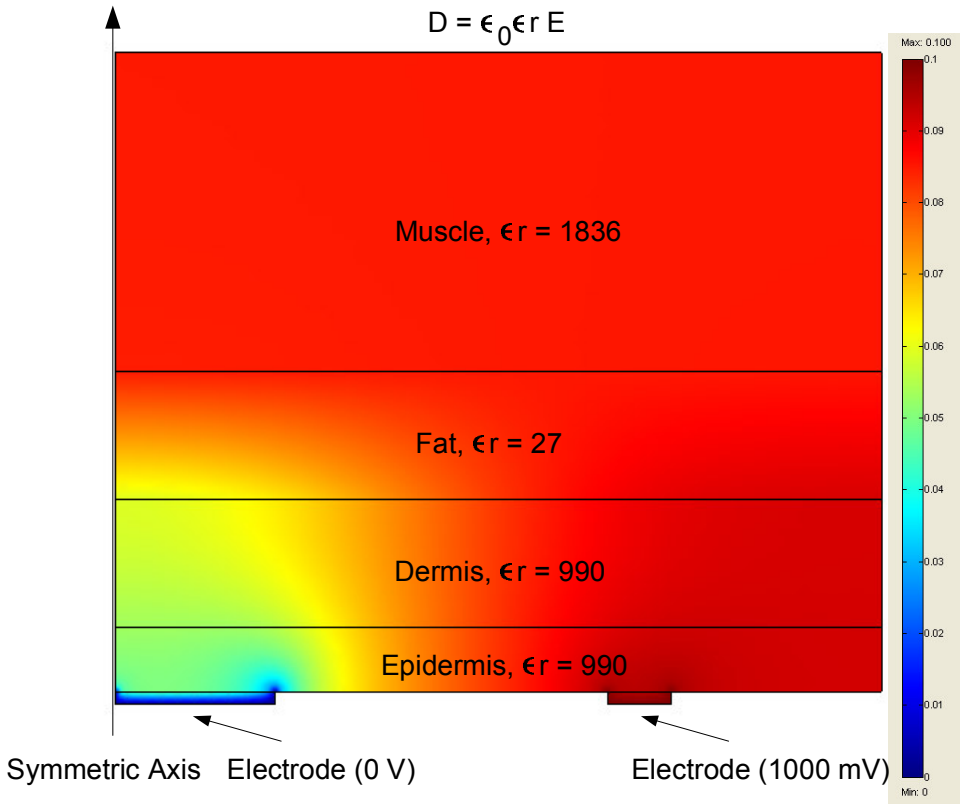

Figure 54 - Distribution of the potential difference in cross section of skin with 100 mV (250 kHz) signal applied through a bipolar sensor. Electrical current is able to cross superficial layers and penetrate in deep tissues with higher glucose concentration.

7.3 IMPEDANCE INSTRUMETATION

The Heinz Nixdorf-Chair for Medical Electronics supported this project with two complex impedance devices that cover the range from μHz up to GHz. The specifications of both equipments are resumed in the following section.

7.3.1 Solartron 1260

The Solartron 1260A impedance/phase analyzer, seen in Figure 55, is able to perform measurements from mΩ until MΩ of modulus, phase, resistance and reactance in bipolar or tetrapolar approaches. Although this device allows the control of current levels, experimental

results showed instability in this configuration. Therefore all tests were done monitoring the voltage amplitude, which can variate from 20 mV until 3 V in frequencies from 10µHz to 32MHz.

Figure 55 – Solartron 1260A analyzer, able to measure complex impedance from 10µHz to 32MHz (SOLARTRON ANALYTICAL, 2004).

The control of this instrument can be performed either through the front panel or remotely with the supervision software ZPlot, illustrated in Figure 56. It is important to note that, whenever only alternated signals are desired, the field DC Potential should be "0" and coupling "AC". Tetrapolar investigations require the setting of the field Input to "Differential".

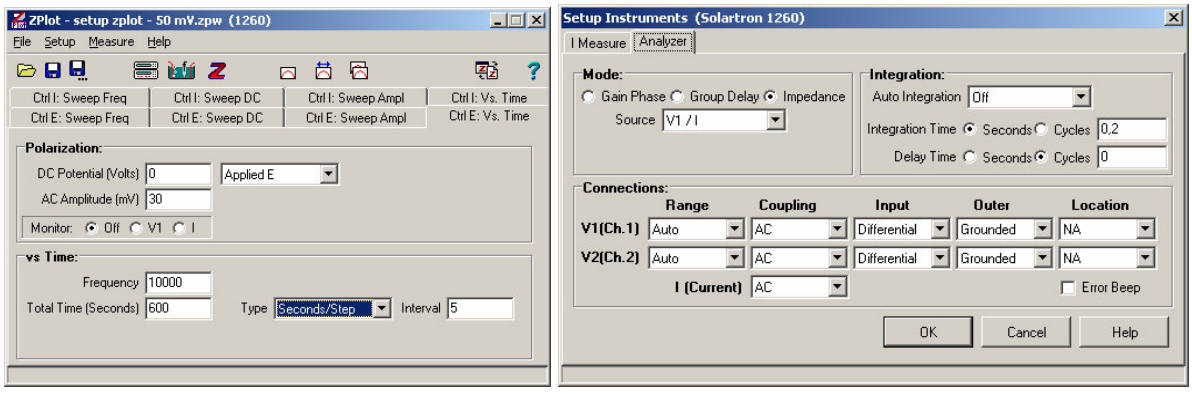

(a) (b)

Figure 56 – Zplot main window (a) and typical instrument setup (b), whenever only alternated signals are desired the field DC Potential should be "0" and coupling "AC".

The measurement results can be seen and processed in the program ZView, which besides showing the curves of the impedance, dielectric and permittivity, can also calculate equivalent circuits that fit the read data. Whenever high frequency assays are desired, the

calibration of the equipment must be done through a nulling procedure (SOLARTRON ANALYTICAL, 2004).

The instrument performance in high frequencies suffers strong influence from the cabling, which should have coaxial characteristics and preferentially short lengths. The Solartron requires that all cable outer wires are connected to each other, as close as possible to the sample, avoiding noises in MHz ranges.

7.3.2 Network analyzer

Figure 57 shows the vector network analyzer ZVCE from Rohde and Schwarz, this impedance spectrometer is able to measure complex transmission and reflection characteristics of two-port devices in the frequency domain from 20 kHz until 8 GHz. The device can simultaneously display up to four traces with independent parameters, which can be scanned in rates of up to 25 sweeps per second from 1 mV to 250 mV. The measurements can be saved on floppy disks or transmitted to the computer via the network cable. Similar to the Solartron, the ZVCE requires a calibration process in order to read the correct parameters from the device undergoing the testing (ROHDE & SCHWARZ, 2004). Some drawbacks of this instrument are the low input impedance and limitation of measuring only two point loads.

Figure 57 - Vector network analyzer ZVCE from Rohde and Schwarz, able to measure bipolar samples from 20 kHz until 8 GHz (ROHDE & SCHWARZ, 2004).

7.4 OPTIC INSTRUMENTATION

Many research works have focussed on glucose measurement in ranges from the visible up to middle-infrared wavelengths. In order to investigate these spectrums two optic devices of the Central Institute of Medical Engineering (IMETUM) at the Technical University of Munich were used.

7.4.1 The UV/VIS/NIR Spectrometer

The Specord 210 from Analytik Jena (Figure 58) is a dispersive device that can measure ultraviolet (UV), visible (VIS) and the beginning of infrared (IR) through two light sources. The spectrometer requires a remote control powered by the software Winaspect, which is able to calculate baseline correction, curves subtraction, convolution, etc… The supervision computer is connected to the measurement instrument through an USB cable.

Figure 58 – UV/VIS/NIR Spectrometer Specord 210 from Analytik Jena, which uses dispersive principle to scan samples in quartz cells (ANALYTIK JENA, 2004).

As shown in Figure 59, a beam of light is separated into its component wavelengths by a prism or a diffraction grating. Each double monochromatic wavelength passes through a small transparent cell of quartz Suprasil. One cell contains a solution of the compound being studied in a transparent solvent (1 mL), the other reference beam crosses an identical bottle containing only the solvent. The intensities of these lights are then measured by electronic detectors and compared. The Specord 210 spectrometer is able to measure spectra of samples in the range from 190 nm up to 1100 nm with resolution of 1 nm (ANALYTIK JENA, 2004).

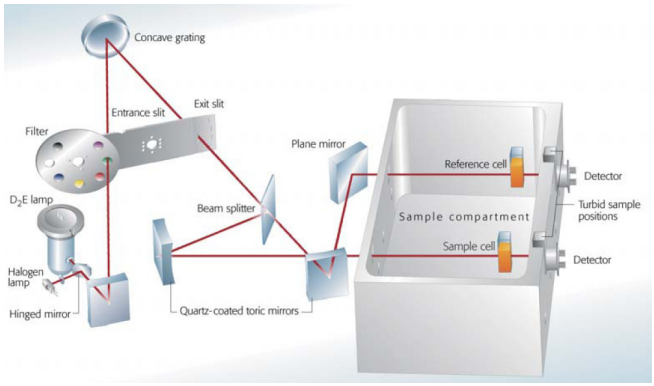

Figure 59 - Measurement principle of UV/VIS/NIR spectrometer, which compares the signal intensities of the sample and the reference cell (ANALYTIK JENA, 2004).

7.4.2 FTIR spectrometer

Most of the infrared information was collected with the Spectrum One FT-IR Spectrometer from the company Perkin-Elmer Instruments, shown in Figure 60. This equipment is built with a deuterated triglycine sulphate detector and measures probes with an ATR accessory, which simplifies the analysis of solids, powders, pastes, gels and liquids. This instrument can measure with 1 cm^{-1} (cm^{-1} = 10000000/nm) resolution from 1282 nm to 28571 nm, but due to the ATR module, the spectrum decreases from 2000 nm to 28571 nm (PERKIN-ELMER, 1998). Before each sampling a background measurement should be done in order to eliminate interference from the local light. The setup of the Spectrum One and the visualisation of the optic spectra are done in the program Spectrum V5.0, which also offers tools for baseline correction and is installed in the same PC as Winaspect.

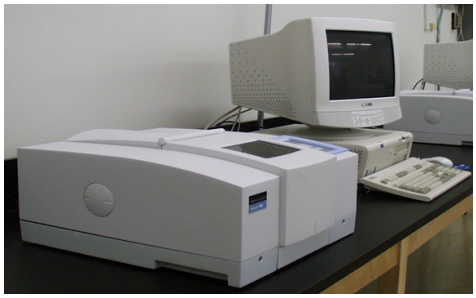

Figure 60 – FTIR spectrometer and supervision computer, this device does not require the use of reference, since it can collect background spectra of the ambient light (PERKIN-ELMER, 1998).

7.5 DESCRIPTION OF MEASUREMENTS

Despite the great number of publications concerning glucose spectral characteristics, there seems to be a disagreement among researchers concerning the optimal site and wavelength/frequency for non-invasive monitoring. Therefore, before transcutaneous measurements are made it is necessary to investigate optical and electrical characteristics of this substance. Liquid samples (volume of 1 mL for Specord 210 and 20 μL for the other devices) were placed in the sensors with a pipette after having their temperature equilibrated to the room conditions. In all fluid assays, each sample scan was only repeated after all other available concentrations had been measured. This allowed the monitoring of possible time drifts in the instrument response. In order to remove any possible residue from the previous series, after measuring the sample with maximal concentration, the test cell, ATR plate and electrodes were washed several times with distilled water.

First, the experiments were carried out using distilled water mixed to different glucose concentrations with the purpose of identifying the relevant bands for analysis, as well as examining the sensitivity of the instruments. After studying aqueous solutions spectra, the best wavelengths and frequencies were compared to blood tests. In addition to correlation results, the choice of best spectral range was also done taking in consideration light penetration depth in biological tissues. Finally non-invasive data were collected using the FTIR spectrometer and impedance devices.

The focus of the research was to demonstrate the technique at constant temperature, thus all measurements took place at 21.5 (+-0.5) degrees Celsius in the laboratory of IMETUM. The Solartron spectrometer requires one minute scanning the range from 100 Hz to 30 MHz (5 points per decade) with 50mV AC for liquids and 500 mV AC to skin. On the other hand, the network analyzer sweeps 101 logarithm frequencies between 20 kHz and 8 GHz in 2 seconds, applying a voltage of 50 mV AC for liquids and 250 mV AC to skin. The Specord 210 range reached from 300 nm to 1100 nm, recording each spectrum 19 times in one and half minutes with a resolution of 1 nm. All light spectra of probes in FTIR were scanned 16 times each, in order to decrease measurement error, and with a resolution of 1 cm^{-1}, taking approximately one minute for measuring from 2000 nm to 28571 nm. Another important procedure to improve Spectrum One experiments was the use of dark covers in the ATR during background and scans, this addition significantly decreases noises due to room light fluctuations.

7.5.1 Preparation of aqueous samples

Distilled water in bottles of 50 mL was mixed with D-glucose powder 30 minutes before starting the measurements at room temperature. The solute was purchased from the company Merck, and its concentration was controlled through a sartorius microbalance with 4µg precision. Since the sugar quantity does not change significantly in aqueous solutions with time, no extra control was realized.

7.5.2 Preparation of blood samples

The assays used heparinized whole blood samples that were collected several hours before measurements from a healthy male subject 29 years old. The samples were first mixed to have the same concentration of anticoagulant, and then distributed in bottles of 5 mL. Distilled water (100 μL) containing different quantities of D-Glucose were added to each probe, and for 30 minutes before starting of measurements, were kept in movement at room temperature. The direct addition of glucose in blood was avoided since this powder dissolves slower in the plasma than in aqueous form. Due to the small volume of water added, one can assume that blood characteristics were not significantly affected, resulting only in variations in the concentration of the analyte of interest. Nevertheless, these values were not constant during assays for blood cells consume glucose continuously due to their metabolism. Therefore it was necessary to control sample concentrations before each scan with a standard blood glucose meter (Accu-Check Sensor from the company Roche Diagnostics).

Whenever blood is not in movement, the cells aggregate in the bottle of the container and only plasma remains in the superficial layers, to avoid this effect, during the whole assays, the probes were slowly mixed. In order to eliminate any contamination, after the end of the experiment, all contact surfaces were disinfected with 70 % alcohol, aqueous solution of 1 % mucocit and finally water.

7.5.3 Impedance assays with fluids

Initial tests with glucose aqueous solutions showed that the impedance spectroscopy has low sensibility to detect variations in the solute concentration when there is no cell metabolism present. In order to determine the spectral correlation of glycemic solutions, samples of distilled water without glucose and with concentrations of 0mg/dL, 25 mg/dL, 50 mg/dL, 100 mg/dL, 200 mg/dL, 400 mg/dL and 800 mg/dL were measured 9 times each in the tetrapolar electrode, connected to the Solartron with 4 centimeter coaxial cables.

Impedance assays with blood probes are important since it is expected that blood cells use glucose as a source of energy, increasing the metabolism and concentration of ions in the liquid. The scans should be done as fast as possible to avoid the effect of cells accumulating on the electrode surface. The samples were measured 16 times each in both spectrometers. The tetrapolar electrode was connected to the Solartron with 4 centimeter coaxial cables and the IDES was connected with port 1 of the network analyzer through similar wires, as well. Short connections were used in order to avoid cable capacitance in high frequency signals. Whole blood concentrations of 77 mg/dL, 150 mg/dL, 200 mg/dL, 300 mg/dL, 400 mg/dL and 1000 mg/dL were investigated.

7.5.4 Optic assays with fluids

Two aqueous glucose measurements with light were done, the first one with high glycemic concentrations and the second one with physiological levels. Due to the wide path deep of quartz cells it was not possible to measure high glucose samples in the Specord 210, but in only FTIR. Reference probes were prepared with 5000 mg/dL of glucose. The solute spectrum could than be obtained in Spectrum One by subtracting this data from pure water results. The probe preparation is similar to the impedance tests, differing only in concentrations from 25 mg/dL to 800 mg/dL for UV/VIS/NIR Spectrometer and to 400 mg/dL for FT-IR spectrometer. The measurements in the Specord 210 were done in a quartz Suprasil cell. After taking the background spectrum, six solutions with glucose concentrations of 25 mg/dL, 50 mg/dL, 100 mg/dL, 200 mg/dL, 400 mg/dL and 800 mg/dL were scanned in the UV/VIS/NIR spectrometer. Similar probes were analyzed in the ATR spectrometer, with

the difference that this instrument requires a background calibration with a dark cover before each sample scan. Glucose concentrations from 25 mg/dL, 50 mg/dL, 100 mg/dL, 150 mg/dL, 200 mg/dL, 250 mg/dL, 300 mg/dL, 350 mg/dL and 400 mg/dL were scanned in this device, in the region between 2000 nm and 28571 nm with Spectrum One.

Blood assays were also realized with concentrations of 50 mg/dL, 75 mg/dL, 100 mg/dL, 125 mg/dL, 150 mg/dL, 200 mg/dL, 250 mg/dL, 300 mg/dL, 350 mg/dL, 400 mg/dL and 700 mg/dL. Based on the previous results from water experiments, the spectrum range from blood tests was focused between 3333 nm and 9600 nm.

7.5.5 Non-invasive assays

Transcutaneous assays were realized with Solartron and the network analyzer for impedance and the FTIR for IR scanning. Measurements took place in the laboratory of IMETUM as well, with controlled humidity (31 % - 32 %). A total of 132 impedance and optical spectra were obtained in a 15 hour period. Procedures were repeated with a 7 minute interval in order to avoid strong changes in skin temperature due to contact with the optic plate.

The volunteer, a healthy 29 years old individual, fasted 10 hours before the procedure and, during the test drank water with 75 g glucose at 11:42 AM, 05:25 PM and 10:12 PM (measurement indexes 16, 65 and 106). Glycemic levels ranged between 58 mg/dL and 115 mg/dL, been controlled through a lancing device Accu-Check Sensor from Roche. All fingers were alternately used to obtain glucose levels with the exception of the thumbs and non-invasive test sites.

Optical spectra from 2500 nm until 15384 nm were scanned with 16 repetitions during one and half minutes in the ATR module of Spectrum One. Before each reading, a background spectrum was collected, avoiding errors due to long term light fluctuations. Chen group in 2005 wrote that changes in the optical properties of tissue could be caused by variable contact pressure between the probe and skin. This is confirmed in Figure 61, where the higher the pressure in the sample, the stronger the absorbance. In order to avoid errors due to changes in pressure and room illumination, a dark chamber with a mechanical arm was added to the ATR module, as shown in Figure 62. In addition to light spectrum, cutaneous temperature was also monitored with contact and infrared thermometers.

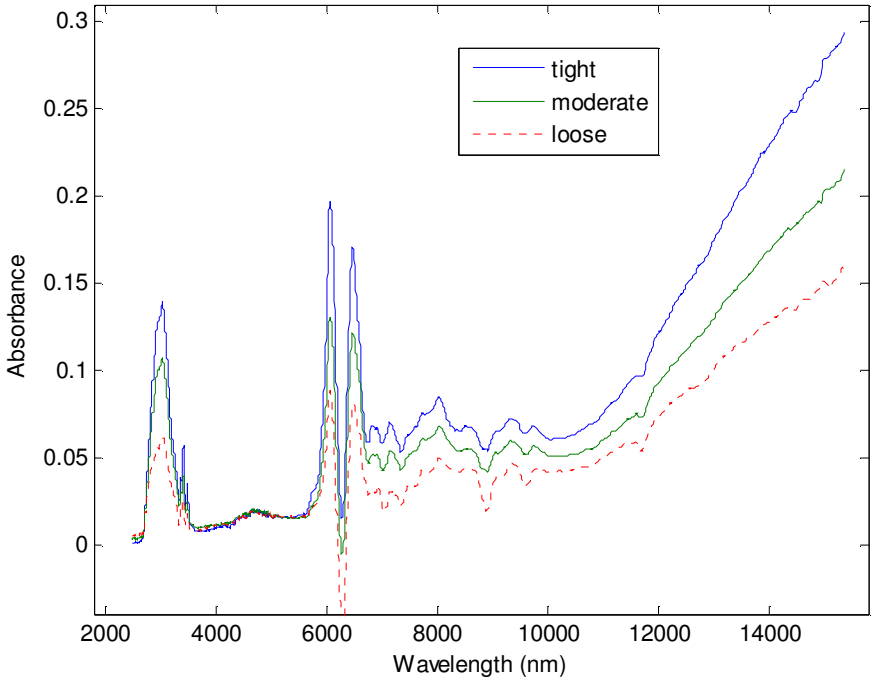

Figure 61 – Pressure effect in finger absorbance spectra, the higher the pressure in the sample, the stronger the absorbance.

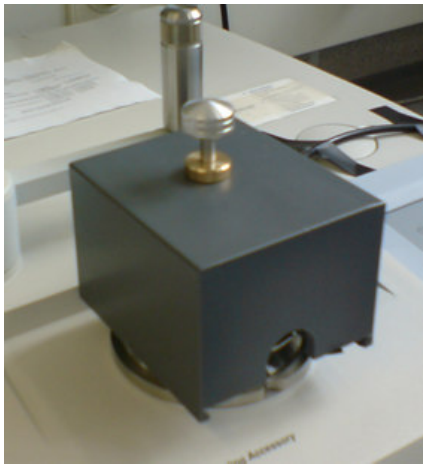

Figure 62 - Dark chamber for transcutaneous measurement of fingertip with pressure arm.

The concentric skin electrode was connected through 4 centimeter coaxial cables in port 2 of the network analyzer. Because this equipment can only measure bipolar loads, the electrodes 1 and 2 were connected to the external contact of the coaxial cable, while 3 and 4 conducted the internal signal. Complex impedance spectra were collected with this instrument in the range from 20 kHz to 8 GHz, with a signal of 250 mV.

Tetrapolar measurements were done in the Solartron 1260, with frequencies from 100 Hz to 30 MHz and amplitude of 500 mV. The current flowed between the external and internal electrode, while the resulting potential was measured in the contacts 2 and 3. Coaxial cables 10 cm long were used to connect the transducer to the measurement device. As in optical assays, pressure arms were used to maintain constant measurement conditions in both impedance instruments. Metal pieces next to the electrodes were avoided since high frequencies can produce parasite currents in such objects. Since the impedance equipment required short cables, as shown in Figure 63, the scanning of impedance and light simultaneously was not possible. Therefore, each spectrometer had to be used in different turns during a 4 minute interval, as shown in the sequences of Table 11. Such delay did not result in significant errors since glucose levels change slowly and can be corrected through algorithms. The change in measurement site also helped the normalization of blood circulation in the finger extremities.

Figure 63 – Measurement setup, each spectrometer had to be used in different turns during a 4 minute interval.

Table 11 – Non-invasive measurement steps, with target site, procedures and duration.

Sequence	Site	Procedure	Duration (s)
1	ring finger (right hand)	IR temperature control	10
2	ring finger (right hand)	impedance spectrum measurement in Solartron	40
2	middle finger (right hand)	conductance temperature control (parallel to impedance in Solartron)	40
3	-	background in FTIR	90
4	ring finger (right hand)	impedance spectrum measurement in network analyzer	15
5	others fingers (except thumbs)	reference glucose level control	30
6	ring finger (left hand)	absorbance spectrum measurement in FTIR	90

7.6 DATA TREATMENT

Both Spectrum V5.0 and Winaspect limited the number of measurements that could be analyzed simultaneously, and therefore the matrices with glucose, wavelength, time and absorbance data were imported in Matlab v 7.0 (The MathWorks, USA), where all the pre-processing, PLS, neural network and statistical analysis were done. With the exception of PLS scripts, obtained from Professor Lars Nørgaard from the Department of Food Science at the Royal Veterinary and Agricultural University in Copenhagen, all the other treatments were done with the available toolboxes from the MathWorks packet on a computer with Duo 1.66 GHz CPU (Intel, USA) and 1 Gigabyte SDRAM, running Windows XP.

7.6.1 Baseline correction

Algorithms for polynomial fitting were written to allow baseline correction in one or two points (line). In addition, procedures for normalization were implemented in order to reduce temperature and pressure effects. Although the shifting of offset level is easily implemented, the analysis of the optimal point requires the calculation of all possible combinations, therefore, spectra with 3500 wavelengths can take approximately 30 minutes of processing in the computer. The visualization of the results is also one important task that consumes memory and time.

7.6.2 PLS

Partial least squares were used to select relevant spectral regions of optical measurements and to compress it into a smaller number of principal components, used either to predict the analyte directly or as input to the ANN. The models were created through the iToolbox for Matlab, whose main methods are interval PLS, backward interval PLS, moving window PLS and synergy interval PLS (LEARDI and NØRGAARD, 2004). To obtain the optimal number of latent variables, each possible factor was analyzed separately with a

resolution of 5 wavelengths. The models with the lower SEP were then chosen to predict a test set of 32 samples. The test set was selected from all the measurement ranges, avoiding errors produced by time and temperature fluctuations.

7.6.3 Neural networks

The neural network structure was a one hidden layer backpropagation ANN with a sigmoidal activation function and the Levenberg–Marquardt update algorithm. The number of nodes in the hidden layer was varied between 1 and 15. The minimum error gradient was also analyzed, with an interval from 0.1 to 10 E^{-6}, and the maximal number of epochs was 100. The dataset was scaled between 0 and 1 together and then separated into training and test components, with the same distribution as the PLS treatment. Feed forward neural networks were trained randomly to model the blood glucose as output, using functions from the Neural Networks Toolbox for Matlab.

CHAPTER 8

RESULTS

8.1 INTRODUCTION

The following chapter describes measurements of the tested fluids and transcutaneous assays with statistical analysis and regression methods. Glucose aqueous assays were required in order to determine the best fingerprint range of this substance. After analysis of this spectrum, blood tests helped to confirm whether other confounding substances could interfere in the efficiency of the methods. Finally non-invasive experiments showed that, although there is difficulty in crossing the skin barrier, the frequencies chosen could still give promising results.

8.2 IMPEDANCE ASSAYS WITH FLUIDS

8.2.1 Solartron spectrum of glucose in water

The use of pretreatment methods does not significantly improve the impedance quantification since the spectra of all four complex components do not have strong peaks. The first analysis of the electrical results compares the correlation influence with signal frequency in aqueous glucose. In Figure 64, the frequency of 15.84 kHz shows higher correlation for the impedance phase (0.55) than the remaining parameters. Figure 65 compares the phase spectra of water with different glucose levels, as a function of the scanning frequency in the Solartron. The signal oscillation, especially at high frequencies, may be one reason for the lack of stability in the performance of this system. Based on the best correlation for θ, predicted glucose concentration is compared with the reference value in Figure 66. This test performance results in a high SEP of 387 mg/dL and standard deviation of 516 mg/dL.

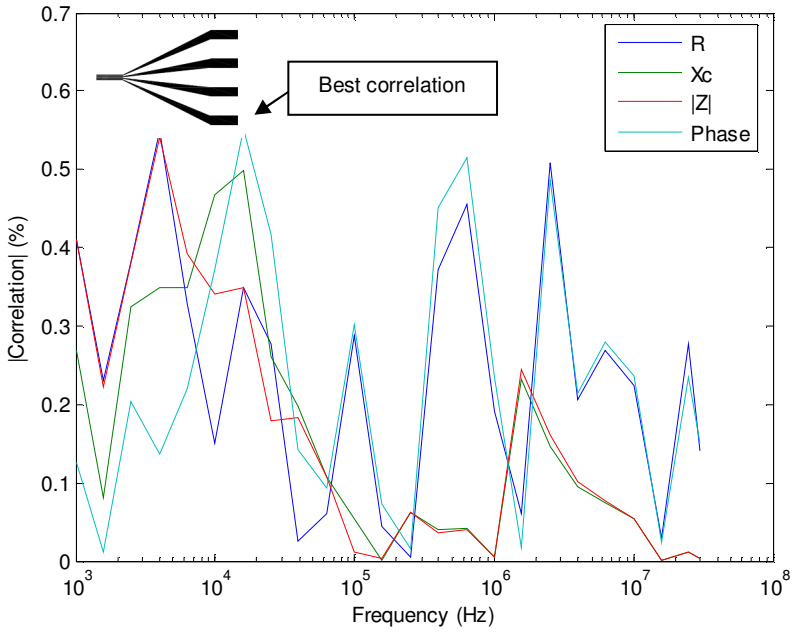

Figure 64 - Correlation spectrum between impedance and glucose of aqueous samples measured in Solartron with a tetrapolar electrode, the highest module is found for the phase in 15.84 kHz. Due to the oscillating response it is difficult to determine a pattern.

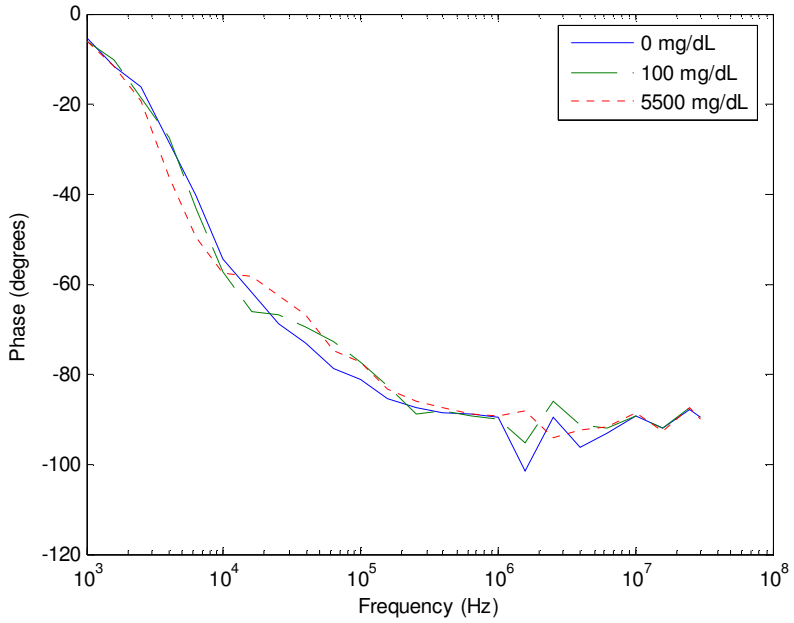

Figure 65 – Phase spectra of water with glucose in the tetrapolar electrode (Solartron), the lack of ions in the sample causes mostly the measurement of electrode characteristics.

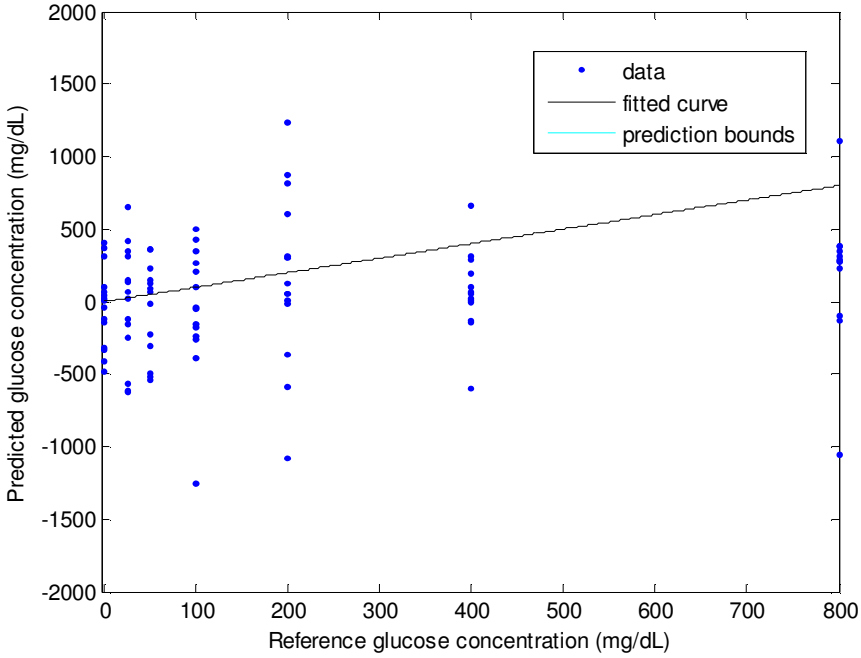

Figure 66 – Glucose prediction with phase information in 15.84 kHz versus reference concentration in water-glucose solutions.

8.2.2 Solartron spectrum of glucose in blood

Blood samples with different glucose concentrations were analyzed in both impedance spectrometers as well. The maximal correlation for the spectrum without treatment is 0.67, which uses the reactance data at 10 MHz (Figure 67). In Figure 68, the higher the frequency, the greater the difference between each spectra of *Xc*. After 10 MHz this effect seems to decrease, also reflecting low values for the correlation. Based on the best result for the imaginary component, predicted glucose concentration is calculated, resulting in the graph in Figure 69. Such performance shows that blood samples in tetrapolar electrodes could reflect glycemic changes better than water, with a SEP of 249 mg/dL and a standard deviation of 156 mg/dL.

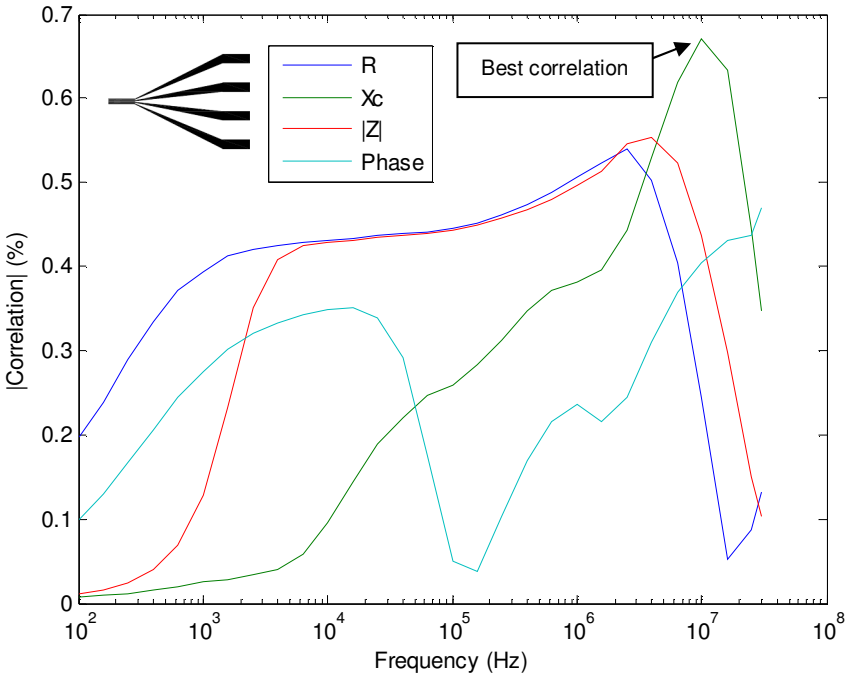

Figure 67 - Impedance correlation spectrum of blood samples measured in Solartron with a tetrapolar electrode, the highest value is found at 10 MHz for the reactance.

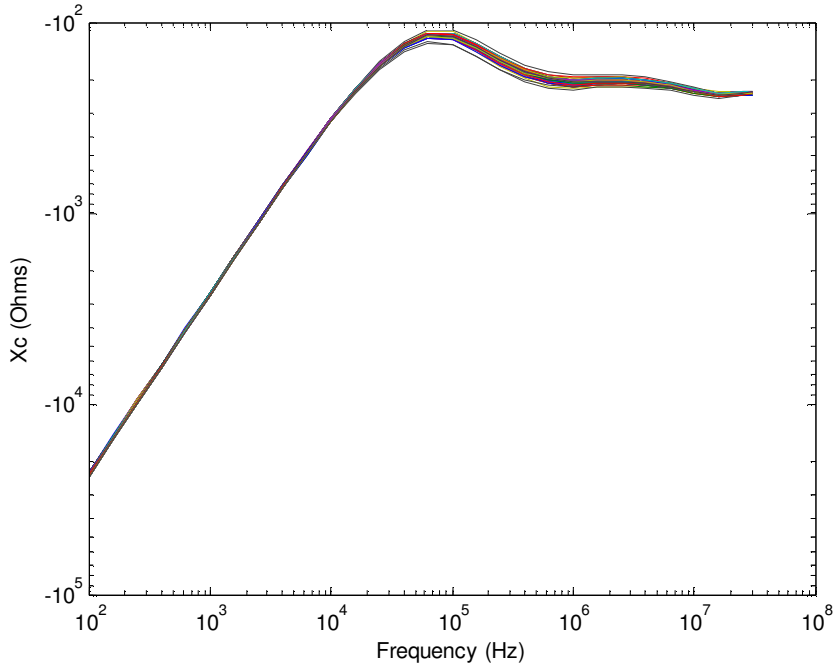

Figure 68 – Reactance spectra of blood with glucose in tetrapolar electrode (Solartron), significant differences between the samples are observed in the interval from 100 kHz to 10 MHz.

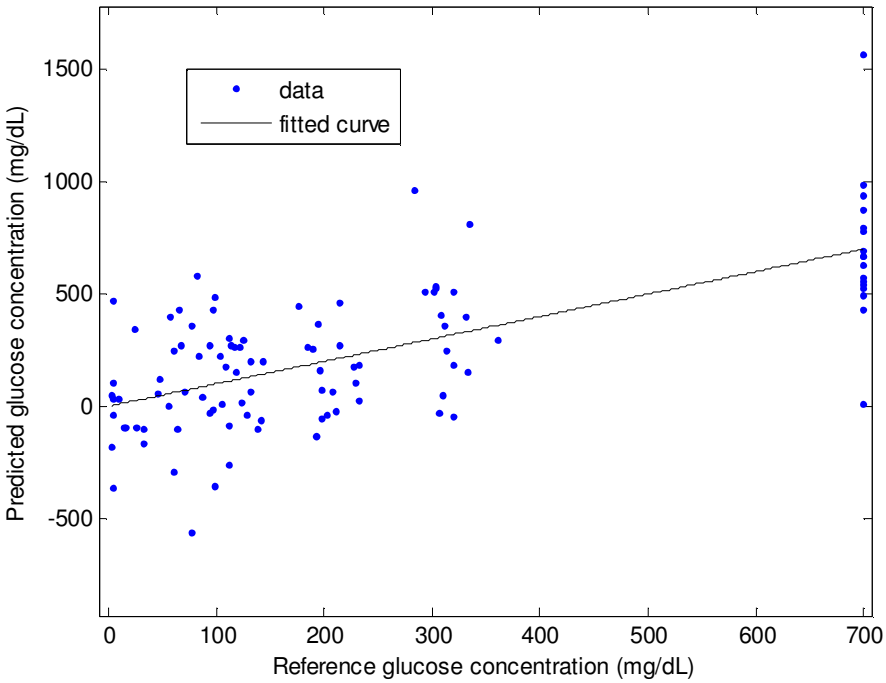

Figure 69 – Glucose prediction with *Xc* data in 10 MHz versus reference values in blood samples.

8.2.3 Network analyzer spectrum of glucose in blood

Measuring blood with IDES in the network analyzer, the maximal correlation in the raw data is 0.43, observed for the modulus at 166.9 MHz (Figure 70). For frequencies higher than 500 MHz the prediction response decreases. In Figure 71 the spectrum of the impedance modulus is shown, where for higher frequencies the signal suffers strong interference from noises. Based on the best correlation result for the imaginary component, predicted glucose concentrations can be calculated resulting in the graphic shown in Figure 72, whose performance has 474 mg/dL of SEP and 300 mg/dL of standard deviation.

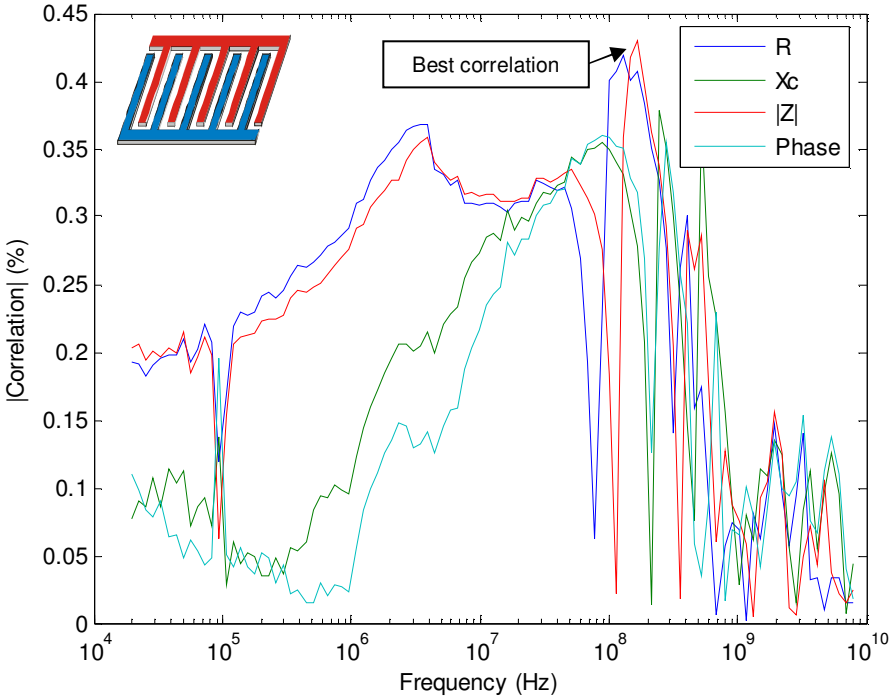

Figure 70 - Impedance correlation spectrum of blood samples measured in the network analyzer through IDES, in the first four decades, the magnitude of all parameters seems to increase with the signal frequency. The highest value is found for|Z| component at 166 MHz.

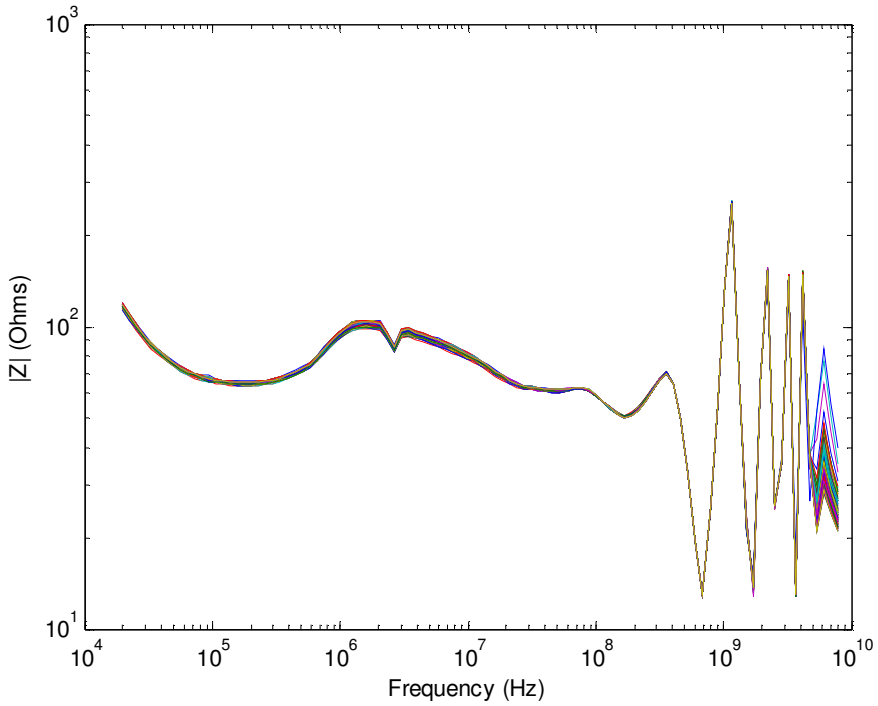

Figure 71 - Modulus spectra of blood with different glucose concentrations in IDES connected to the network analyzer. High frequency noise can be seen after 300 MHz.

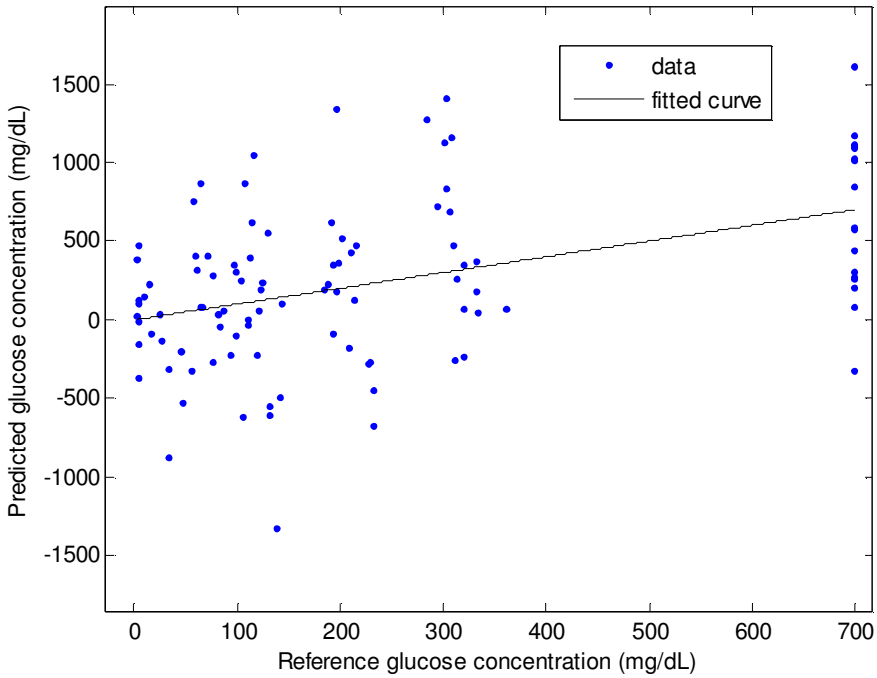

Figure 72 - Glucose prediction with |Z| component at 166 MHz compared with reference levels in blood samples.

8.3 OPTICAL ASSAYS WITH FLUIDS

8.3.1 Specord 210 spectrum of glucose in water

The first analysis of the results tried to reduce temperature and instrument fluctuations, through the elimination of offset differences in one specific wavelength (baseline correction). This calculation was repeated for all available points, which required approximately 30 minutes of processing in a computer with a Duo 1.66 GHz CPU and 1 Gigabyte SDRAM. In Figure 73, the Specord measurements of glucose in water showed an optimal wavelength for baseline correction in 972 nm. After treating all spectra, 960 nm was the wavelength with higher correlation (0.91), as seen in Figure 74. In Figure 75 one can see the absorbance spectrums that result when all samples are normalized in 972 nm. The best correlation absorbance predicts the glucose concentration as shown in Figure 76, with a SEP of 125.57 mg/dL and a standard deviation of 66.32 mg/dL.

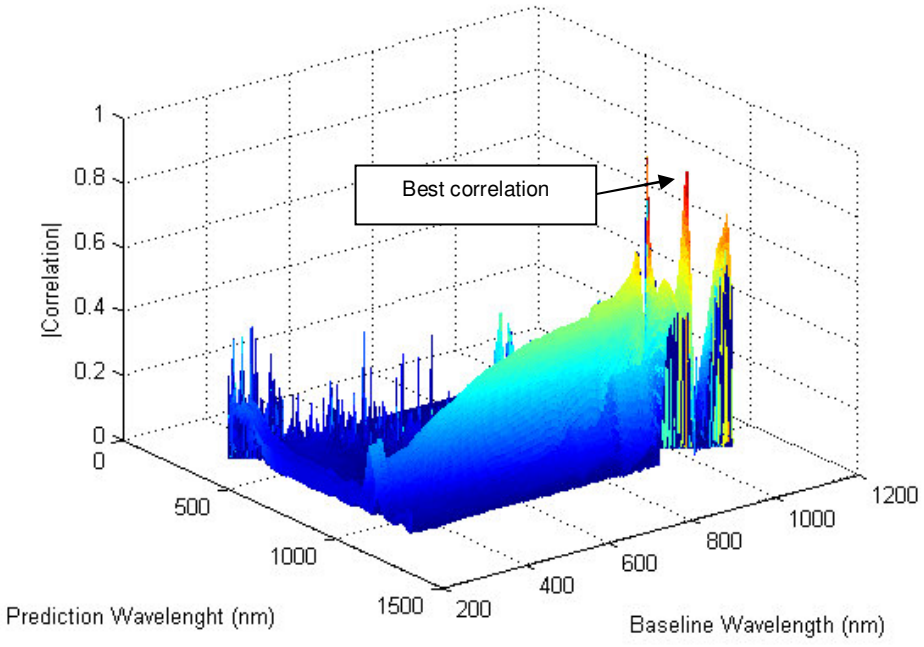

Figure 73 - 3D analysis of optimal value for baseline correction of water samples in Specord 210. The highest peak in the baseline axis corresponds to 972 nm, while 960 nm shows the best prediction performance.

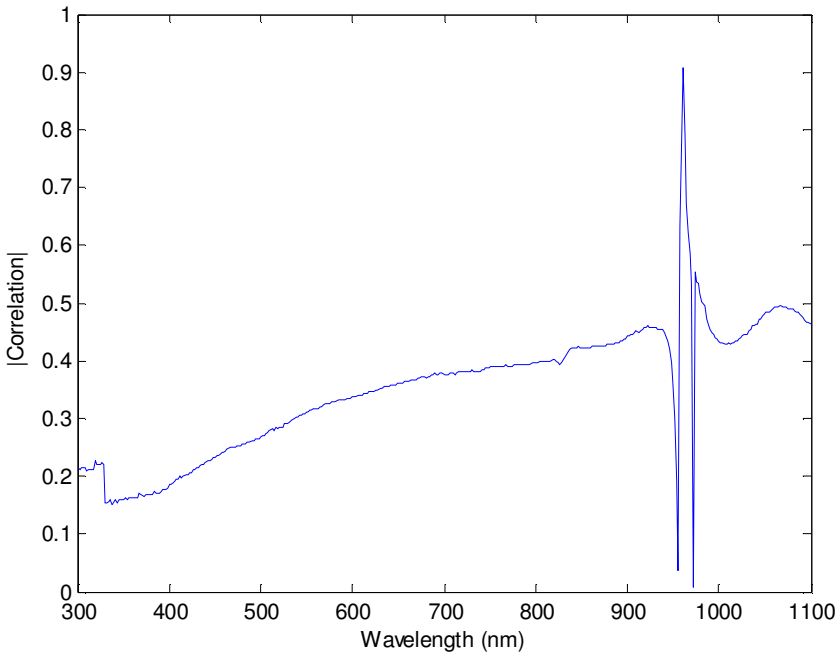

Figure 74 - Correlation spectrum of aqueous samples after baseline correction in 972 nm. The proximity between the prediction wavelength and the value of offset correction causes great variations of the magnitude around this range.

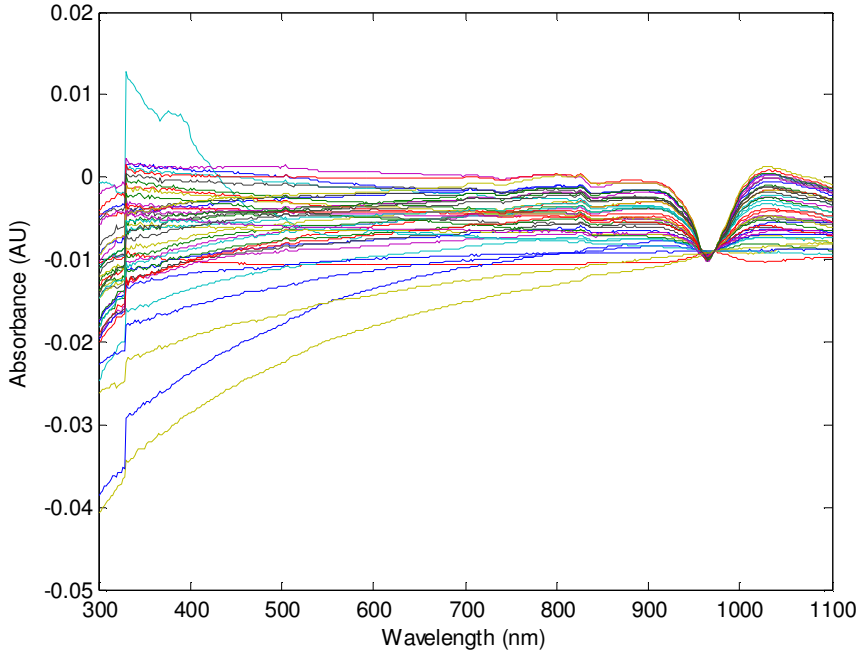

Figure 75 - Absorbance spectrums of water with glucose after baseline correction in 972 nm. Negative absorbance values are probably caused by instrumentation drifts.

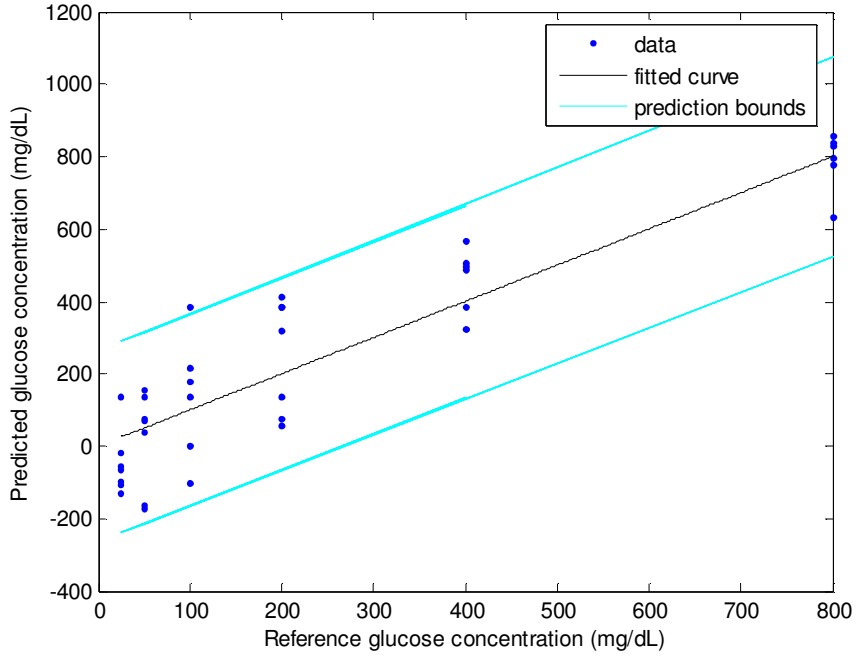

Figure 76 - Comparison of absorbance prediction in 960 nm and known glucose concentrations in water samples.

8.3.2 FTIR spectrum of glucose in water

The middle infrared range is known as the spectrum where glucose has distinct absorption peaks. This can be verified around 3380 nm and especially in the interval between 8333 nm and 10526 nm as shown in Figure 77. Therefore, 20 μL aqueous samples with different glucose concentrations were analyzed in the FT-IR spectrometer as well.

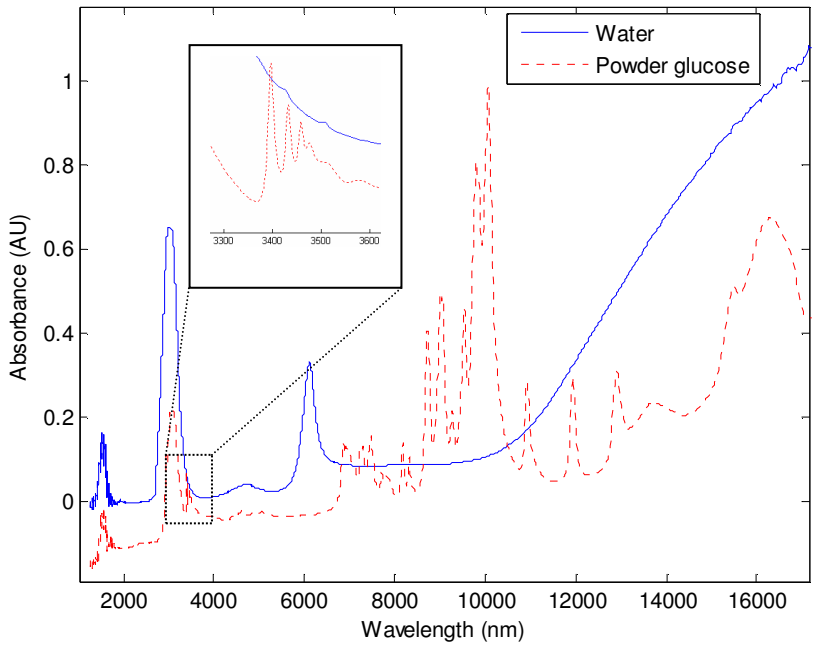

Figure 77 - MIR spectrum of powder glucose and water in the Spectrum One. The range between 8333 nm and 10526 nm shows the most significant glycemic peaks. Nevertheless, the region in 3380 nm also shows glucose characteristics, with lower water absorbance.

Figure 78 shows the baseline analysis of glucose aqueous solutions measured in Spectrum One. The best wavelength for baseline correction is located in 8453 nm, allowing a correlation of 0.983 for measurements in 9259 nm, as seen in Figure 79. The signal in 3380 nm also reflects signal elevation in the 3D graphic, with magnitude of 0.56. Figure 80 illustrates the water-glucose absorbance spectra after all samples are normalized. In Figure 81, the best predicted glucose concentrations are plotted as a function of the reference data,

resulting in a prediction error of 25.04 mg/dL and standard deviation of 15.18 mg/dL, which has much better precision than the Specord 210 measurements.

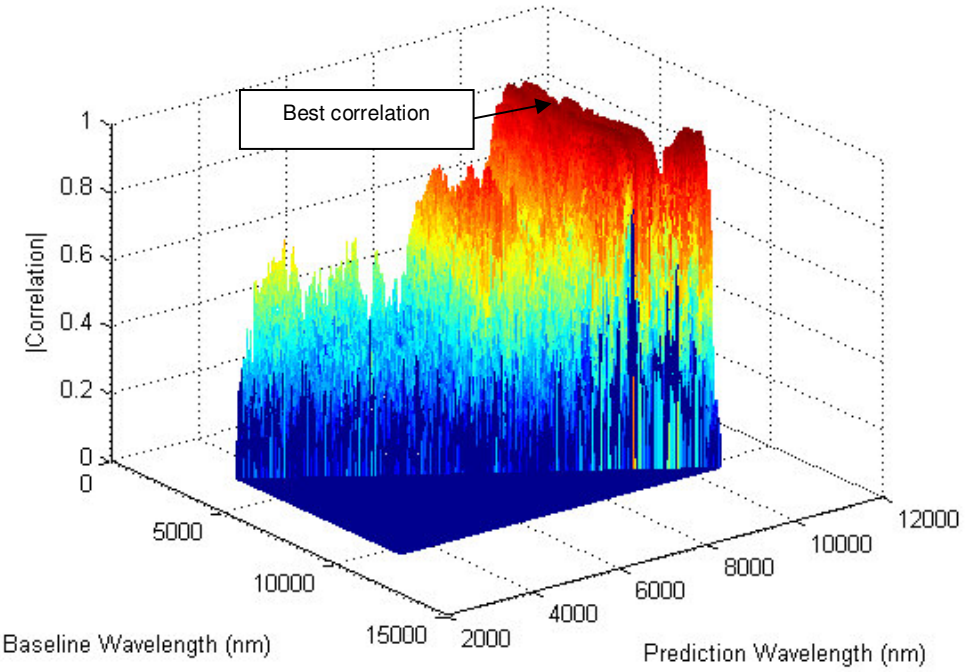

Figure 78 - 3D analysis of optimal value for baseline correction of water samples in FTIR, prediction around 9259 nm offers good results independent of the baseline point.

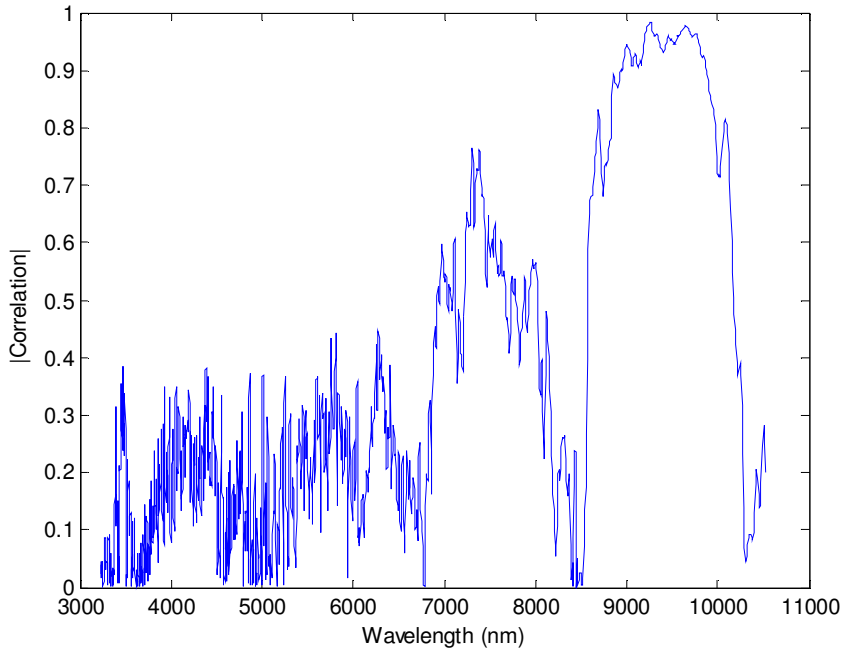

Figure 79 - Correlation spectrum of aqueous samples after baseline correction in 8453 nm. The glucose finger print can be easily detected in the intervals from 8333 nm to 10526 nm.

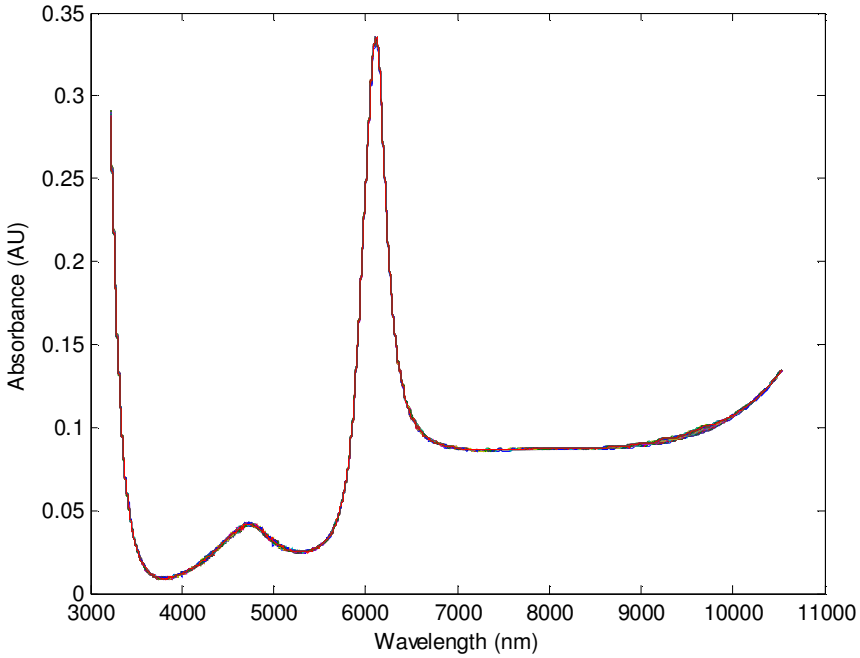

Figure 80 - Absorbance spectra of water with glucose, after baseline correction in 8453 nm. Physiological glycemic concentrations are attenuated by this solvent and, therefore, cannot be easily distinguished.

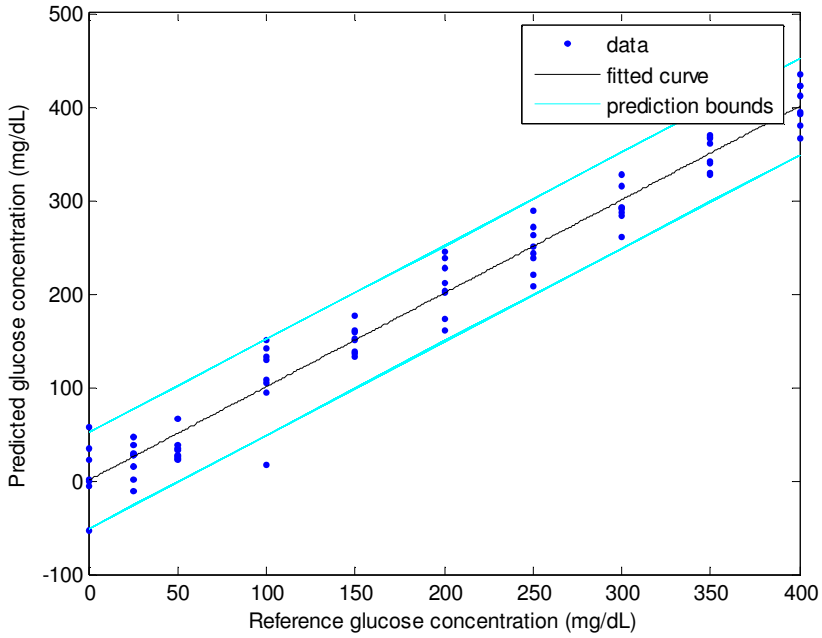

Figure 81 - Absorbance prediction in 9259 nm, versus glucose concentration in aqueous solutions. The correlation between both values corresponds to 0.983

8.3.3 FTIR spectrum of glucose in blood

In Figure 82 one can observe the difference between blood spectra with glucose concentrations of 77 mg/dL and 8000 mg/dL. Again, the strongest analyte fingerprint is between 8333 nm and 10526 nm. Nevertheless it is already possible to detect changes from 3300 nm to 3650 nm and 6500 nm to 11500 nm.

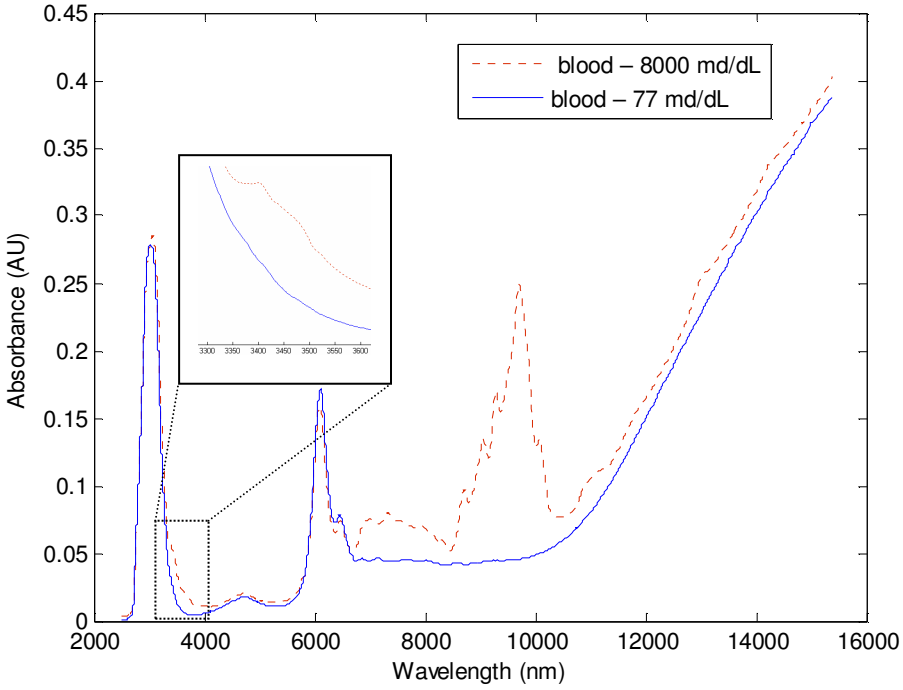

Figure 82 – MIR spectra of blood samples with glucose concentrations of 77 mg/dL and 8000 mg/dL. The strongest analyte characteristic is found between 8333 nm and 10526 nm. Nevertheless, glucose characteristics can be seen in the region around 3380 nm.

Blood probes with different glucose concentrations were analyzed in both optical spectrometers as well. Like water assays, the best results were also found in the MIR range, therefore, only such wavelengths are described in this section. Although wavelengths around 3380 nm also show elevations (0.62), the best offset correction point in Figure 83 is 8347 nm, located in the same region as water tests. The maximal correlation after baseline correction is 0.992 at 9680 nm, as shown in Figure 84. Figure 85 shows the blood spectra after the normalization procedure. Based on the best correlation result, predicted glucose concentrations were calculated resulting in the graph in Figure 86.

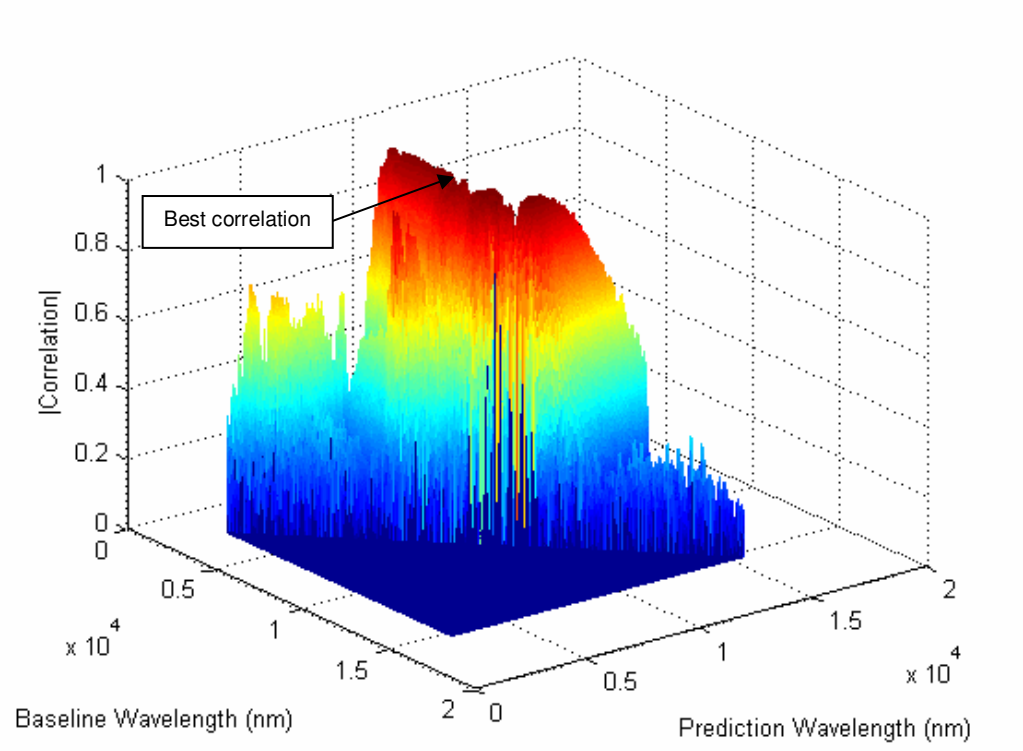

Figure 83 – Offset analysis for blood samples in the FTIR spectrometer. The highest peak in the baseline axis corresponds to 8347 nm, while 9680 nm shows the best prediction performance.

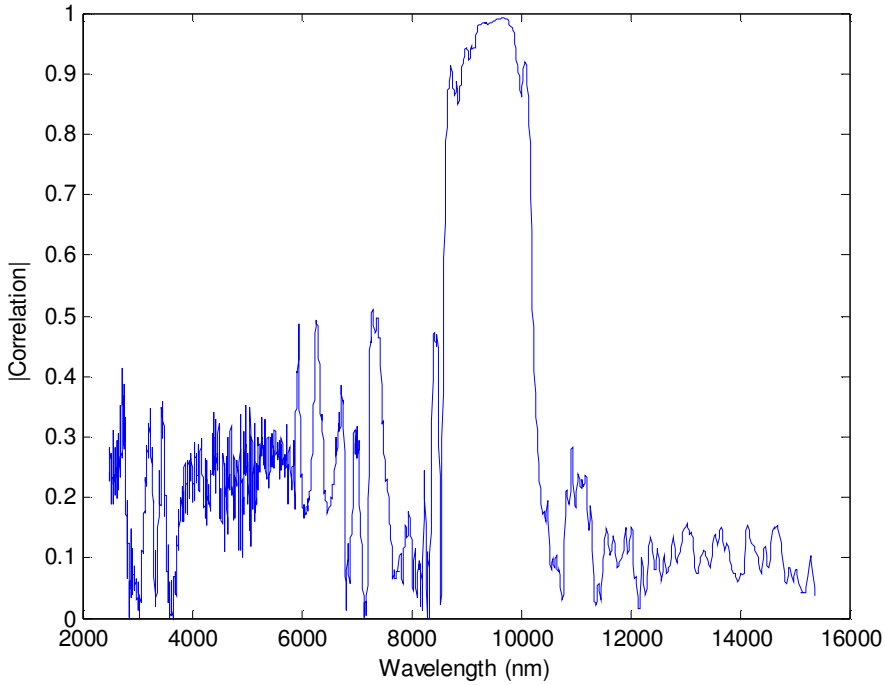

Figure 84 - Correlation spectrum of blood samples after baseline correction in 8347 nm.

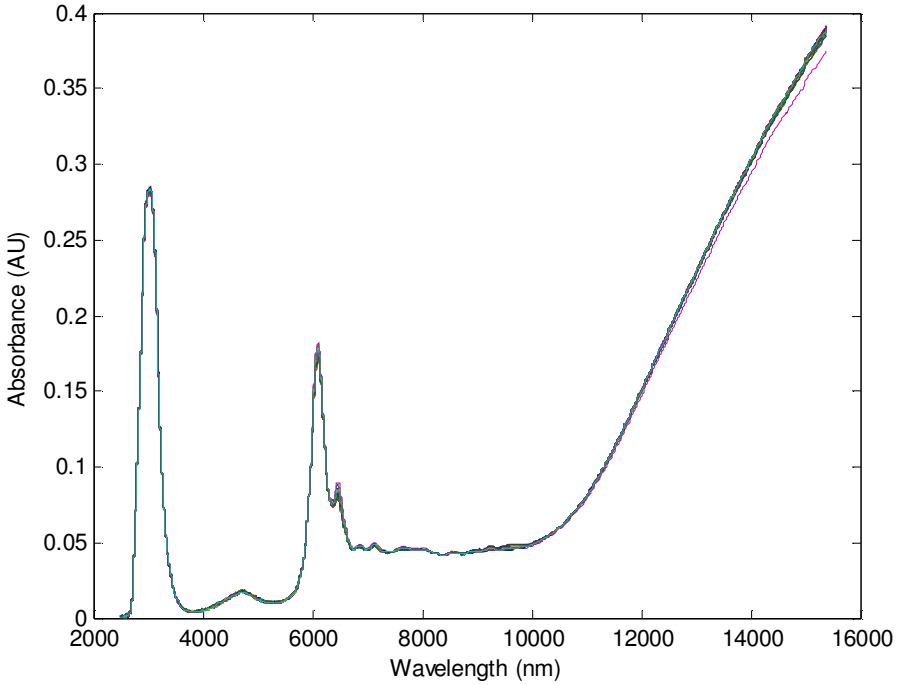

Figure 85 - Absorbance spectra of blood with different glucose values, after baseline correction in 8347 nm.

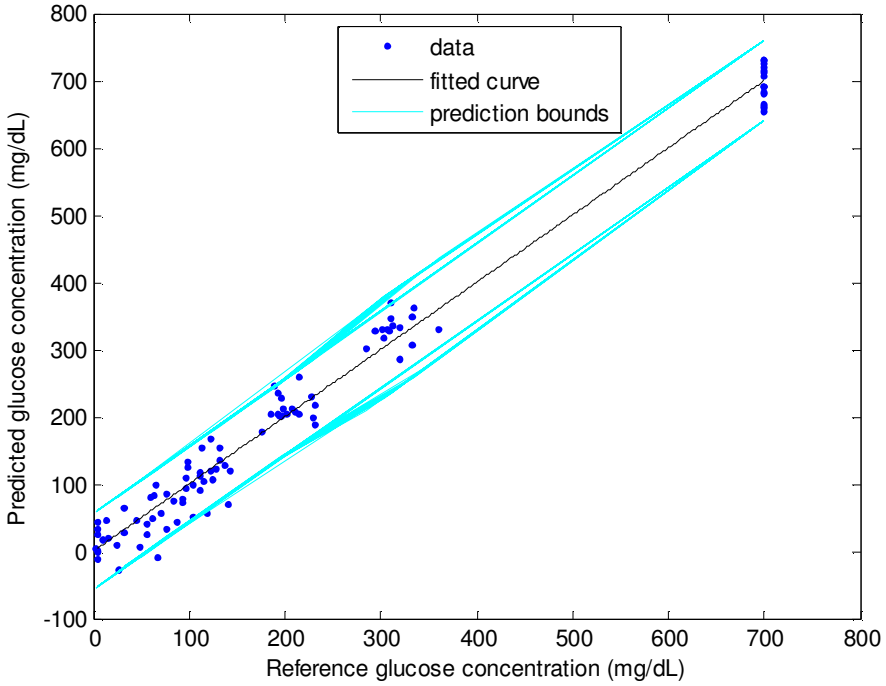

Figure 86 - Absorbance prediction (9680 nm) versus glucose concentration in blood samples, with 27.75 mg/dL SEP and 16.78 SD.

This test resulted in a prediction error of 27.75 mg/dL and a standard deviation of 16.78 mg/dL. The glucose range of 700 mg/dL did not have any variation in the x-axis because the glucometer was not able to reach high concentrations. Nevertheless, the blood cells consumption is not supposed to significantly change this value. Even the variation in 400 mg/dL range is probably caused by imprecision of instrumentation.

8.4 NON-INVASIVE ASSAYS

8.4.1 Solartron non-invasive spectrum

The last assay realized in our work was the transcutaneous measurement of glucose in the finger site. Although this technique is still in the process of improvement, initial results indicate that there is a possibility to monitor glycemic variations in the organism without invasive approaches. The impedance method does not change its performance when compared with blood tests. Figure 87 shows the correlations for the spectra in the Solartron without any pretreatment, the maximum is 0.33, again for the reactance component at high frequencies (1 MHz).

In Figure 88, the spectra of *Xc* in the finger are shown, the greater variations can be observed at lower frequencies, probably due to pressure and temperature changes. The graph from Figure 89 shows the predicted blood glucose of skin for the imaginary component at 1 MHz, with a SEP of 35.95 mg/dL and standard deviation of 20.99 mg/dL. Figure 90 compares both values with the index of measurement, with each point corresponding to 7 minute intervals.

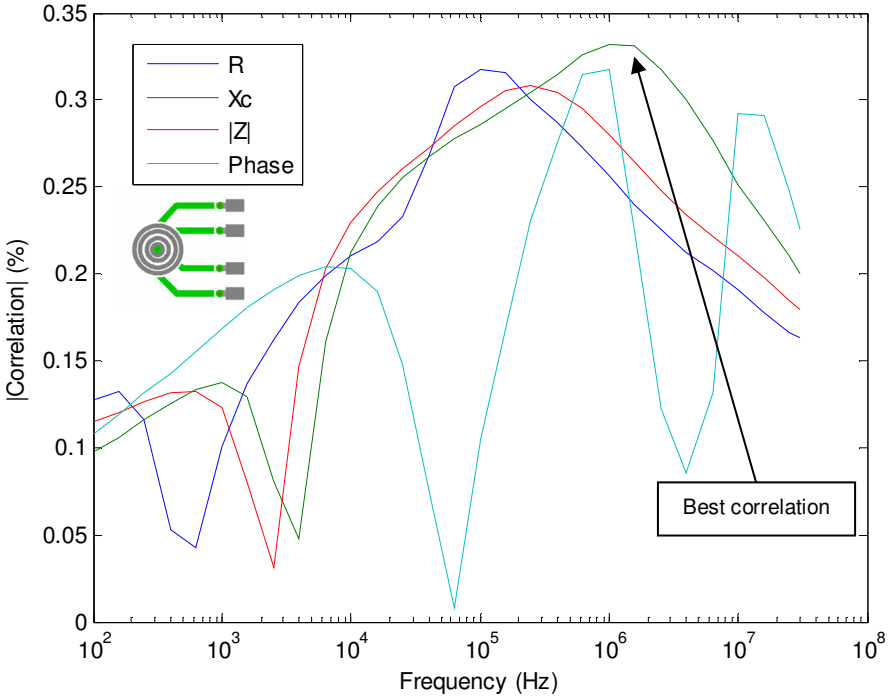

Figure 87 - Correlation spectrum of finger skin samples in Solartron with a tetrapolar electrode. The maximal magnitudes is found for *Xc* at 1 MHz.

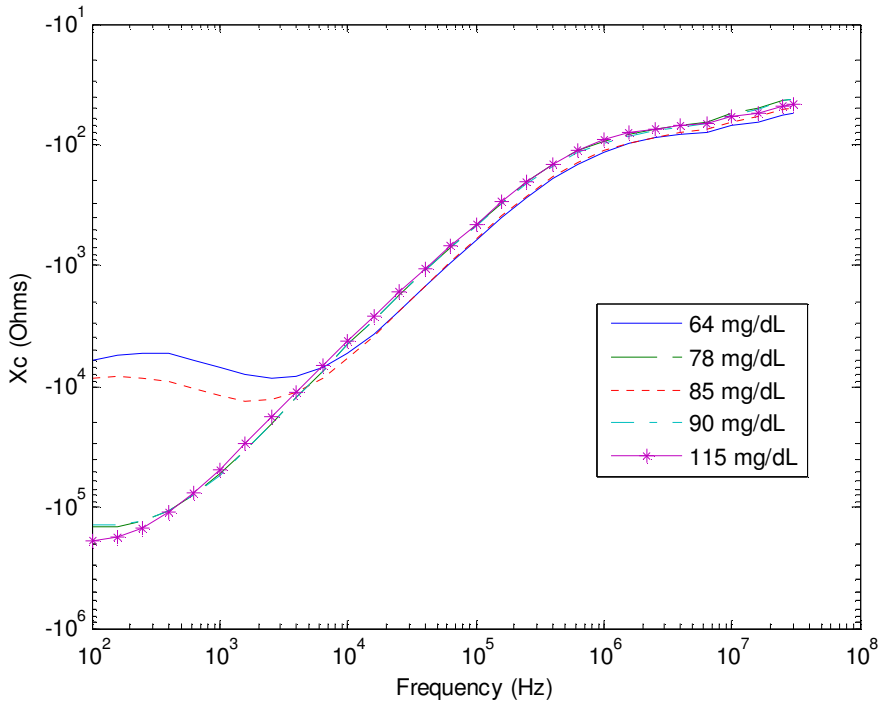

Figure 88 – Reactance spectra of transcutaneous measurements in Solartron. Variations at lower frequencies are probably due to pressure and temperature changes.

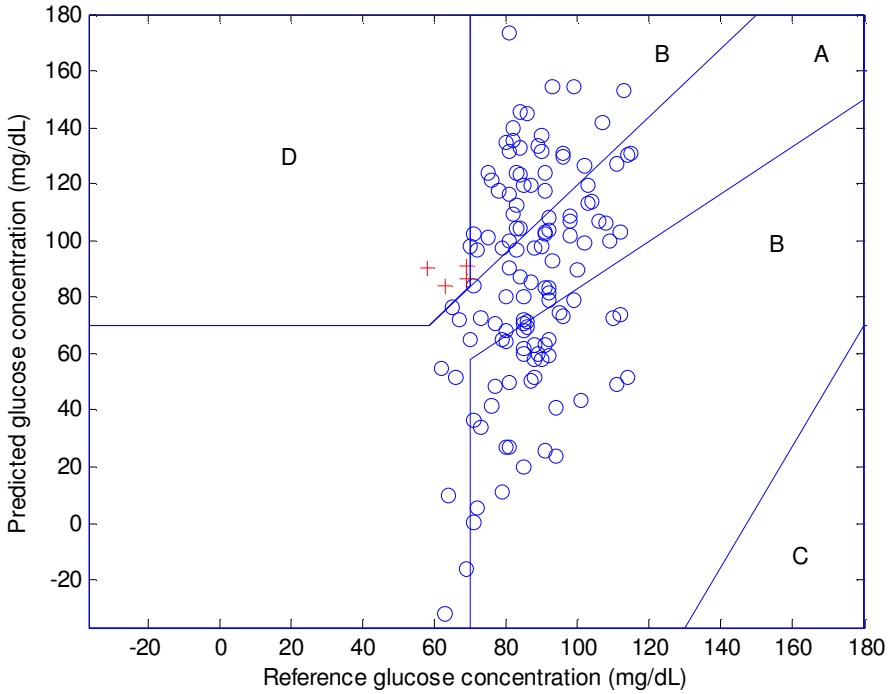

Figure 89 – Transcutaneous prediction (*Xc,* 1 MHz) as a function of the reference glucose controlled with a finger-stick device.

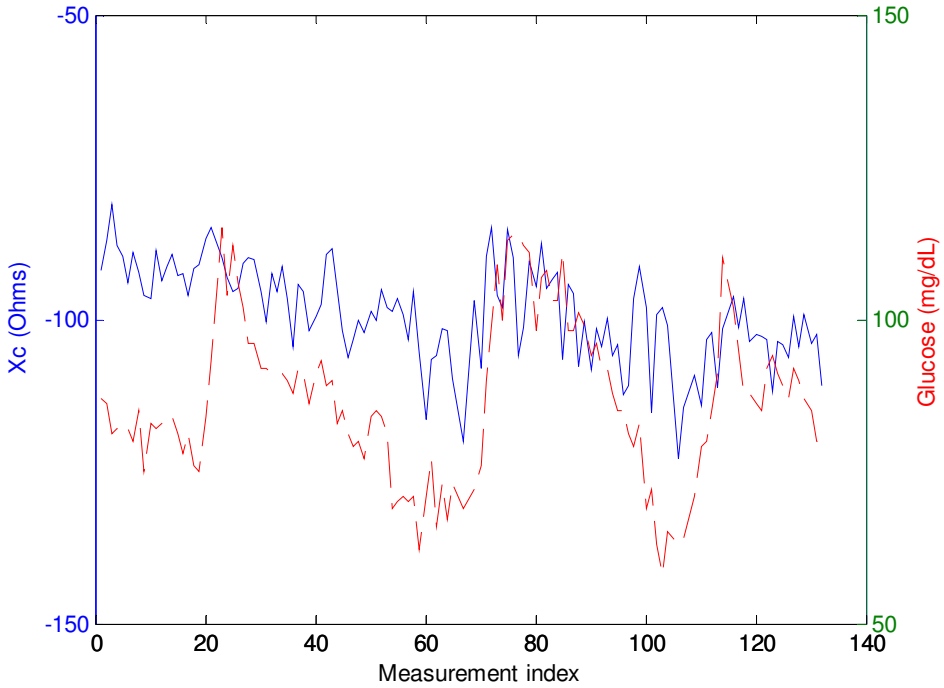

Figure 90 - *Xc* skin prediction at 1 MHz compared with reference glucose for each measurement point (7 minutes).

8.4.2 Network analyzer non-invasive spectrum

The maximal correlation of the transcutaneous raw data in the network analyzer is 0.46 for phase at 4.5 MHz, as shown in Figure 91. In Figure 92 the spectra of the impedance phase are shown, where above 70 MHz the signal noise is increased. Figure 93 shows the glucose prediction with phase at 4.5 MHz, which has an error of 23.93 mg/dL and standard deviation of 14.02 mg/dL. Figure 94 compares skin phase and invasive data with the index of measurement, where each point corresponds to 7 minutes interval.

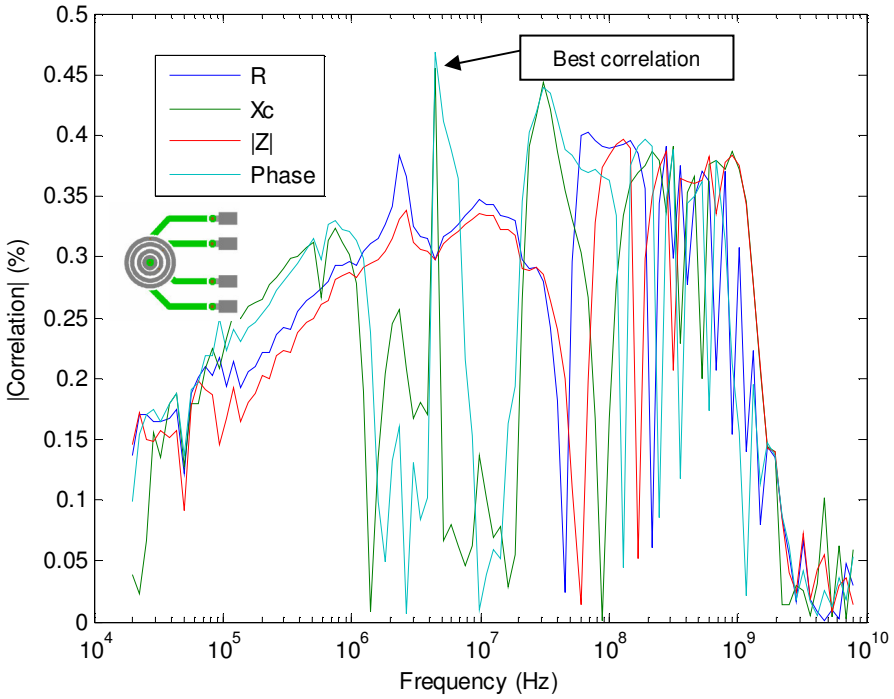

Figure 91 - Correlation spectrum of non-invasive measurements in network analyzer. Values above 70 MHz should be avoided due to the high levels of instability. The impedance phase shows best prediction at 4.5 MHz.

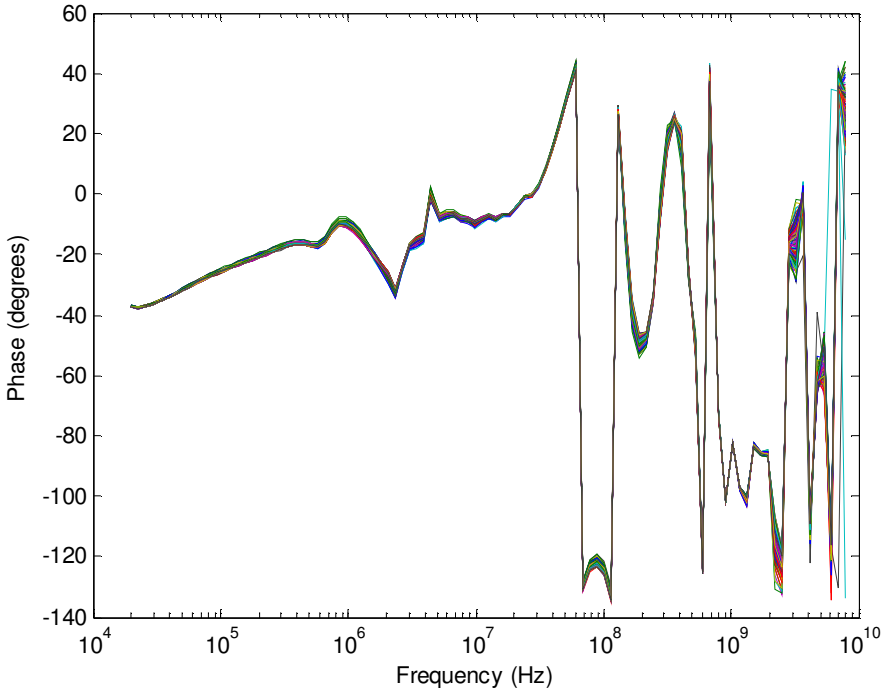

Figure 92 – Phase spectra of fingertip skin in the network analyzer, frequencies above 70 MHz show a high signal noise.

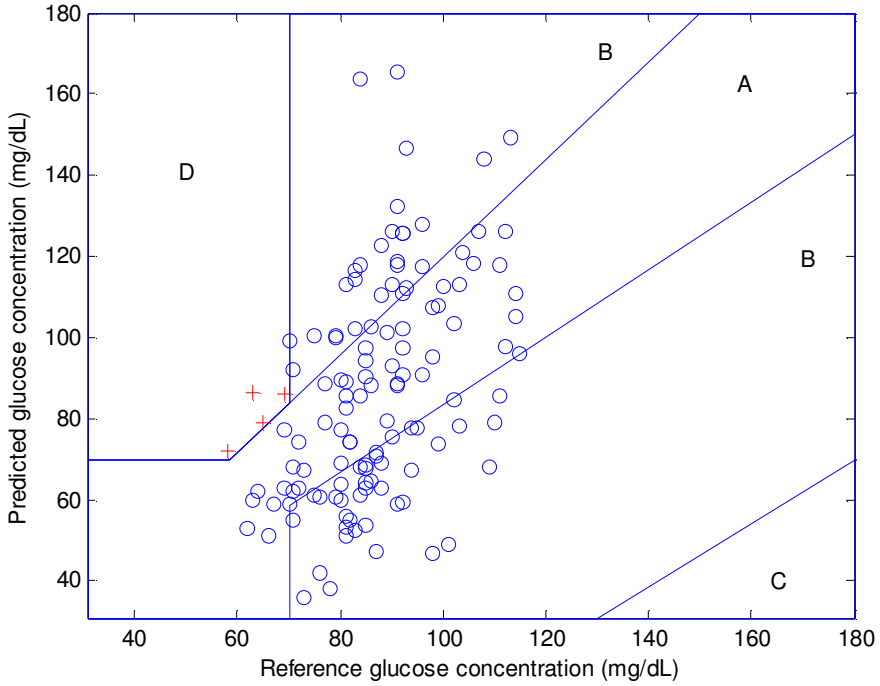

Figure 93 – Phase prediction (4.5 MHz) versus reference glucose in non-invasive samples, with 23.93 mg/dL SEP and 14.02 mg/dL SD.

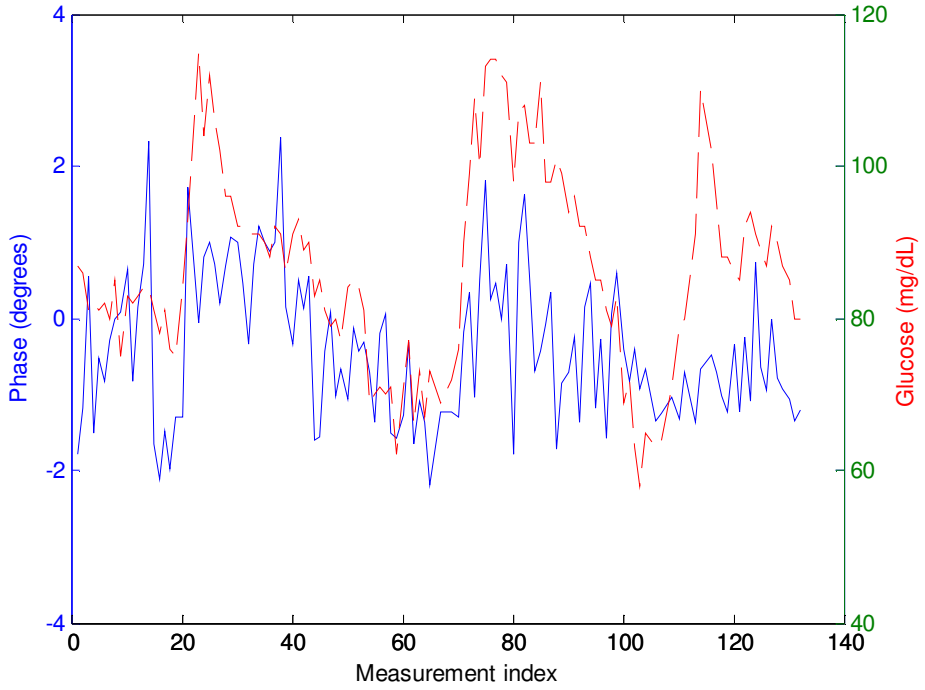

Figure 94 – Phase prediction (4.5 MHz) and reference glucose versus measurement index.

8.4.3 FTIR non-invasive spectrum

The optical correlation showed similar performance as impedance in transcutaneous approaches, especially when correcting the spectrum baseline in 3328 nm, seen in the correlation peak of Figure 95. Although the great number of wavelengths allows the use of filtering and derivative techniques, none of these treatments reached the same prediction as baseline correction, therefore only these results will be described. The maximal correlation after such procedure is 0.46, located in 3335 nm, as seen in Figure 96. Figure 97 shows the absorbance spectrums when all samples are normalized in 3328 nm. In Figure 98, the predicted glucose concentration based on the best correlation result for absorbance (3335 nm) is compared with the reference value. This graph has a prediction error of 24.18 mg/dL and standard deviation of 14.34 mg/dL. Finally, in Figure 99, one can observe skin and invasive data with the index of measurement, where each point corresponds to 7 minute intervals.

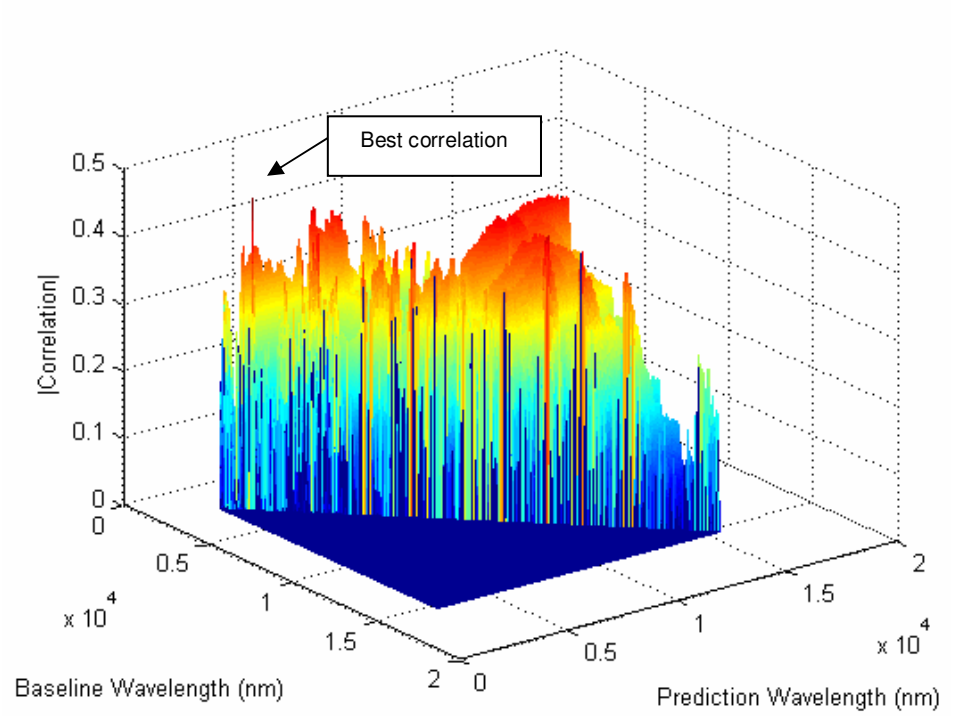

Figure 95 - 3D analysis of optimal value for baseline correction of non-invasive optic assays, the best offset result corresponds to 3328 nm, while the best prediction is found in 3335 nm.

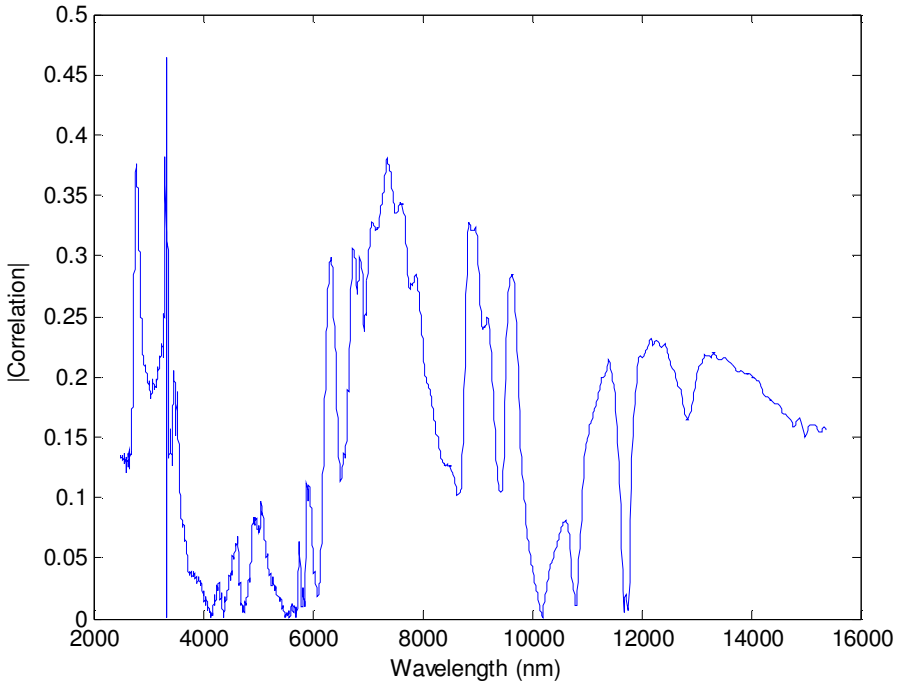

Figure 96 - Correlation spectrum of cutaneous tests after baseline correction in 3328 nm. The proximity between the prediction wavelength and the value of offset results in variations of the magnitude around this range.

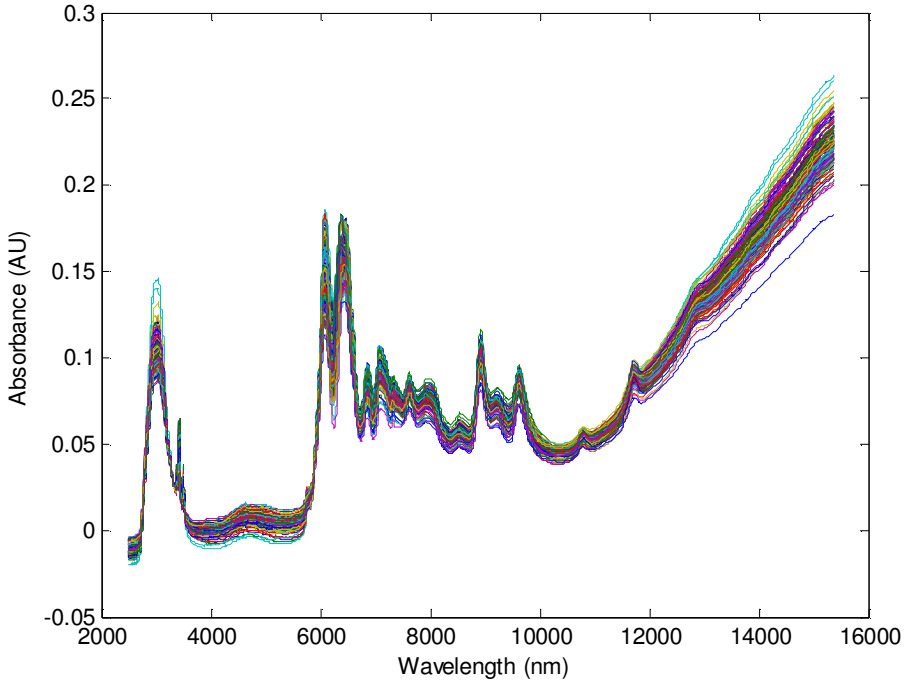

Figure 97 - Transcutaneous absorbance spectra with baseline correction. Pressure changes are probably the cause of levels shifting between the samples.

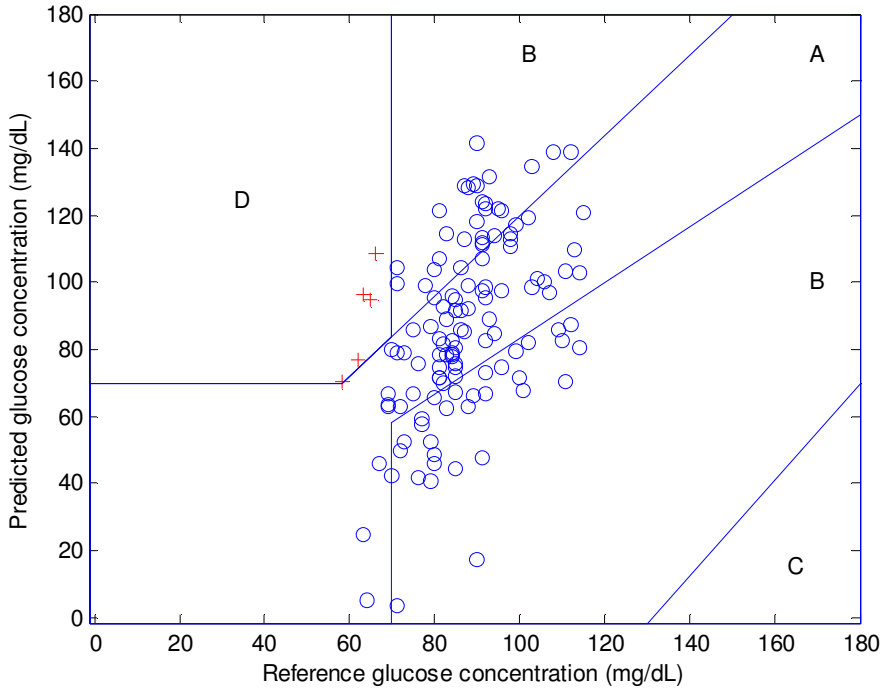

Figure 98 - Invasive reference and non-invasive absorbance prediction (3335 nm) after baseline correction.

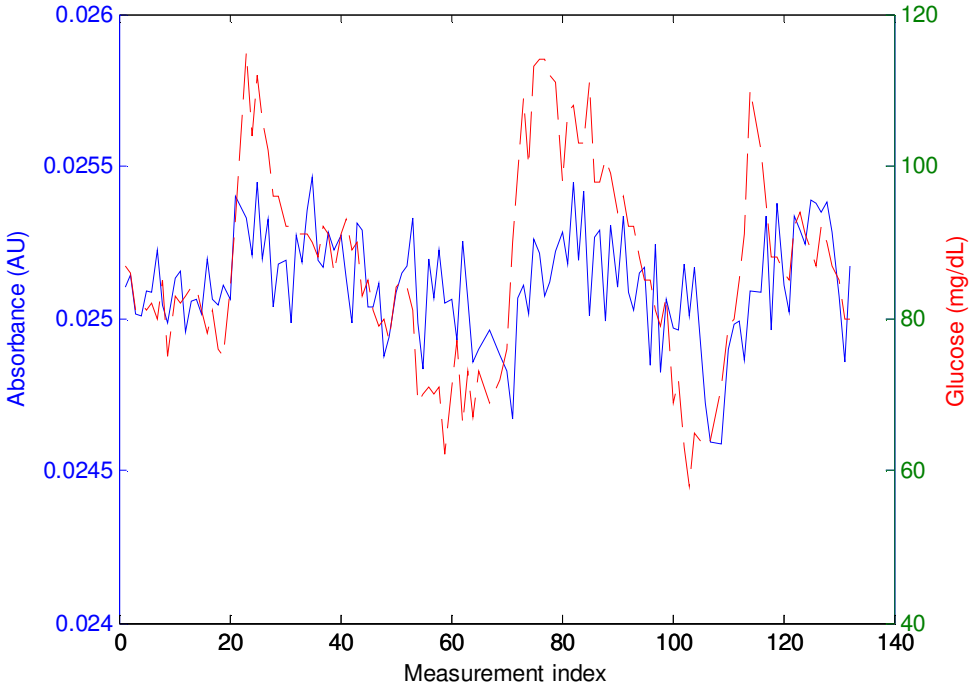

Figure 99 – Absorbance prediction (3335 nm) and reference glucose versus measurement index.

In Figure 95 one can see that the interval where water and blood showed better results also has correlation peaks in non-invasive assays, therefore a second spectrum processing between 8333 nm and 10000 nm was done. In this approach, the best wavelength for baseline is found in 9746 nm and for prediction in 9990 nm, reaching a correlation of 0.34, SEP of 34.42 mg/dL and standard deviation of 20.67. Predicted glucose concentrations in relation to the reference values can be seen in Figure 100, and Figure 101 shows both parameters with the measurement index, where each point corresponds to a 7 minute period.

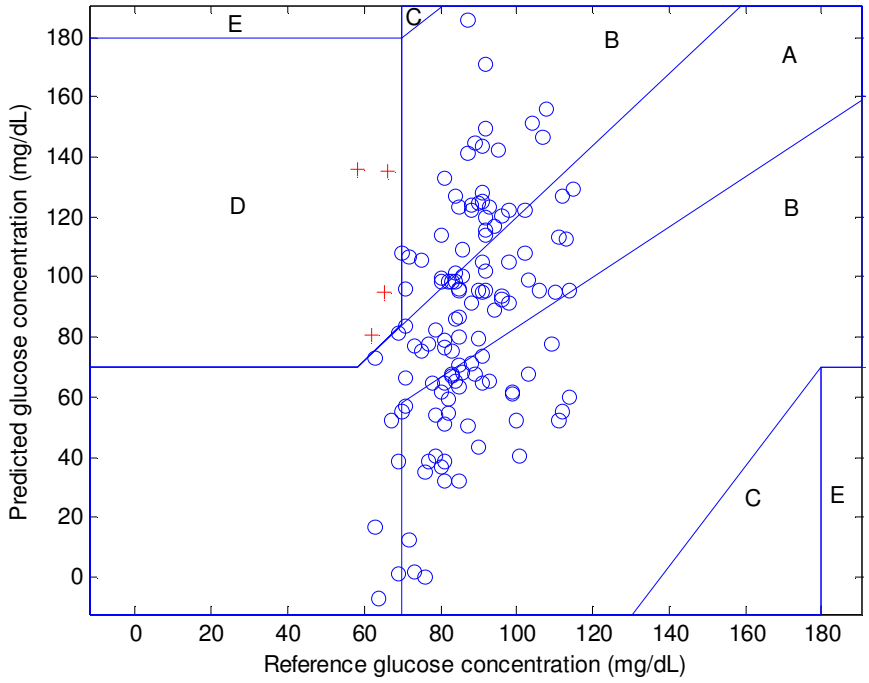

Figure 100 – Error grid with absorbance prediction at 9990 nm and reference glucose concentration, controlled by finger stick device.

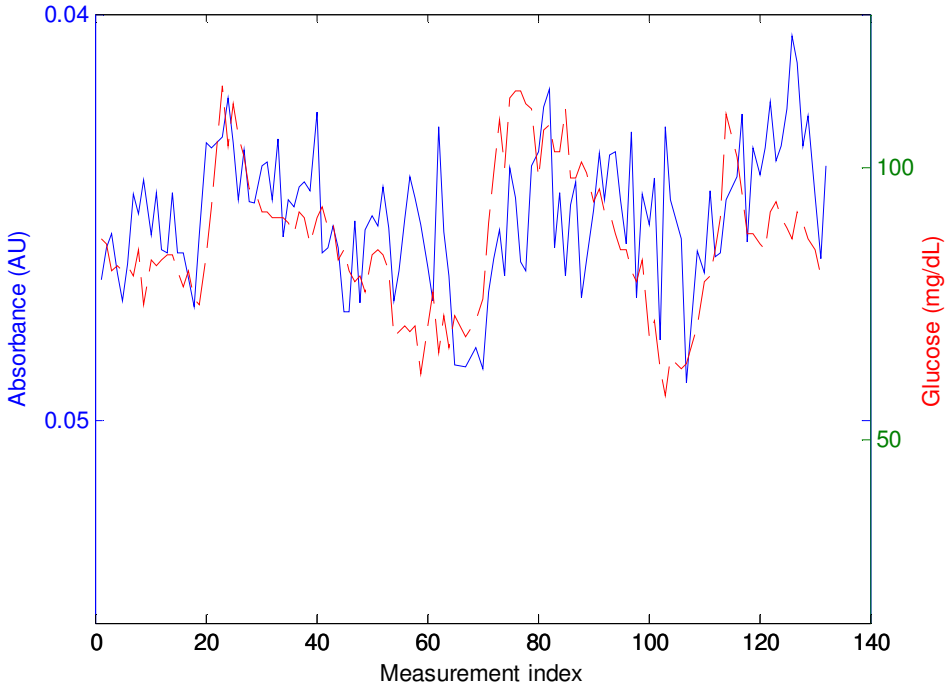

Figure 101 - Absorbance prediction (9990 nm) and reference glucose versus measurement index.

8.5 CALIBRATION MODELS

8.5.1 PLS applied to optical spectra

The first step in PLS regression is the analysis of the error, as a function of the number of components (factors that may have influence in the glucose prediction), shown in Figure 102. Three components were chosen since they seem to be the valley of the error curve.

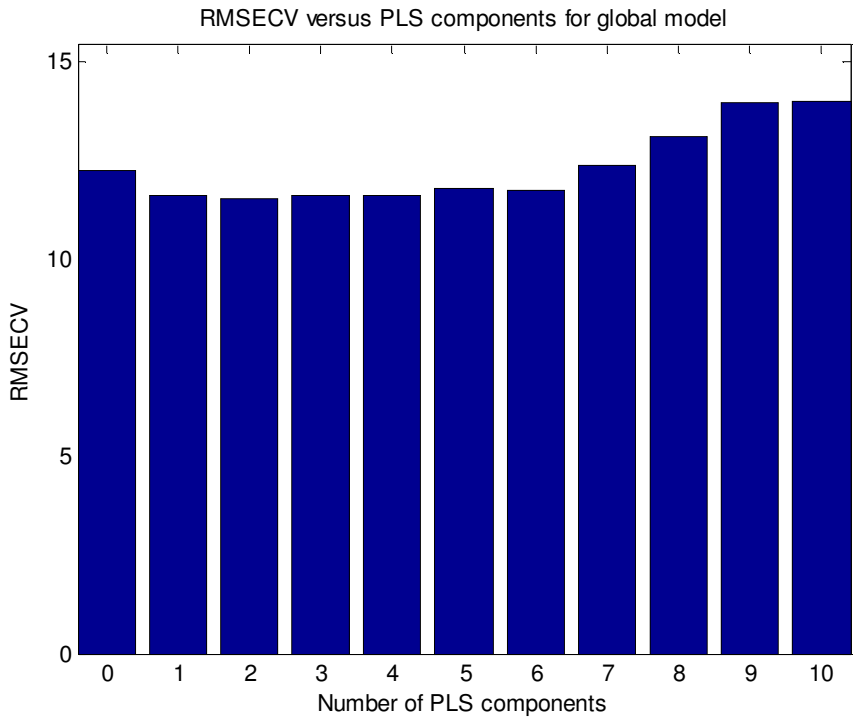

Figure 102 – Prediction error performance with the number of components, three factors are found in a performance valley and, therefore, are chosen for regression.

The most significant ranges of the spectrum are seen in Figure 103, despite the low errors in intervals 2 and 10, the fourth segment is chosen because it contains the wavelengths with the best correlation.

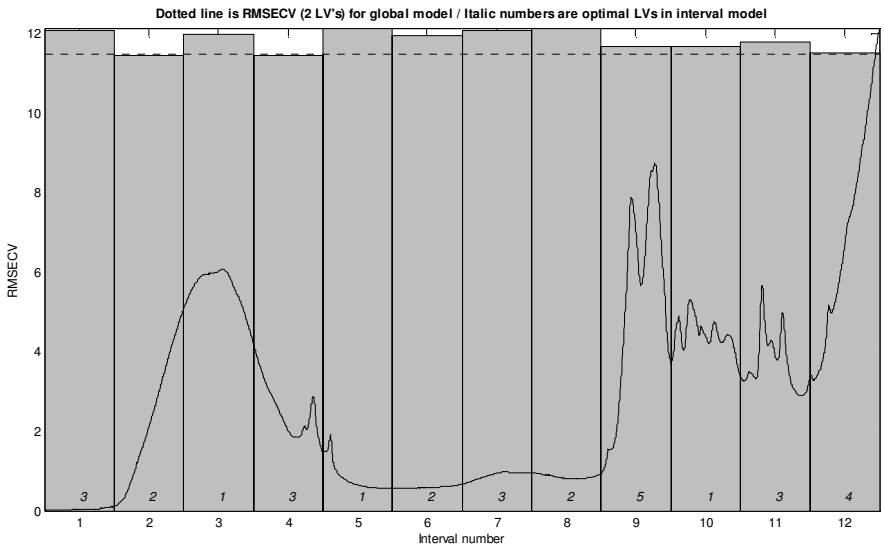

Figure 103 – Low error versus interval of prediction, the fourth range corresponds to the best result in the baseline analysis, therefore this spectrum was chosen to factor calculation.

The 3 components PLS model for the spectrum between 3160 nm and 3466 nm was trained with 94 samples. After the learning phase, 32 test values were analyzed, resulting in a correlation of 0.4, and a SEP of 12.86 mg/dL as shown in Figure 104.

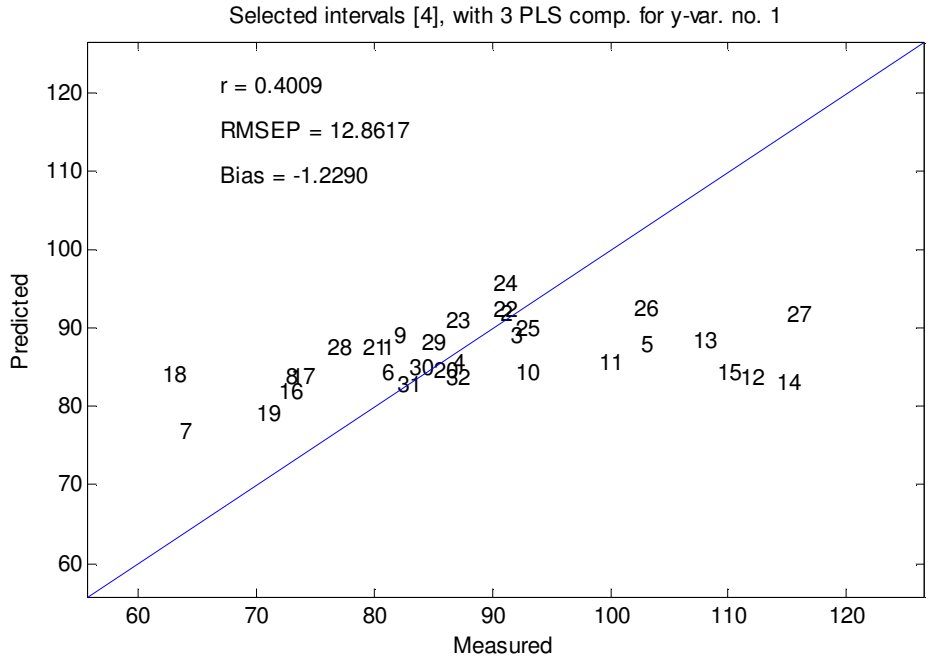

Figure 104 – Prediction values for test set with 32 samples, the correlation corresponds to 0.4, with a SEP of 12.86 mg/dL.

The same test data was analyzed without any regression algorithm, resulting in the distribution of Figure 105. The concentrations calculated seem to fit better than the glucose values of the PLS model. In this case the same correlation (0.46) of all the 126 samples is reached, nevertheless the SEP (17.35 mg/dL) and SD (9.13 mg/dL) show values much lower than the original set.

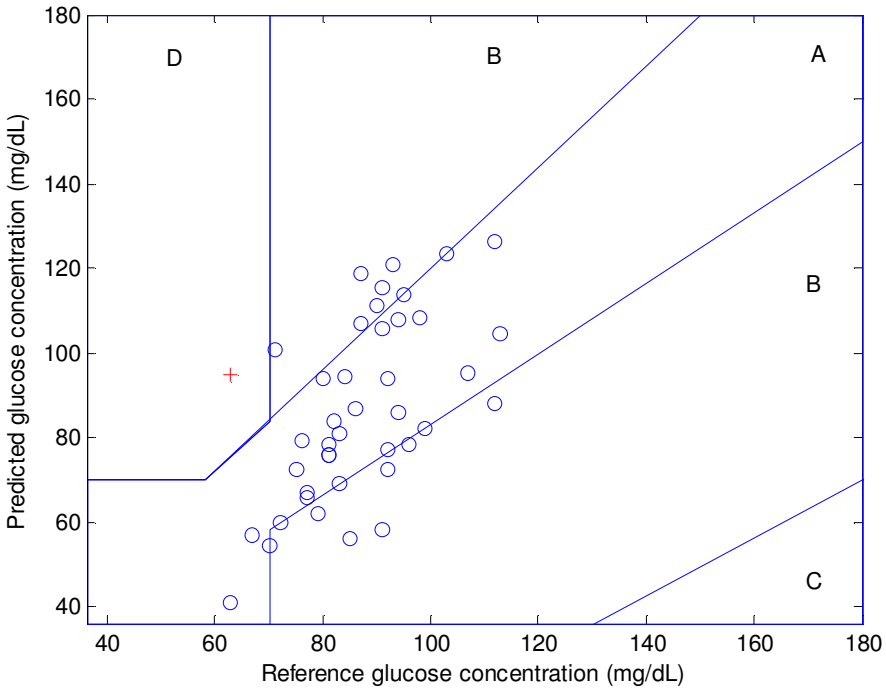

Figure 105 – Optical Prediction (3335 nm) for a test set of 32 samples with baseline correction

8.5.2 ANN prediction of non-invasive assays with best correlation data

In order to improve the performance of the transcutaneous tests, finger conductance and IR temperature were also controlled (Figure 106), which together with the predicted results by impedance (Solartron and network analyzer) and optical assays (FTIR), serve as input for artificial neural networks.

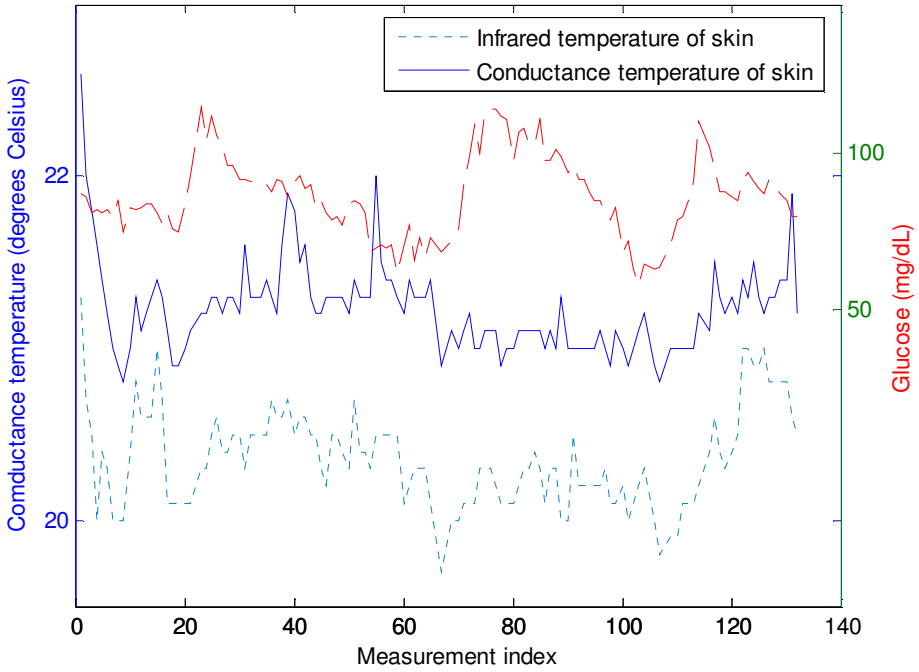

Figure 106 – Conductance and infrared temperatures from skin compared with blood glucose.

Again the training set of 94 samples is used with a goal of 0.01 mg/dL, while 32 points are separated for testing the algorithm. The choice of the optimal number of hidden nodes is based on Figure 107, which shows the mean error as a function of the cells in the intermediary layer. Although 4 neurons have lower error, the control of the results showed overfitting. The system only becomes stable above 9 nodes, and this value also gives satisfactory performance. Figure 108 shows the results after training the net with optic, impedance and temperature values. The error of this prediction model is 15.31 mg/dL, with a standard deviation of 9.92 mg/dL.

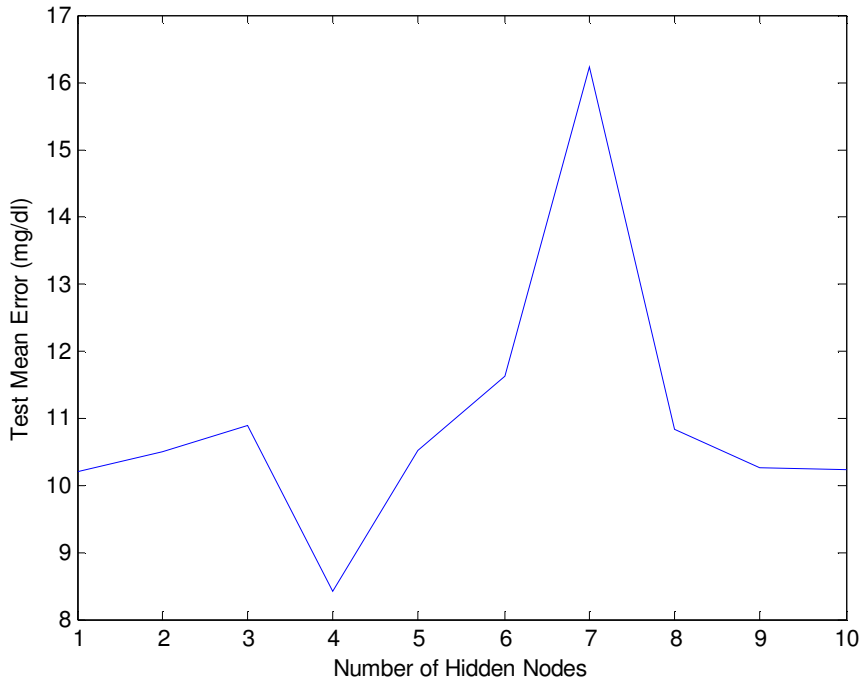

Figure 107 – Mean error analysis of neural network with different number of hidden nodes, the lower value was found for 4 neurons, but 9 values showed better correlation.

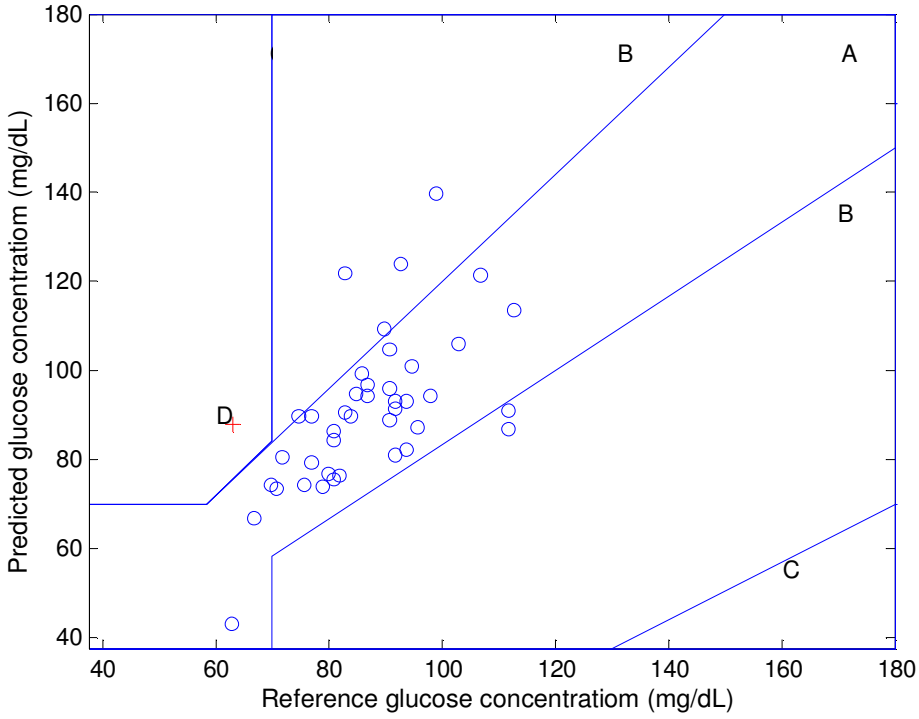

Figure 108 – Predicted glucose values for neural network with 9 hidden layers, trained with temperature, impedance and optic data.

8.5.3 ANN prediction of non-invasive assays with PLS factors

One alternative to improve the ANN prediction is to replace the absorbance data for the PLS factors already calculated. Such values, together with the impedance (Solartron and network analyzer) and temperature, improve the performance of the network (0.01 mg/dL goal), as illustrated in Figure 109. At this time, 5 nodes in the hidden layer were enough to determine a satisfactory prediction of 14.43 mg/dL SEP and SD of 8.04 mg/dL.

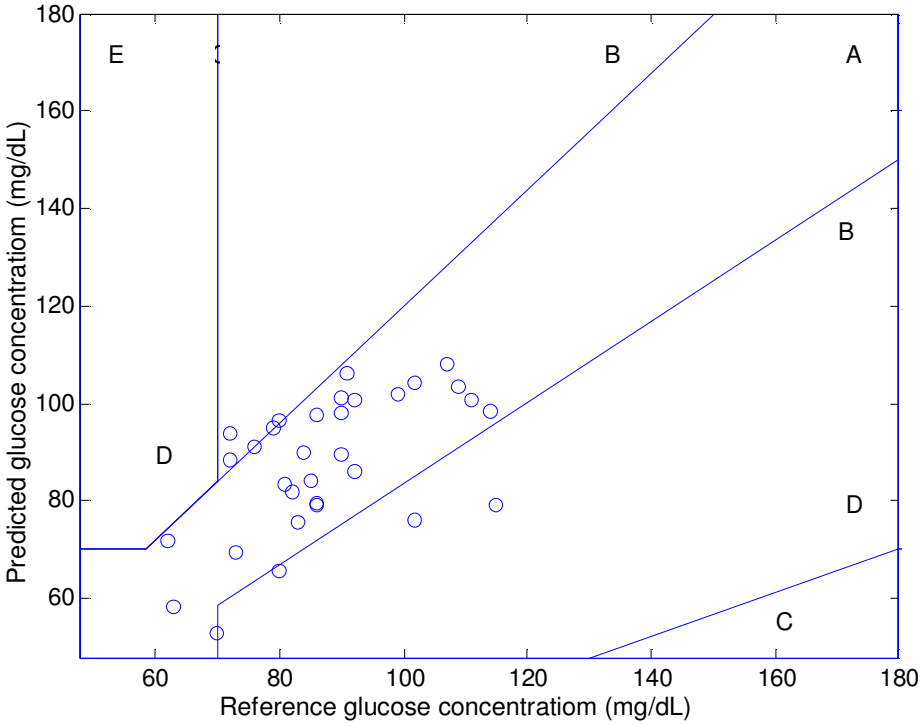

Figure 109 – Predicted glucose values for neural network with 5 hidden layers, trained with temperature, impedance and PLS factors from light spectra.

CHAPTER 9

DISCUSSION AND CONCLUSIONS

9.1 INTRODUCTION

Due to the great amount of data available, it is necessary to interpret the results carefully in order to avoid wrong conclusions. The first important task is the elimination of outlines, from a set of 132 non-invasive points measured, only 6 samples are incorrect, been therefore excluded.

Tests with the preprocessing of the impedance show low performance and lack of reproducibility, which does not encourage the use of such algorithms. However, significant improvements for optical spectrum were seen through these techniques, probably due to the strong absorbance peaks of glucose.

The aim of this section is to compare the prediction efficiency of the measurements and regression methods. Besides the individual analysis of each procedure, the comparison between invasive and non-invasive tests encourages further investigations on this theme, which corresponds to the last section.

9.1.1 IMPEDANCE ASSAYS WITH FLUIDS

9.1.2 Impedance spectrum of glucose in water

The correlation spectrum from aqueous glucose in the tetrapolar electrode connected to Solartron (Figure 64) shows that simple glucose solutions do not offer enough information for dielectric investigations. The location of the best prediction in the low frequency range can be observed in Figure 65, which shows higher phase differences from 500 Hz until 100 kHz. It is also interesting to note that all four components showed similar performance for prediction.

9.1.3 Impedance spectrum of glucose in blood

In Figure 67 one can observe that the tetrapolar measurement of blood in the Solartron tends to increase correlation of glucose concentration with the frequency. The valley of the phase around 100 kHz can be explained since in this range there is an inversion of inclination in this curve, observed in the *Xc* spectrum of Figure 68. Nevertheless, the glucose prediction, seen in Figure 69, requires an improvement of sensitivity that can only be accomplished through covering the electrode surface with enzymes, such as glucose oxidase.

The correlation spectrum of blood in IDES for the network analyzer (Figure 70) also shows the same comportment as the results with the Solartron, with the difference that the impedance modulus reflects the glycemic concentrations with lower error. This effect is probably caused by the high capacitance of the electrode that decreases the phase component in the β dispersion region. In Figure 71 one can see that above 500 MHz there is a strong oscillation in the modulus value. In such frequencies the electrical signal suffers reflection depending on the connection characteristics and, therefore, does not detect changes in the transducer's surface. The lack of clusters in Figure 72 confirms the need of additional substances in invasive glucose sensing.

9.1.4 OPTICAL ASSAYS WITH FLUIDS

9.1.5 UV/VIS/NIR spectrum of glucose in water

Although ultraviolet light has higher energy than visible and infrared, no data from glucose was noted in this area. Figure 73 and Figure 74 show 0.91 as the best correlation in Specord 210, which was observed in near infrared range (960 nm for prediction and 972 nm for baseline correction). Many research works have already been done in this interval, especially because of the large number of optical components available in the market and the penetration depth. However, one did not detect any prominent peak of the analyte in this

region, even with concentrations of 8000 mg/dL. The lack of strong spectrum differentiation may be one reason why NIR scans of aqueous solutions showed a prediction error of 125.57 mg/dL, which is approximately 20 times higher than standard home glucose devices.

Measurements of low concentrations can also be influenced by sample cell optic properties (which can be changed after cleaning procedures), drifts in the equipment response with time and temperature or even non-compliance of reference calibration. These factors could be the cause of negative absorbance values (transmittance higher than 100 %) of the UV/VIS/NIR tests in Figure 75, as well as the cause of the glucose variation in Figure 76. It is known that glucose concentrations decrease with time due to the metabolism by micro organisms in the medium. Nevertheless, this phenomenon can be ignored in our research since some of the last measurements showed higher predictions values. In addition, glucose concentrations in distilled water should not change significantly during the 3 hours of testing. Time fluctuations in the instrument response can also be discarded because each reference point in Figure 76 showed a different prediction comportment. Therefore the most likely causes of low signal-to-noise ratio in this experiment are the low energy light source available and the limited sensibility of photo detectors to low concentrations of analyte.

9.1.6 MIR spectrum of glucose in water

Spectrums with the FT-IR spectrometer showed better results than the UV/VIS/NIR instrument as shown by the strong glucose differences in Figure 77, especially in the interval between 8333 nm and 10526 nm. This spectrum has good correlations as seen in Figure 78 and Figure 79, and it is interesting to note in Figure 78 that this value stays almost constant independent of wavelength chosen for baseline correction. In this case, the elimination of the offset in 8453 nm improves the correlation in 9259 nm only from 0.973 to 0.983. In all spectra of Figure 80, one can observe that water absorption curves are much more intense than glucose changes. Nevertheless Figure 81 shows that it is possible to measure this element with a SEP of 25.04 mg/dL.

9.1.7 MIR spectrum of glucose in blood

Blood contains many substances that may interfere with the glucose signal, it is important to note that the MIR spectrum of glucose in this fluid (Figure 82) shows similar characteristics to the samples of aqueous glucose. Figure 83 and Figure 84 confirm that the maximal correlation interval is located from 8333 nm to 10526 nm. At this time, baseline subtraction in 8347 nm resulted in correlation improvement from 0.976 to 0.992. One can see in Figure 85 that peaks of complex blood elements appear especially in the wavelength of 9680 nm. This is also confirmed by the error of 27.75 in Figure 86. The source of reference values in this case was the invasive equipment with a precision of 7 %. Therefore it is possible that MIR results could have even a lower error than measured.

9.2 NON-INVASIVE ASSAYS

9.2.1 Impedance of skin

Although the non-invasive glucose range did not show great variations in the concentration (58 mg/dL to 115 mg/dL), it was expected that dielectric changes of living cells could respond better to shifts in the metabolism level. Figure 87 shows that all four impedance parameters have approximately the same performance of correlation (R – 0.31, Xc – 0.33, $|Z|$ - 0.3 and θ - 0.31), while resistance and modulus peaks are found around 15 kHz, phase and reactance require higher frequencies to reach the same result. It is interesting to note that, although bloods tests and non-invasive assays used different transducer shapes, the correlation spectrum of the tetrapolar approaches from Solartron in the finger surface maintains the same characteristics as solution tests. One difference between both cases is that the skin phase has an additional valley located in 15 MHz, due to an inversion of its inclination. Another important effect is that, the resistance, reactance and modulus show a significant increase of correlation from several kHz until approximately 100 kHz. The main cause of this comportment is the polarization in low frequencies, and the high sensibility to extracellular fluids in biological tissues, resulting in variations in this range (Figure 88). The prediction performance in Figure 89 contains 3.17 % of the samples in the D zone

(inaccurate) on the Clarke error grid analysis (EGA), with the remaining data in A (35.71 %) and B (61.11 %) ranges. Negative glucose concentrations of three samples also reflect the weakness of this model alone, which can be observed through the high SEP of 35.95 mg/dL and standard deviation of 20.99 mg/dL. The time analysis of Figure 90 shows that impedance requires approximately 2 hours to equilibrate, which is in agreement with previous non-invasive research. After this period the reactance component starts to change in proportion to the glycemic rates.

In Figure 91, although the dielectric characteristics of the cutaneous tissue in the network analyzer showed noises at high frequencies, similarity with correlation of blood measurements can be observed, especially for R and $|Z|$. In this case, the modulus (0.39) and resistance (0.4) peaks are not as significant as phase (0.46) and reactance (0.45) contributions, both of which are located at 4.5 MHz. Figure 92 shows that the transducer tends to have the phase increasing with the frequency, and above 30 MHz suffers effects of signal reflection. The use of bipolar transcutaneous electrode in the network analyzer showed lower SEP of 23.93 mg/dL and SD of 14.02 mg/dL than Solartron results (Figure 93). Although 3.17 % of samples are also found in the D region of the EGA, there are no negative value is predicted and the number of points in the A zone increased to 42 %, with the remaining 53 % in the B area. Figure 94 helps the visualization of the prediction improvement, where the equilibration phase is reduced to one and half hours and the phase mean value seems to have a better response to blood glucose levels.

9.2.2 Optical absorbance of skin

It is already known that MIR light can penetrate the skin surface deep enough to reflect glucose levels in interstitial fluid. Due to the large number of interference factors it was expected that the last experiment involving non-invasive procedures would not show results as good as liquid assays. In Figure 95 and Figure 96 one can observe that correlation values did not gather in a specific area as in water and blood tests. Nevertheless it is interesting to observe that, using 3328 nm to correct offset changes, light beams of 3335 nm result in a correlation peak of 0.46, much higher than the other wavelength values (0.37 and 0.38). The different offset levels in Figure 97, which can be caused by fluctuations in contact pressure or temperature, could be a cause of imprecision of the skin absorbance. In addition,

strong noise peaks can be seen in the glucose fingerprint region, therefore the best results were found in other ranges with small peaks in the glycemic absorbance. Figure 98 has a prediction error of 24.18 mg/dL and standard deviation of 14.34 mg/dL, with EGA distributions of 3.96 % (D), 50 % (A) and 46.03 % (B). The visual control of the prediction shows a reduction in the number of errors at higher ranges and an increase in the lower values. Even after losing the sensibility for fast changes of blood glucose levels in Figure 99, the regression model for such analyte seems to answer with a lower signal noise ratio than impedance data. Figure 100 helps to compare the efficiency of 3335 nm versus 9746 nm, which resulted in a correlation of 0.34, SEP of 34.42 mg/dL and standard deviation of 20.67. While the EGA concentration for this wavelength still contains 4 samples (3.17 %) in the region D, A zone decreases to 36.5 % and B region increases to 60.31 %. Therefore, lower wavelengths can predict blood glucose with better precision.

9.3 CALIBRATION MODELS

In contrast to previous literature, Figure 102 shows that 3 significant factors were optimal for the PLS model in non-invasive assays, which is also confirmed through Figure 103. The fact that PLS detected high correlation in the spectrum between 3160 nm and 3466 nm confirms the confiability of the baseline method. The reduction of the error in the calibration methods compared to the total raw data readings is result of the test set being reduced to 32 samples, with the rest being used as training. Despite the prediction distribution in Figure 104 gives a SEP of 12.86 mg/dL, the correlation of 0.4 and the visual control of Figure 105 shows that using PLS alone may not improve the results, since the same data reaches correlation of 0.46 with baseline correction in one wavelength. This fast processing has 64.28 % in the A zone, 33.33 % in B zone and 2.38 in D zone.

Although the conductance temperature in Figure 106 does not reflect the glycemic variations, the IR thermometer seems to be more sensitive to this factor. It is interesting to note that both parameters require approximately one and half hours to stabilize, which may be the main cause for the impedance imprecision in the same samples. Therefore, it is important to use the room and skin temperatures as input in the ANN systems. Also significant to the regression model are all the four impedance parameters, which were chosen based on the peaks of the correlation spectra. The last loaded data is the best reading by the optic method. The analysis of hidden nodes for the 12 input network showed a low error and good

distribution for 9 elements, avoiding the overfitting between 4 and 7 components of Figure 107. The error grid analysis after the network training showed 3.13 % of data in zone D (one sample), 18.75% in B and 78.13 % in the A area of Figure 108, which is an appealing result for the use of multiparameter techniques.

The best performance was finally obtained when 3 factors from the PLS models replaced the absorbance data in the input of the net. Again an analysis of hidden nodes was required resulting in an optimal value of 5 elements, which corresponds to 0.57 correlation, 14.43 mg/dL SEP and SD of 8.04 mg/dL as shown in Figure 109. Finally, in this last model, only regions A (84.38 %) and B (15.63 %) contain predicted data, which is the expected performance of non-invasive blood glucose devices.

9.4 CONCLUSION

Table 12 lists the results of optical and impedance experiments to quantify glucose concentration in 126 samples. The low performance of impedance applied to aqueous glucose is probably caused by the weak quantities of ions available in this solution. Therefore most of the read spectra reflect only the electrode characteristic. On the other hand, biological fluids such as blood, are rich in ions, and can be easily studied by BIA. The correlation spectra of impedance for blood samples and skin showed similar curves in Figure 67, Figure 70 and Figure 91, with peaks in the high frequency ranges, therefore, confirming Caduff‘s affirmation that glucose causes significant dielectric changes in this area. One reason may be the fact that the majority of the blood glucose is found in the extracellular fluid (plasma), which is only crossed by currents with high frequency. It is also interesting to note that the better performance was found in non-invasive experiments, but does not occur in optical cases. Because of the wide peak in almost all impedance correlations, the choice of the measurement interval of impedance will have good flexibility. Another important phenomenon is that, the best results were mostly related to capacitance changes, which can be seen either in phase or in reactance sensibility.

There is still a lack of agreement in scientific publications about the optimal wavelengths for non-invasive glucose investigation. In Table 2 one can see that much research has been done in visible and near infrared (NIR) range, around 590 nm – 950 nm, 1500 nm – 1850 nm and 2120 nm – 2380 nm. These spectra are chosen because water absorbance is weak, the measuring signal has higher energy and there are many commercial

light transducers available. Water measurements in the UV/VIS/NIR Spectrometer confirm the importance of this region demonstrated by the good baseline correction in 972 nm and prediction in 960 nm. Middle infrared research, mostly conducted between 8382 nm and 9708 nm, also measured glucose and validated the results with Spectrum One. The importance of baseline correction in blood was also observed, improving the results of the measurement in 9680 nm. The efficiency of optic assays in the skin is decreased due to the great absorbance of the light in biological tissue. The error value does not only depend on the prediction efficiency, but also in the glucose range available for the measurements. Therefore, although non-invasive measurements in the FTIR show lower SEPs and SDs than water and blood tests, their correlation reflect that the performance still needs to be improved. The fact that the better prediction range for transcutaneous assays is found around 3400 nm reflects that, although such beams have smaller glucose peaks than higher wavelengths, the lower water absorbance and the greater signal energy, allow a higher penetration power in this tissue.

Table 12 – Performance of glucose assays with impedance and light methods.

Experiment	Reference (mg/dL)	Wavelength/ frequency	Correlation	SEP (mg/dL)	SD (mg/dL)
Impedance of aqueous solutions in Solartron	0 to 800	Phase 15.84 kHz	0.55	516	387
Absorbance of aqueous solutions in Specord 210	0 to 800	960 nm (972 nm)	0.91	125.57	66.32
Absorbance of aqueous solutions in FTIR	0 to 400	9259 nm (8453 nm)	0.983	25.04	15.18
Impedance of blood samples in Solartron	5 to 700	Xc 10 MHz	0.67	249	156
Impedance of blood samples in network analyzer	5 to 700	Modulus 166.9 MHz	0.43	474	300
Absorbance of blood samples in FTIR	5 to 700	9680 nm (8347 nm)	0.992	27.75	16.78
Impedance of skin in Solartron	58 bis 115	Xc 1MHz	0.33	35.95	20.99
Impedance of skin in network analyzer	58 bis 115	Phase 4.5 MHz	0.46	23.93	14.02
Absorbance of skin in FTIR	58 bis 115	3335 nm (3328 nm)	0.46	24.18	14.34

The difference in the efficiency of optical and impedance technologies in the fluid measurement occurs because light can detect characteristics of the chemical structure from the glucose molecule, whereas electrical current is sensible to changes in the ionic concentration in the sample. Therefore transcutaneous BIA should only monitor blood glucose through secondary phenomenons such as metabolism, temperature or pH changes. Although both non-invasive methods showed the same correlation (0.46), optic sensing does not require a long equilibration process. In addition, this approach seems to fit the mean value of the glucose curve better.

Both algorithms analyzed allow the quick training of the model, nevertheless, the choice of the number of hidden layers and components required careful analysis. In Table 13

the statistical and EGA results of the different methods can be observed. Although the network analyzer response did not contain any data in the D zone, its correlation is lower than using PLS techniques. Nevertheless, Clarke error grid help the differentiation between feeding the network with absorbance raw data or 3 partial least squares factors. Besides eliminating occurrences in the D region, the principal components also condensed the data between the A limits, and therefore is the best alternative for non-invasive prediction.

Table 13 – Prediction performance for non-invasive assays with test set of 32 samples.

Prediction method	Correlation	SEP (mg/dL)	SD (mg/dL)	EGA A (%)	EGA B (%)	EGA D (%)
Xc: 1 MHz (Solartron)	0.37	37.47	22.9	31.25	65.62	3.13
phase: 4.5 MHz (Network analyzer)	0.43	24.1	15.59	53.12	46.87	0
light: 3335 nm - baseline correction in 3328 nm (FTIR)	0.46	17.34	9.13	64.28	33.33	2.38
neural network input: temperature, impedance and optic absorbance	0.6	15.31	9.92	78.13	18.75	3.13
neural network input: temperature, impedance and PLS factors	0.57	14.43	8.04	84.38	15.63	0

9.5 FUTURE WORKS

Although there are some products commercially available for *in vivo* non-invasive glucose monitoring, many improvements are still needed in order to have the same precision as standard methods with blood samples. In controlled conditions of research laboratories it is relatively simple to find correlation between transcutaneous data and blood glucose levels. The challenge is to establish stable regression models able to measure in normal day-to-day activities of a patient's life. In order to accomplish this goal many techniques and procedures still need to be studied.

Despite the good reproducibility of the tests described, the addition of more training and test sets will help the validation of the calibration algorithms. Future experiments should try to improve glucose readings, which besides the error of 6%, due to the Accu-chek limitation, also depends on the blood circulation in the target site. In our case, lancing was repeated every 30 minutes in each finger, and although the sample site was alternated (fingertip left, right and centre), vasoconstriction could be observed after several hours of

measurement. The use of the Biostator artificial pancreas in Figure 110 may be an interesting alternative, since this device is able to continuously monitor venous blood glucose (CLEMENS, HOUGH and D'ORAZIO, 1982). Due to the wide range of data available, further study of the classification analysis algorithms can improve this technology by researching the optimal ranges in the PLS models or the addition of extra relevant frequencies/wavelengths as input in the ANN.

Figure 110 – Biostator artificial pancreas which is able to continuously monitor venous blood glucose.

The aim of this work is to validate the parallel use of temperature, impedance and light in the non-invasive prediction of blood glucose. Both spectral techniques offer many alternatives for further investigation, and while few publications describe glucose research associated with skin permittivity, no transcutaneous report is known on monitoring with light in the 3335 nm range. These factors, in addition to the successful performance of the error grid analysis in the initial tests, appeals to the development of a more accurate multiparameter prototype.

In this case, improvements in the transducers, hardware and calibration methods are still possible. Although other layouts of the sensor contacts can be used for skin measurement, the actual concentric electrode was chosen in consideration of the placement of light, temperature and pressure sensors, without changing the symmetry of the electrical current in the target site. The parallel monitoring of all parameters can improve the efficiency of this approach, since the actual dataset has several minutes delay between each different spectra. Significant improvements of the MIR correlation were observed when measuring the fingertip inside of dark chamber, which needs to maintain the mechanical arm in order to apply a constant pressure in this site.

Optical and impedance circuits with few sensors can be easily implemented, however, if an increase in the performance from non-invasive testing is desired, PLS association with ANN is strongly recommended, and requires the acquisition of a wide spectrum to build the models. Fast sampling rates (100 spectra/s) in the impedance and optical circuits should allow the separation of pulsatile blood signal from interference factors (YAMAKOSHI, 2006). The development of vector impedance circuits with these characteristics is a complex task and requires a good knowledge of high frequencies techniques to avoid external sources of electromagnetic noise.

Photo-spectrometers with a fast response also require a carefully approach. The fact that the optimal wavelength for detection is in the proximity of the baseline reference also increases the difficulty of the prototype manufacturing since the detector element, probably a charge coupled device (CCD), should have narrow band ranges. One requisite to improve the optical SNR is the increase of light energy, without crossing secure limits. This can be accomplished with acquisition of laser diodes (Figure 111), whose actual price is around 50 €. If laser diodes are not available in the frequency of interest, another possibility is the use of high energy LEDs in association with interference filters, which cost approximately 400 €.

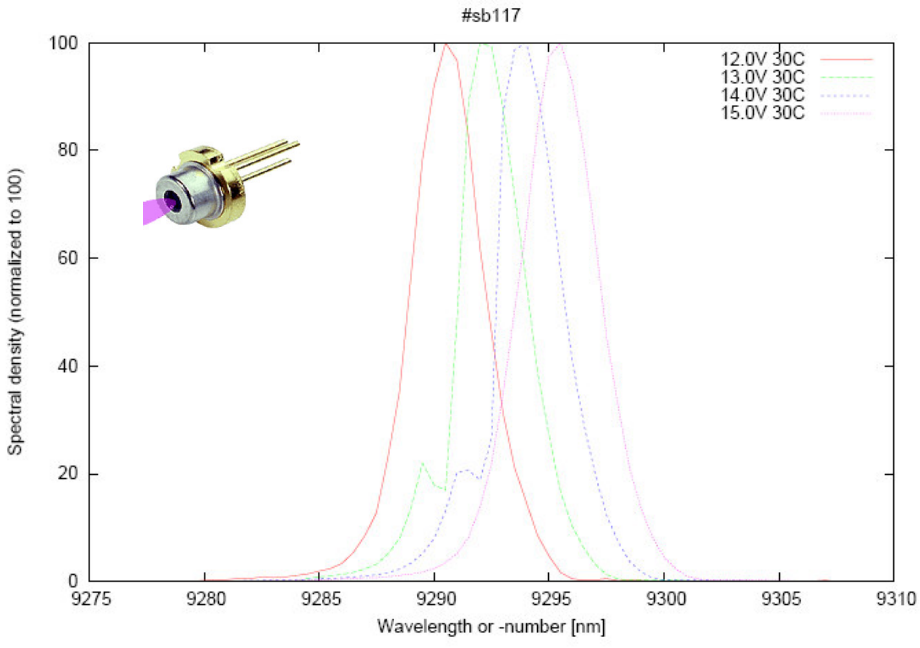

Figure 111 – Spectrum of laser diode signal, the measurement wavelength can be controlled changing the voltage applied to its terminals.

Figure 112 shows the block diagram from the prototype that should be made for non-invasive measurement of blood glucose through the parallel acquisition of impedance, light, temperature and moistness of skin. As a result of all the non-invasive research completed to date, it is expected that in a few years, a new generation of non-invasive glucose instruments could be available in the market. These devices should have low cost, fast response simple calibration procedures, and improve the patients comfort. This in turn, will increase compliance to monitoring blood glucose levels, thus decreasing the long-term complications of diabetes.

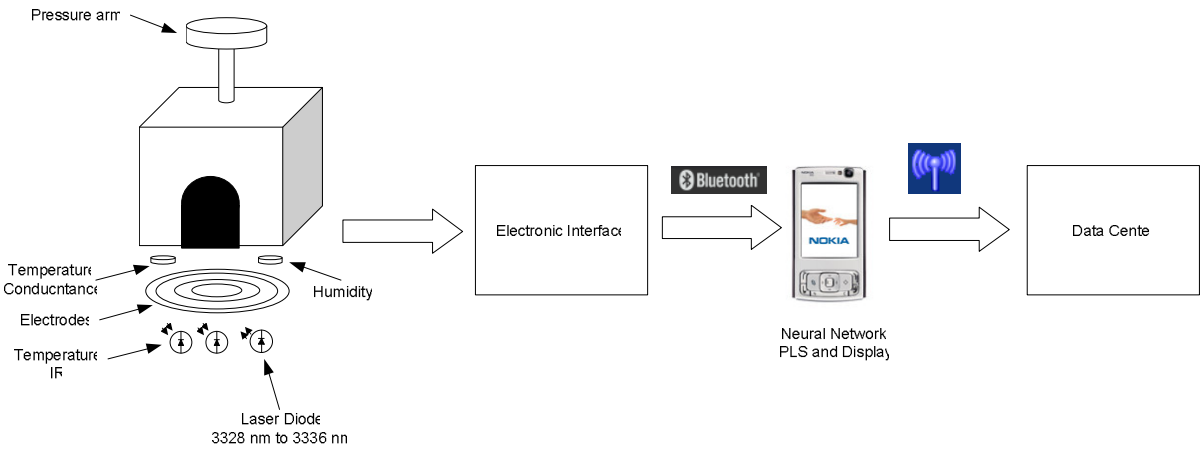

Figure 112 – Block diagram from prototype for parallel measurement of impedance, light, temperature and humidity, the calibration algotiyhms and the display fuction can be performanced through a cell phone, which also sends the results to a data server.

CHAPTER 10

REFERENCES

ANALYTIK JENA, **SPECORD**, Analytik Jena AG, 2004.

ACKMANN, J.J. Complex bioelectric impedance measurement system for the frequency range from 5 Hz to 1 MHz. **Annals of Biomedical Engineering**, v. 21, p. 135-146, 1993.

ALAVI, S.M., GOURZI, M., ROUANE, A., NADI, M., An original method for non-invasive glucose measurement: preliminary results, Proceedings **of the 23rd Annual International Conference of the IEEE**, v. 4, p. 3318- 3320, 2001.

ABERG, P., GELADI, P., NICANDER, I., OLLMAR S. Variation of skin properties within human forearms demonstrated by non-invasive detection and multi-way analysis. **Skin Res Technol**, v. 8, n.3, p. 194-201, 2002.

ALLEN, T.J., COX, B.T., BEARD, P.C. Generating photoacoustic signals using high peak power laser diodes, **Proceedings of the SPIE**, v. 5697, p. 233-242, 2005.

AMARAL, C.E.F., HARA, M.S., LOPES, H.S., ARRUDA, L.V.R.A., GONÇALVES, A. J., DIAS, A. A. Diagnóstico de câncer de cabeça e pescoço baseado em redes neurais e dados de impedanciometria. In: **Proceedings of the VI Brazilian Conference on Neural Networks**, p. 139–142, June 2–5, 2003.

ANSELL, J., HASENKAM, J.M., VOLLER, H., JACOBSON, A., LEVY, J. Guidelines for implementation of patient self-testing and patient self-management of oral anticoagulation. **International Journal of Cardiology**, v. 99, p. 37-45, 2004.

ARNOLD, M. A., SMALL, G.W. Perspectives in Analytical Chemistry: Noninvasive glucose sensing; **Analytical Chemistry**, v. 77, n. 17, p. 5429-39, 2005.

BABA J.S., CAMERON, B.D., COTÉ, G.L. Effect of temperature, pH, and corneal birefringence on polarimetric glucose monitoring in the eye. **Journal of Biomedical Optics**, v. 7, n. 3, p. 321-328, 2002.

BADUGU, R., LAKOWICZ, J.R., GEDDES, C.D. A glucose-sensing contact lens: From bench top to patient. **Current Opinion in Biotechnology**, v. 16, p. 100–107, 2005.

BAYOD, S., HERMANT, A., FARGES, G. Les applications effectives, en routine, des mesures de bioimpédance et la présentation des appareils sur le marche. 1999. Available in: http://www.utc.fr/~farges/dess_tbh/98-99/Projets/Bio_Imp/BioZ.htm. Accessed in 09/07/2006.

BERGER, A.J., ITZKAN, I., FELD, M.S. Feasibility of measuring blood glucose concentration by near-infrared Raman spectroscopy. **Spectrochim, Acta A**, v. 53, p. 287–292, 1997.

BEVING, H., ERIKSSON, L.E.G., DAVEY, C.L., KELP, D. B. Dielectric properties of human blood and erythrocytes at radio frequencies (0.2-10 MHz); dependence on cell volume fraction and medium composition, **European Biophysics Journal**, v. 23, p. 207-215, 1994.

BLAD, B., BALDETORP, E.B. Impedance spectra of tumor tissue in comparison with normal tissue; a possible clinical application for electrical impedance tomography. **Physiological Measurements**, v. 17, n. 4A, p. A105 – A115, 1996.

BLAD, B., WENDEL, P., JÖNSON, M., LINDSTRÖM, K. An electrical impedance index to distinguish between normal and cancerous tissues. **Journal of Medical Engineering & Technology**, v. 23, n 2, p. 57 – 62, March/April 1999.

BOONE, K.G., HOLDER, D.S. Current approaches to analogue instrumentation design in electrical impedance tomography. **Physiological Measurements**, v. 17, n. 4, p. 229 – 247, 1996.

BOZKURT A, ONARAL B. Safety assessment of near infrared light emitting diodes for diffuseoptical measurements. **Biomedical Engineering Online**, v.3, p. 1-10, 2004.

BOYD, C., BRUNS, D.E. Quality Specifications for Glucose Meters: Assessment by Simulation Modeling of Errors in Insulin Dose, **Clinical Chemistry**, v. 47, p. 209 – 214, 2001.

BURMEISTER, J.J., ARNOLD, M.A. Evaluation of measurement sites for noninvasive blood glucose sensing with near-infrared transmission spectroscopy, **Clinical Chemestry**, v. 45, n. 9, p. 1621-1627, 1999.

CADUFF, A., HIRT, E., FELDMAN, Y., ALI, Z., HEINEMANN, L. First Human Experiments with a Novel Non-Invasive, Non-Optical Continuous Glucose Monitoring System. **Biosensors and Bioelectronics**, v. 19, p. 209-217, 2003.

CADUFF, A., DEWARRAT, F., TALARY, M., STALDER, G., HEINEMANN, L., FELDMAN, Y. Biosens Bioelectron. Non-invasive glucose monitoring in patients with diabetes: A novel system based on impedance spectroscopy. v. 22, p. 598-604, 2006.

CAFFEE, A.E., TEICHMAN, P.G. Improving anticoagulation management at the point of care. **Family Practice Management**, v.9, n. 2, p.35-37, 2002.

CAMERON, B.D., BABA, J.S., COTÉ, G.L. Optical polarimetry applied to the development of a noninvasive vivo glucose monitor. **Proceedings of SPIE**, v. 3923, p. 66-77, 2004.

CASAS, O., ROSELL, J., BRÁGÓS, R., LOZANO, A., RIU, P. A parallel broadband real-time system for electrical impedance tomography. **Physiological Measurements**, v. 17, n. 4A, p. A1 – A6, 1996.

CHAOSHI, R., HUIYAN, W., HONG, S., GUOJING, L. Development of electrical bioimpedance technology in the future. In: **Proceedings of the IEEE/EMBS 20th Annual International Conference**, p. 1052 – 1053, 1998.

Chen, W., Liu, R., Xu, K., Wang, R.K., Influence of contact state on NIR diffuse reflectance spectroscopy in vivo, **Journal of Physics, D, Applied Physics**, 38, p. 2691-2695, 2005.

CHO, O. K., KIM, Y.O., MITSUMAKI, H., KUWA, K. Noninvasive Measurement of Glucose by Metabolic Heat Conformation Method. **Clinical Chemistry**, v. 50:10, p. 1894-1898, 2004.

CHOUDHARY, P. Review of dietary recommendations for diabetes mellitus, **Diabetes Research & Clinical Practice**, v. 65, p. S9-S15, 2004.

CINCA, J., WARREN, M., RODRÍGUEZ-SINOVAS, A., TRESÀNCHEZ, M., CARREÑO, A., BRAGÓS, R., CASAS, O., DOMINGO, A., SOLER-SOLER, J. Passive transmission of ischemic ST segment changes in low electrical resistance myocardial infarct scar in the pig. **Cardiovascular Research**, v. 40, n. 1, p. 103-112, 1998.

CLARKE, W.L., ANDERSON, S., FARHY, L., BRETON, M., GONDER-FREDERICK, L., COX, D., KOVATCHEV, B., Evaluating the Clinical Accuracy of Two Continuous Glucose Sensors Using Continuous Glucose–Error Grid Analysis. **Diabetes Care**, v. 28, p. 2412-2417, 2005.

CLEMENS, A.H., HOUGH, D.L., D'ORAZIO, P.A. Development of the Biostator Glucose clamping algorithm. **Clinical Chemistry**, v. 28, n. 9, p. 1899–1904, 1982.

COHEN O., FINE I., MONASHKIN E., KARASIK A., Glucose Correlation with Light Scattering Patterns-A Novel Method for Non-Invasive Glucose Measurements. **Journal of Diabetes Technology & Therapeutics**, v. 5, n. 1, p. 11-17, 2003.

CORNISH, B.H., THOMAS, B.J., WARD, L.C. Effect of temperature and sweating on bioimpedance measurements. **Journal of Applied Radioisotopes**, v. 49, n. 5/6, p. 475 – 476, 1998.

COTE, G.C. Innovative non- or minimally-invasive technologies for monitoring health and nutritional status in mothers and young children. **The Journal of Nutrition**, v. 131, p. 596S–604S, 2001.

DESPAGNE, F., MASSART, D.L. Neural networks in multivariate calibration. **Analyst**, v. 123, p.157R-178R, 1998.

DING, Q., SMALL, G.W., ARNOLD, M.A. Evaluation of nonlinear model building strategies for the determination of glucose in biological matrices by near-infrared spectroscopy. **Analytica Chimica Acta**, vol. 384, p. 333-343, 1999.

DORF, R.C. **The Electrical Engineer Handbook**. Boca Raton, FL: CRC Press, 1993.

EHRET, R., BAUMANN, W., BRISCHWEIN, M., SCHWINDE, A., WOLF, B. On-line control of cellular adhesion with impedance measurements using in-terdigitated electrode structures, **Medical & Bio-logical Engineering & Computing**, v. 36, p. 365-370, 1998.

ELLIS, D.I., GOODACRE, R. Metabolic fingerprinting in disease diagnosis: biomedical applications of infrared and Raman spectroscopy. **The Analyst**, v. 131, p. 875-85, 2006.

ERGIN, A.,THOMAS, G.A. Non-invasive detection of glucose in porcine eyes, **31st IEEE Annual Northeast Bioengineering Conference**, p. 246-247, 2005.

FAUSETT, L. **Fundamentals of Neural Networks, Architectures, Algorithms and Applications**. Prentice Hall, Englewood Cliffs, 1994.

FINE, I., SHPIGELMAN, E., FIKHTE, B., MONASHKIN, E., KARASIK, A. Progress in Glucose Quantification. **Diabetes Technology Meeting**, San Francisco, November, 2003

FUNAKI, T., MATSUURA, K., TANAKA S. Error estimation and correction of detected phase by real time DFT. **Transactions of IEEE of Japan**, v. 120-B, n.12, p. 1682-1690, 2000.

GEDDES, L.A., BAKER, L.E. **Principles of Applied Biomedical Instrumentation**, 3rd edition, New York: John Wiley & Sons, p.537 –651, 1989.

GIVENS, T.B., BRAUN, P.J. Classification of factor deficiencies from coagulation assays using neural networks. **International Journal of Medical Informatics**, v. 46, n. 3, p. 129-143, 1997.

GLUCON A personal, non-invasive, real-time and continuous blood glucose monitoring device. 2002. Available in: http://www.glucon.com. Accessed in 19/08/2006.

GOURZI, M., ROUANE, A., GUELAZ, R., ALAVI, M.S., MCHUGH, M.B., NADI, M., ROTH, P. Non-invasive glycaemia blood measurements by electromagnetic sensor: study in static and dynamic blood circulation. **Journal of Medical Engineering & Technology**, v. 29, p. 22-26, 2005.

GRAEME, J.G., TOBEY, G. E., HUELSMAN, L. P. **Operational Amplifiers Design and Applications**. New York: McGraw-Hill, 1971.

GRIMNES, S., MARTINSEN, G.O. **Bioimpedance and Bioelectricity Basics**. London: Academic Press, 2000.

GROSS, T.M., BODE, B.W., EINHORN, D. Performance Evaluation of the MiniMed Continuous Glucose Monitoring System During Patient Home Use, **Diabetes Technology & Therapeutics**, v. 2, p. 49-56, 2000.

GÜNZLER, H., GREMLICH, H.U. **IR Spectroscopy: An Introduction**, Wiley-VCH, Weinheim, Germany, 2002.

GUO, B., Y.WANG, C. PENG, H.L. ZHANG, G.P. LUO, H.Q. LE, C. Laser-Based Mid-Infrared Reflectance Imaging of Biological Tissues, **Optics Express**, v. 12, p. 208–219, 2004.

HAALAND, D.M., THOMAS, V.T. Partial least-squares methods for spectral analyses. Relation to other quantitative calibration methods and the extraction of qualitative information. **Analytical Chemistry**, v. 60, p. 1193-202, 1988.

HAM, F.M., COHEN, G.M., KOSTANIC, I., GOOCH, B.R. Multivariate determination of glucose concentrations from optimally filtered frequencywarped NIR spectra of human blood serum. **Physiological Measurement**, v. 17, p. 1-20, 1996.

HARVEY, L.M., MCNEIL, B. At-line monitoring of ammonium, glucose, methyl oleate and biomass in a complex antibiotic fermentation process using attenuated total reflectance-mid-infrared (ATR-MIR) spectroscopy, **Analytica Chimica Acta**, v. 561, p. 218–224, 2006.

HEBDEN, J.C., BOAS, D.A., GEORGE, J.S., DURKIN, A.J. Topics in biomedical optics: introduction, **Applied Optics**, v. 42, p. 2869-2870, 2003.

HEISE, H. M. Glucose, In Vivo Assay of. In: Meyers, R.A. **Encyclopedia of analytical chemistry**, John Wiley Press , v. 1, p. 56-83, 2000.

HENNING, G.T., BRISCHWEIN, M., BAUMANN, W., EHRET, R., FREUND, I., KAMMERER, R., LEHMANN, M., SCHWINDE, A., WOLF, B. Approach to a multiparametric sensor-chip-based tumor chemosensitivity assay. **Anti-Cancer Drugs**, v. 12, n. 1, p. 21-32, 2001.

HOF, M. Basics of optical spectroscopy. Gauglitz, G., Vo-Dinh, T. **Handbook of Spectroscopy**, v. 1, WILEY-VCH GmbH, Weinheim, Germany, pp. 39–47, 2003.

HOLLIS, V., Non invasive monitoring of brain tissue temperature by near infrared spectroscopy, **PhD Thesis**, University of London, 2002.

HUANG, J.J., HONG, Y.N. CHENG, K.S., CHEN, C.W. A real-time monitoring system for the cardiac and respiratory parameters using bioimpedance technique. In: **Proceedings of the 11th IEEE Symposium on Computer-Based Medical Systems**, p. 216-221, 1998.

HUANG, J.J., CHENG, K., PENG, C. Temperature-compensated bioimpedance system for estimating body composition. **IEEE Engineering in Medicine and Biology Magazine**, v. 19, n. 6, p. 66 – 73, 2000.

INDIANA UNIVERSITY – BLOOMINGTON, Laser Safety Manual Available in: http://www.research.indiana.edu/rschcomp/radsafety/laser2004a.htm. Accessed in 06/02/2006.

JACKSON, M. From biomolecules to biodiagnostics: Spectroscopy does it all. **Faraday Discuss**, v. 126, p. 1-8, 2004.

JANG, S., FOX, M.D. Optical Glucose Sensor Using a Single Faraday Rotator, **Proceedings of the IEEE 1997 23rd Northeast**, p. 11-12, 1997.

JOSSINET, J., TRILLAUD, C. Technical improvement of a dual frequency EIT tomography for bioelectrical tissue characterization. In: **Proceedings of the IEEE/EMBS 14th Annual International Conference**, p. 1712, 1992.

JOSSINET, J., TOURTEL, C., RISACHER, F. A 2 MHz wide band full wave distributed impedance tomograph. In: **Proceedings of the IEEE/EMBS 16th Annual International Conference**, p. 543 – 544, 1994.

KANG, N. KASEMSUMRAN, S., WOO, Y.A., KIM, H.J., OZAKI, Y. Optimization of informative spectral regions for the quantification of cholesterol, glucose glucose and urea in control serum solutions using searching combination moving window partial least squares regression method with near infrared spectroscopy. **Chemometrics and Intelligent Laboratory Systems**, v. 82, p. 90 – 96, 2006.

KASEMSUMRAN, S., DU, Y., MARUO, K., OZAKI, Y. Improvement of Partial Least Squares Models for in vitro and in vivo Glucose Quantifications by Using Near-Infrared

Spectroscopy and Searching Combination Moving Window Partial Least Squares, **Chemometrics and Intelligent Laboratory Systems**, v. 82, p. 97-103, 2006.

KHALIL, O.S. Noninvasive Photonic-Crystal Material for Sensing Glucose in Tears. **Clinical Chemistry**, v. 50, p. 2236-2237, 2004.

KHALIL, O.S. Non-invasive glucose measurement technologies: an update from 1999 to the dawn of the new millennium. **Diabetes Technology & Therapeutics**, v. 6, p. 660-697, 2004.

KHALIL, O.S. Spectroscopic and clinical aspects of noninvasive glucose measurements, **Clinical Chemistry**, v. 45, n. 2, p. 165–177, 1999.

KINNUNEN, M. Comparison of optical coherence tomography, the pulsed photoacoustic technique, and the time-of-flight technique in glucose measurements in vitro. **PhD Thesis**, Oulu Graduate School, 2006.

KLONOFF, D. C. Continuous glucose monitoring: Roadmap for 21st. century diabetes therapy. **Diabetes Care**, v.28, p. 1231–1239, 2005.

KO, J.B., CHO, O.K., KIM, Y.O., YASUDA, K. Body metabolism provides a foundation for noninvasively monitoring blood glucose concentration. **Diabetes Care**, v. 27, p. 1211-1212, 2004.

KOSCHINSKY T., HEINEMANN L. Sensors for glucose monitoring: technical and clinical aspects. **Diabetes/Metabolism Research and Reviews**, v. 17, p. 113-123, 2001.

KOST, J., MITRAGOTRI, S., GABBAY, R.A., PISHKO, M., LANGER, R. Transdermal monitoring of glucose and other analytes using ultrasound. **Nature Medicine**, v. 6, p. 347-350, 2000.

KOVATCHEV, B.P., GONDER-FREDERICK, L.A., COX, D.J., CLARKE, W.L., Evaluating the Accuracy of Continuous Glucose-Monitoring Sensors: Continuous glucose-error grid analysis illustrated by TheraSense Freestyle Navigator data, **Diabetes Care**, v. 27, p. 1922 – 1928, 2004.

LEARDI, R., NØRGAARD, L. Sequential application of backward interval PLS and Genetic Algorithms for the selection of relevant spectral regions, **Journal of Chemometrics**, v. 18, n. 11, p. 486-497, 2004.

LACKERMEIER, A., PIRKE, A., MCADAMS, E., JOSSINET, J. Non-linearity of the skin's AC impedance. In: **Proceedings of the IEEE/EMBS 18th Annual International Conference**, p. 1945 – 1946, 1996.

LEBOULANGER, B., GUY, R.H., DELGADO-CHARRO, M.B. Reverse iontophoresis for non-invasive transdermal monitoring, **Physiological Measurement**, v.25, p. R35-R50, 2004.

LEE, S., NAYAK, V., DODDS, J., PISHKO, M., SMITH, N.B. Glucose measurements with sensors and ultrasound. **Ultrasound in Medicine & Biology**, v. 31, p. 971-977, 2005.

LEGER, M.N., RYDER, A.G. Comparison of Derivative Preprocessing and Automated Polynomial Baseline Correction Method for Classification and Quantification of Narcotics in Solid Mixtures. **Applied Spectroscopy**, v. 60, p. 182-193, 2006.

LIN, C.W., HSIAO, T.C., ZENG, M.T., CHIANG, K.H.H. Quantitative multivariate analysis with artificial neural networks. **Bioelectromagnetism, 1998. Proceedings of the 2nd International Conference on2nd International Conference on Bioelectromagnetism**, Melbourne, Australia, p. 59-60, 1998.

LISZKA-HACKZELL, J.J. Prediction of blood glucose levels in diabetic patients using a hybrid AI technique. **Computers and biomedical research, an international journal**, v. 32, n. 2, p. 132–144, 1999.

LIEDTKE, R.J. Principles of bioelectrical impedance analysis. 1997. Available in: http://www.rjlsystems.com/research/bia-principles.html. Accessed in 22/07/2004.

LO, Y.L., YU, T.C. A polarimetric glucose sensor using a liquid crystal polarization modulator driven by a sinusoidal signal. **Optics Communications**, v. 259, p. 40-48, 2006.

LOBANOV A.V., BORISOV, I.A., GORDON, S.H., GREENE, R.V. LEATHERS T.D. RESHETILOV, A.N. Analysis of ethanol-glucose mixtures by two microbial sensors:

application of chemometrics and artificial neural networks for data processing. **Biosensors & Bioelectronics**, v. 16, p. 1001-1007, 2001.

LÓPEZ, M.G., MADRID, R.E, FELICE, C.J. Medidor de biomasa por espectroscopia dieléctrica. In: **Anales del XIII Congreso Argentino de Bioingeniería**, Tucumán, Argentina, p.327, 2001.

MAGNENAT-THALMANN, N., KALRA, P., LÉVÊQUE, J-L., BAZIN, R., BATISSE, D., QUERLEUX, B., A computational skin model: fold and wrinkle formation. **IEEE Transactions on information technology in biomedecine**, v. 6, n. 4, p.317-323, 2002.

MALCHOFF, C.D., SHOUKRI, K., LANDAU, J.I., BUCHERT, J.M. A. novel noninvasive blood glucose monitor. **Diabetes Care**, v. 25, p. 2268–2275, 2002.

MALICH, A., BOHM, T., FRITSCH, T., FACIUS, M., FREESMEYER, M.G., ANDERSON, R., FLECK, M., KAISER, W.A. Animal-based model to investigate the minimum tumor size detectable with an electrical impedance scanning technique. **Academic Radiology**, v. 10, p. 37-44, 2003.

MARCH, W., LAZZARO, D., RASTOGI, S. Fluorescent measurement in the non-invasive contact lens glucose sensor. **Diabetes Technology & Therapeutics,** v. 8, p. 312-317, 2006.

MARTIN, W.B., MIROV, S., VENUGOPALAN , R., Using two discrete frequencies within the middle infrared to quantitatively determine glucose in serum, **Journal of Biomedical Optics**, v. 7, p. 613-618, 2002.

MARUO, K., TSURUGI, M., CHIN, J., OTA, T., ARIMOTO, H., YAMADA, Y., TAMURA, M., ISHII, M., OZAKI, Y. Noninvasive Blood Glucose Assay Using a Newly Developed Near-Infrared System, I**EEE Journal of Selected Topics in Quantum Electronics**, v. 9, p. 322-330, 2003.

MATTHIE, J., ZAROWITZ, B., DE LORENZO, A., ANDREOLI, A., KATZARSKI, K., PAN, G., WITHERS, P. Analitic assessment of the various bioimpedance methods used to estimate body water. **Journal of Applied Physiology,** v. 85, n. 5, p. 1801 – 1816, 1998.

MCADAMS, E.T., JOSSINET, J., LACKERMERMAIER, A., WOOLFSON, D., MCCAFFERTY, D., ANDERSON, J. Epidermal A.C. impedance: low frequency distortions. In: **Proceedings of the IEEE/EMBS 15th Annual International Conference**, p. 1497 – 1498, 1993.

MCNICHOLS, R.J., COTÉ, G.L. Optical glucose sensing in biological fluids: an overview, Journal of Biomedical Optics, v. 5, p. 5–16, 2000.

MENDELSON, Y. Optical Sensors, in **The Biomedical Engineering Handbook**, Bronzino, J.D., Ed. Boca Raton, FL: CRC, p. 764–778, 1995.

MENDELSON, Y., CLERMONT, A.C., PEURA, R.A., LIN, B. Blood Glucose Measurement by Multiple Attenuated Total Reflection and Infrared Absorption Spectroscopy. **IEEE Transactions on Biomedical Engineering**, v. 3, n. 5, 1990.

MIN, M., MÄRTENS, O., PARSE, T. Lock-in measurement of bio-impedance variations. **Measurement**, v. 27, n. 1, p. 21-28, 2000.

MIN, M., PARVE, T., KUKK, V., KUHLBERG, A. An implantable analyzer of bio-impedance dynamics: mixed signal approach. In: **Proceedings of the 18th IEEE Instrumentation and Measurement Technology Conference**, p. 38-43, 2001.

MOSCHOU, E.A., SHARMA, B.V., DEO, S.K., DAUNERT, S. Fluorescence Glucose Detection: Advances Toward the Ideal in vivo Biosensor, **Journal of Fluorescence**, v. 14 p. 535-547, 2004.

N. I. H. - NATIONAL INSTITUTES OF HEALTH Bioelectrical impedance analysis in body composition measurement. December, 1994. Available in: http://consensus.nih.gov/ta/015/015_intro.htm. Accessed in 18/08/2004.

NEVES, C.E.B., LEITE, B.B., SOUZA, M.N. Body Impedance spectroscopy based on a step response. **Physiological Measurement**, v. 21, n 3, p. 395 – 408, 2000.

NYSTROM, J., LINDHOLM-SETHSON, B., STENBERG, L., OLLMAR, S., ERIKSSON, J.W., GELADI, P. Combined nearinfrared spectroscopy and multifrequency bioimpedance investigation of skin alterations in diabetes patients based on multivariate analyses. **Medical and Biological Engineering and Computing**, v. 4, p. 324-329, 2003.

O'CONNELL, P., HAWTHORNE, W., HOLMES-WALKER, D., NANKIVELL, B., GUNTON, J., PATEL, A., WALTERS, S., PLEASS, H., ALLEN, R., CHAPMAN, J. Clinical islet transplantation in type 1 diabetes mellitus: results of Australia's first trial. **The Medical journal of Australia,** v. 184, p. 221-225, 2006.

OLDHAM, N.M. Overview of bioelectrical impedance analysers. **American Journal of Clinical Nutrition**, v. 64, suppl., p. 405S – 412S, 1996.

OLESBERG, J.T., LIU, L., VAN ZEE, V., ARNOLD, M.A. In vivo near-infrared spectroscopy of rat skin tissue with varying blood glucose levels, **Proceedings of the SPIE 2004**, v. 5325, p.11–20, 2004.

OZ, G., HENRY, P.G., SEAQUIST, E.R., GRUETTER, R. Direct, noninvasive measurement of brain glycogen metabolism in humans. **Neurochemistry International**, v. 4, p. 323-329, 2003.

ORSYPKA, M., GERSING, E. Tissue impedance spectra and the appropriate frequencies for EIT. **Physiological Measurements**, v. 16, n. 3A, p. A49 – A55, 1995.

PALLÁS-ARENY, R., WEBSTER, J.G. AC instrumentation amplifier for bioimpedance measurements. **IEEE Transactions on Biomedical Engineering**, v. 40, n. 8, p. 830 – 833, August 1993.

PANCHAGULA, R., PILLAI, O., NAIR, V.B., RAMARAO, P. Transdermal iontophoresis revisited. **Current Opinion in Chemical Biology**, v. 4, p. 468-473, 2000.

PARK, H.D., LEE, K.J., YOON H., R., NAMB, H.H. Design of a portable urine glucose monitoring system for health care. **Computers in Biology and Medicine**, v. 35, p. 275-286, 2005.

PÉREZ, P., SANTOS, A., VAQUERO, J.J. Potential use of the undersampling technique in the acquisition of nuclear magnetic resonance signals. **Magnetic Resonance Materials in Physics, Biology and Medicine,** p. 109–117, v. 13, n. 2, 2001.

PERKIN-ELMER, **Spectrum One User's Guide**, Perkin-Elmer Corporation, 1998.

PICKUP J. C., HUSSAIN F., EVANS N. D., SACHEDINA N. In vivo glucose monitoring: the clinical reality and the promise. **Biosensors and Bioelectronics**, v. 20, p.1897-1902, 2005.

POTTS R.L O., TAMADA J.A., TIERNEY M. J. Glucose monitoring by reverse iontophoresis. **Diabetes Metabolism Research and Reviews**, v. 18 Suppl 1, S49-S53, 2002.

PFÜTZNER, A., CADUFF, A., LARBIG M., SCHREPFER, T., FORST, T. Impact of posture and fixation technique on impedance spectroscopy used for continuous and noninvasive glucose monitoring. **Diabetes Technology & Therapeutics**, v. 6, n. 4, p. 435-441, August, 2004.

PRESS, W.H., VETTESLING, W.T., TEUKOLSKY, S.A., FLANNERY, B.F. **Numerical Recipes in C.** Cambridge: Cambridge University Press, 1992.

PRISCO, D., PANICCIA, R. Point-of-Care Testing of Hemostasis in Cardiac Surgery. **Thrombosis Journal**, v. 1, p. 1-10, 2003

RANDALL, T.D. An Introduction to Partial Least Squares Regression. SUGI Proceedings, 1995.

RAWER, R., STORK, W., KREINER, C.F. Non-invasive polarimetric measurement of glucose concentration in the anterior chamber of the eye, **Graefe's Archive for Clinical and Experimental Ophthalmology**, v. 242, 1017-1023, 2004.

REN, C., WANG, H., AN, Y., HONG, S., LIN., G. Development of electrical bioimpedance technology in the future. In: **Proceedings of the IEEE/EMBS 20th Annual International Conference**, v. 20, n. 2 p. 1052 – 1054, 1998.

RENARD E. Monitoring glycemic control: the importance of self-monitoring of blood glucose. **American Journal of Medicine**, v. 118 p. 12S-19S, 2005.

RIGAUD, B., HAMZAOUI, L., CHAVEUAU, N., MARTINEZ, E., MORUCCI, J. Tissue characterization and modeling by electrical bioimpedance spectrometry. In: **Proceedings of the IEEE/EMBS 16th Annual International Conference**, p. 866 – 867, 1994.

RISTIC, B., KUN, S., PEURA, R. Development of an impedance spectrometer for tissue ischemia monitoring: instrument realization and performance. In: **Proceedings of the IEEE/EMBS 17th Annual International Conference**, p. 1643 – 1644, 1995.

RODVIEN, R., MIELKE, C. Role of Platelets in Hemostasis and Thrombosis. **The Western Journal of Medicine**, v. 125, n.3, p.181–186, 1976.

ROHDE & SCHWARZ, Universal sweep generators for network analysis **News from Rohde & Schwarz**, n. 184, p. 39-41, 2004.

ROHRSCHEIB, M., ROBINSON, R., EATON, R.P. Non-invasive glucose sensors and improved informatics-the future of diabetes management. **Diabetes, Obesity and Metabolism**, v. 5, p. 280-284, 2003.

ROSELL, J., COLOMINAS, J., RIU, P., PALLAS-ARENY, R., WEBSTER, J.G. Skin impedance from 1 Hz to 1 MHz. **IEEE Transactions on Biomedical Engineering**, v. 35, n. 8, p. 649 – 651, 1988.

ROSEN, A., ROSEN, H.D., HSI, R.A., ROSEN, D., HAPPAWANA, G., EVANS G., FATHY, A. , STERN, L. Advances in RF-microwave and light sources for applications in therapeutic medicine. In: **Microwaves, Radar and Wireless Communications, 2004. MIKON-2004**, v. 2, p. 461- 466, 2004.

SABLINSKAS, V. Instrumentation. In: Gauglitz, G., Vo-Dinh, T. (Ed.) **Handbook of Spectroscopy**, v. 1, WILEY-VCH GmbH, Weinheim, Germany, pp. 48–69, 2003.

SAVAGE M.B., KUN, S.,HARJUNMAA, H. Development of a non-invasive bloodg lucose monitor. Application of artifi-cial neural networks for signal processing. **Proceedings of the IEEE 26th Annual Northeast**, p. 229-230, 2000.

SATO, S., ISHIGURE, M., INABA, H. Optical trapping and rotational manipulation of microscopic particles and biological cells using higher-order mode Nd:YAG laser beams, **Electronics Letters**, v. 27, n. 20, p. 1831-1832, 1991.

SCHNECK, D.J. An Outline of Cardiovascular Structure and Function, in **The Biomedical Engineering Handbook**: Bronzino, J.D., Ed. Boca Raton, FL: CRC, p. 1.1-1.13, 1995.

SCOLARO, K.L., STAMM, P.L., LLOYD K.B. Devices for ambulatory and home monitoring of blood pressure, lipids, coagulation, and weight management, part 2. **American Journal of Health-System Pharmacy**, v. 62, p. 1894-1903, 2005.

SCHRADER, W., MEUER, P., POPP, J., KIEFER, W., MENZEBACH, J.-U., SCHRADER, B. Non-invasive glucose determination in the human eye. **Journal of Molecular Structure**, v. 299, p. 735-736, 2005.

SEARLE, A., KIRKUP, L. Real time impedance plots with arbitrary frequency components **Physiological Measurements**, v. 20, n. 1, p. 103 – 114, 1999.

SEKIGUCHI, N., KOMEDA, T., FUNAKUBO, H., CHABICOVSKY, R., NICOLICS, J., STANGL, G. Microsensor for the measurement of water content in the human skin. **Sensors and Actuators B: Chemical**, v. 78, n. 1, p. 326-330, 2001.

SHAW, R.A., MANTSCH, H.H. Infrared Spectroscopy in Clinical and Diagnostic Analysis;, in **Encyclopedia of Analytical Chemistry**, Meyers, R. A., John Wiley & Sons Ltd, Chichester, 2000.

SHEN, Y.C., DAVIES, A.G., LINFIELD, E.H., ELSEY, T.S., TADAY, P.F., ARNONE, D.D., The use of Fourier-transform infrared spectroscopy for the quantitative determination of glucose concentration in whole blood. **Physics in Medicine and Biology**, v. 48(13) p. 2023-2032, 2003.

SHERMAN, C.P. Infrared Spectroscopy. In: Settle, F.A. (Ed.) **Handbook of. Instrumental Techniques for Analytical. Chemistry**. Prentice Hall, New Jersey, p. 247 - 283, 1997.

SIEG, A., GUY, R.H., DELGADO-CHARRO, M.B. Noninvasive and minimally-invasive methods for transdermal glucose monitoring. **Diabetes Technology & Therapeutics**, v. 7 p. 174-97, 2005.

SIMONS, J.P., SCHOLS, A.M., WESTERTERP, K.R., TEN VELDE, G.P., WOUTERS, E.F. Bioelectrical impedance analysis to assess total water in patients with cancer. **Clinical Nutrition**, v. 18, n. 1, p. 35 - 39, 1999.

SLINEY D.H. Optical radiation safety of medical light sources, **Physics in Medicine and Biology**, v. 42, p. 981-996, 1997.

SMALL, G.W., ARNOLD, M.A., MARQUARDT, L.A. Strategies for Coupling Digital Filtering with Partial Least-Squares Regression: Application to the Determination of Glucose in Plasma by Fourier Transform Near-Infrared Spectroscopy. **Analytical Chemistry**, v. 65, p. 3279-3289, 1993.

SRINIVASAN, V., PAMULA, V.K., POLLACK, M.G., FAIR, R.B. Clinical diagnostics on human whole blood, plasma, serum, urine, saliva, sweat, and tears on a digital microfluidic platform, **Proceedings of MicroTAS**, p. 1287–1290, 2003.

SMITH, D.G., POTTER, S.R., LEE, B.R., KO, H.W., DRUMMOND, W.R., TELFORD, J.K. PARTIN A.W. In vivo measurement of tumor condutiveness with the magnetic bioimpedance method. **IEEE Transactions on Instrumentation and Measurement,** v. 47, n. 10, p. 310 – 313, October 2000.

SOLARTRON ANALYTICAL, 1260 Impedance/gain-phase Analyzer, **Solartron Analytical**, 2004.

SONG, K., JANG, P., CHO, H. JUN, C. Partial least square-based model predictive control for large-scale manufacturing processes. **IIE Transactions**, v. 34, p.881–890, 2004.

SOSA, M., BERNAL-ALVARADO, J., JIMENEZ-MORENO, M. Magnetic field influence on electrical properties of human blood measured by impedance spectroscopy. **Bioelectromagnetics**, v. 26, n.7, p. 564-570, 2005.

TAMURA, K., FUJITA, K., KANEKO, W., NGUYEN TUONG LINH NISHIMATSU, T., ISHIZAWA, H., TOBA, E. Noninvasive measurement of blood glucose based on optical sensing, **Proceedings of the 21st IEEE**, v. 3, p. 1970- 1974, 2004.

THENNADIL, S.N., RENNERT, J.L., WENZEL, B.J., HAZEN, K.H., RUCHTI, T.L., BLOCK, M.B., Comparison of glucose concentration in interstitial fluid, and capillary and venous blood during rapid changes in blood glucose levels, **Diabetes Technology & Therapeutics**, v. 3 p. 357-365, 2001.

THERMO NICOLET **FT-IR vs. Dispersive Infrared Theory of Infrared Spectroscopy Instrumentation**, Thermo Nicolet Corporation, 2002.

THOMAS, B.J., WARD, L.C., CORNISH, B.H. Bioimpedance spectrometry in the determination of body water compartments: accuracy and clinical significance. **Applyed Radiation and Isotopes**, v. 49, n. 5/6, p. 447 – 455, 1998.

THOMASSET, A.L. Bio-electrical impedance analysis. 1997. Available in: http://home.worldnet.fr/~althomas/HomePage.shtml Accessed in 20/05/2004.

TIERNEY, M.J., JAYALAKSHMI, Y., PARRIS, N.A., REIDY, M.P., UHEGBU, C., VIJAYAKUMAR, P. Design of a biosensor for continual, transdermal glucose monitoring. **Clinical Chemistry**, v. 45, p. 1681–1683, 1999.

TIERNEY, M.J., TAMADA, J.A., POTTS, R.O., JOVANOVIC, L., GARG, S. Clinical evaluation of the GlucoWatch biographer: a continual, non-invasive glucose monitor for patients with diabetes. **Biosensors and Bioelectronics**, v. 16, p. 621-629, 2001.

TORRENTS, J., PALLÀS-ARENY, R. Compensation of impedance metres when using an external front-end amplifier. **IEEE Transactions on Instrumentation and Measurement.** v. 51, n. 2, p. 310 – 313, April 2002.

TOSO, S., PICCOLI, A., GUSELLA, M., MENON, D., BONONI, A., CREPALDI, G., FERRAZZI, E. Altered tissue electric properties in lung cancer patients as detected by bioelectric impedance vector analysis. **Basic Nutritional Investigation**, v. 16, p. 120 – 124, 2000.

TRAJANOSKI, Z., REGITTNIG, W., WACH, P. Simulation studies on neural predictive control of glucose using the subcutaneous route. **Comput Meth Programs Biomed**, v. 56, p. 133-139, 1998.

TURA, A., MARAN, A., PACINI, G. Non-invasive glucose monitoring: Assessment of technologies and devices according to quantitative criteria. **Diabetes Research & Clinical** Practice v. 1, 2006.

ÜLGEN, Y., SEZDI, M. Electrical parameters of human blood. In: **Proceedings of the IEEE/EMBS 20th Annual International Conference**, v. 6, p. 2983 - 2986, 1998.

WANG, R.K., HEBDEN, J.C., TUCHIN, V.V. Special issue on recent developments in biomedical optics. **Physics in Medicine and Biology**, v. 49, n. 7, 2004.

WANG, W., YAN, L., LIU, B., ZHANG, H. Multisensors Information Fusion with Neural Networks for Noninvasive Blood Glucose Detection, **Lecture Notes in Computer Science**, Springer Berlin / Heidelberg, 2005.

WEBSTER, J.G. **Design of pulse oximeters**. Institute of Physics publishing Ltd, Philadelphia, 1997.

WEBSTER, J.G. **Medical Instrumentation: Application and Design**. 3rd edition, New York: John Wiley & Sons, 1998.

WEBSTER, J.G. **The Measurement, Instrumentation, and Sensors Handbook.** Boca Raton, FL: CRC Press, 1999.

WENTHOLT, I., M., E., HOEKSTRA, J., B., L., ZWART, A., DEVRIES, J., H., Pendra goes Dutch: lessons for the CE mark in Europe. **Diabetologia**. v. 48, n.6, p. 1055-1058, 2005.

WHITTON, J.T., EVERALL, J.D. The thickness of the epidermis. **British Journal of Dermatology,** v. 89, p. 467–476, 1973.

WICKRAMASINGHE, Y., YANG, Y., SPENCER, S.A. Current problems and potential techniques in in-vivo glucose monitoring. **Journal of Fluorescence**, vol.14, n. 5, p. 513-520, 2004.

WILKINS, E., ATANASOV, P. Glucose Monitoring: State of the Art and Future Possibilities. A Review, **Medical Engineering & Physics**, v.18, p. 273-288, 1996.

WILLIAMS, C.M.J. MAIER, N.A., POTOCKY-PACAY, K.A. The ABC of Metabonomics-Automated Baseline Correction", Orlando, Florida, **Advanced Chemistry Development**, Williams, 2001.

WOJCICKI J. M., LADYZYNSKI P. Toward the improvement of diabetes treatment: recent developments in technical support. **Journal of Artificial Organs**, v. 6, p. 73-87. 2003.

YAMAKOSHI, K., YAMAKOSHI, Y. Pulse glucometry: a new approach for noninvasive blood glucose measurement using instantaneous differential near-infrared spectrophotometry. **Journal of Biomedical Optics**, v. 11, 2006.

YEH, S.J., HANNA, C.F., KHALIL, O.S. Monitoring blood glucose changes in cutaneous tissue by temperature-modulated localized reflectance measurements, **Clinical Chemistry**, v. 49(6), p. 924-934, 2003.

VICKERS, T.J., WAMBLES, R.E., MANN C.K. Curve fitting and linearity: Data processing in Raman spectroscopy. **Applied Spectroscopy**, v. 55, p. 389-393, 2001.

YOKOTA, M., SATO, Y., YAMAGUCHI, I., KENMOCHI, T., YOSHINO T. A compact polarimetric glucose sensor using a high-performance fibre-optic Faraday rotator. **Measurement Science and Technology**, p. 143-147, 2004.

YOTTER, R.A., WILSON, D.M. A review of photodetectors for sensing light-emitting reporters in biological systems, **IEEE Sensors Journal**, v. 3, p. 288–303, 2003.

ZAMANIAN, A., HARDIMAN, C. Electromagnetic Radiation and Human Health: A Review of Sources and Effects. **High Frequency Electronics**, p. 16-26, 2005.

ZHAO, Z.M. **Pulsed photoacoustic techniques and glucose determination in human blood and tissue**. Ph.D thesis,University of Oulu, 2002.

ZHAO, R.T., Electrical Impedance and Haematocrit of Human Blood with Various Anticoagulants. **Physiological Measurements**. , v. 14, p. 299-307, 1993.

ZHU, F., SCHNEDITZ, D., WANG, E., LEVIN, N.W. Continuous measurement of segmental and whole body bio-impedance. In: **Proceedings of the IEEE/EMBS 19th Annual International Conference**, Oct. 30 – Nov. 2, p. 2086 – 2088, 1997.